SOLID-STATE ELECTROCHEMISTRY AND THERMODYNAMIC ASSESSMENT IN THE Al-In-Sb SYSTEM

By

CORINNE ANN COUGHANOWR

A DISSERTATION PRESENTED TO THE GRADUATE SCHOOL
OF THE UNIVERSITY OF FLORIDA IN
PARTIAL FULFILLMENT OF THE REQUIREMENTS
FOR THE DEGREE OF DOCTOR OF PHILOSOPHY

UNIVERSITY OF FLORIDA

1989

Vere didici verum laborem,
autem didici et veritatem.

ACKNOWLEDGEMENTS

In that the production of this dissertation has been a very difficult process which I could not have finished without the help of numerous others, I would like to acknowledge those who have given me so much invaluable assistance.

I would like first to thank Ted Lazo, my husband, who provided me with excellent advice, support and inspiration throughout the project.

I would like to thank Tim Anderson for providing support and guidance as my committee chairman. I would also like to thank Jim Egan and Ursula Kattner, who supervised various portions of this project.

A myriad thanks go to the many people who provided technical advice and assistance, including Ray Heus, Jim McBreen, John Johnson, Georges Bougnot, Pete Horton and Bob Sabatini.

I would particularly like to thank Glenn Price, Don Metz and Bruce Klemm for their administrative and financial support at Brookhaven National Laboratory. I would like to acknowledge a Junior Research Associate Appointment, supported by the Brookhaven National Laboratory Co-Op Program.

Special thanks go to Arleen Lancsarics for her unflagging support and assistance.

I would like to thank my committee members, Mark Orazem, Gerry Westermann-Clark, Sam Colgate and Bob De Hoff, for patiently bearing with me and for showing up for the big day. I would also like to thank Shirley, Peggy and Nancy in the Chemical Engineering

Department office, who helped me get through many long-distance registrations and other University of Florida red tape.

Many, many thanks go to my parents, who headed me in this direction from childhood, and to my parents-in-law, who provided housing, care and support during the latter portion of the project. I would especially like to thank Tina Coughanowr, Tom Trull and Sherie Michaile for their invaluable support from the trenches.

Finally, I would like to thank the many, many friends and supporters without whom this project would have been much more difficult.

TABLE OF CONTENTS

Page

ACKNOWLEDGMENTS iii

ABSTRACT viii

CHAPTERS

I INTRODUCTION 1

II EXPERIMENTAL METHODS 3

Introduction 3

Apparatus 6

Materials 10

Experimental Procedure 15

III THE Al-In SYSTEM 18

Introduction 18

Experimental 18

Results and Discussion 20

IV THE Al-Sb SYSTEM 40

Introduction 40

Experimental 40

Results and Discussion 43

Liquid Al-Sb Results 43

Solid AlSb Results 52

V ASSESSMENT AND CALCULATION OF THE THERMOCHEMICAL PROPERTIES AND PHASE DIAGRAMS FOR THE Al-In AND Al-Sb SYSTEMS 59

The Al-In System 59
Introduction 59
Experimental Data 60
Phase diagram data 60
Thermodynamic data 63
Method of Calculation 65
Results and Discussion 67

The Al-Sb System 77
Introduction 77
Experimental Data 78
Phase diagram data 78
Enthalpy data 82
Partial molar Gibbs energy data 85
Method of Calculation 86
Results and Discussion 90
Results using the Redlich-Kister model 90
Results using the associated solution model 95
Results using the Wagner-Schottky model 103
Comparison with previous calculations 106

VI EXTRAPOLATION AND OPTIMIZATION OF THE Al-In-Sb SYSTEM . . 111

Introduction 111

Experimental Data 111

Results and Discussion 112
Extrapolation from the Binary Subsystems 112
Ternary Optimization 116
Comparison with Previous Calculations 124

VII SUMMARY AND CONCLUSIONS 130

APPENDICES

A EXPERIMENTAL DATA FOR THE Al-In SYSTEM 133

B EXPERIMENTAL ERRORS 148

LIST OF REFERENCES 151

BIOGRAPHICAL SKETCH 156

Abstract of Dissertation Presented to the Graduate School
of the University of Florida in Partial Fulfillment of the
Requirements for the Degree of Doctor of Philosophy

SOLID-STATE ELECTROCHEMISTRY AND
THERMODYNAMIC ASSESSMENT IN THE
Al-In-Sb SYSTEM

By

Corinne Ann Coughanowr

December, 1989

Chairman: Timothy J. Anderson
Major Department: Chemical Engineering

Thermodynamic studies of the Al-In and Al-Sb systems have been carried out using solid electrolyte galvanic cells. Using the sensitive coulometric titration technique, aluminum activities were obtained for both systems. In addition, liquidus data were obtained for the Al-Sb system, and the Gibbs energy of formation of AlSb was determined. All of the data obtained match the values reported in the literature very closely.

For the Al-Sb system, the coulometric titration technique was also used to investigate, for the first time, the very narrow region of homogeneity in the AlSb compound. The width of the compound was found to be 0.002 mole fraction at 850 $^{\circ}C$, and the deviation from stoichiometry was determined to occur primarily on the Al-rich side.

The experimental data obtained in this study were used along with the available literature data in the critical assessment and calculation of the Al-In and Al-Sb systems. The Al-In system was successfully modeled using the Redlich-Kister polynomial to describe the liquid phase, and the Al-Sb system was described with the associate model as well as the

polynomial model. In addition, the Wagner-Schottky model was able to give a description of the AlSb homogeneity region that was consistent with the solid-phase titration data obtained in this study.

Finally, the calculated binary descriptions for the Al-In and Al-Sb systems were used in the calculation of the Al-In-Sb system. The ternary description using only the binary parameters gave a very reasonable fit to the available Al-In-Sb data. Two ternary parameters were determined from optimization of the ternary data, and the resulting Al-In-Sb description agreed excellently with the ternary data.

CHAPTER I

INTRODUCTION

While silicon is well-established as a device material in the electronics industry, the use of Group III-V semiconductors is becoming increasingly important as device design requirements become more complex. The elemental nature of silicon has allowed its properties to be well-characterized, and its behavior in electronic processing steps has been extensively studied. The inherent complexity of the Group III-V compounds makes their characterization more difficult, but they offer a wide range of electrical and optical properties, often superior to those of pure silicon. Moreover, the ability of these compounds to form completely miscible substitutional solid solutions among themselves provides the electronics industry with a virtually continuous spectrum of properties from which to choose.

The use of III-V materials in semiconductor devices has been hampered by the technological difficulties of processing compound materials rather than elemental materials. In the interest of facilitating the development of III-V processing technology, studies of the thermodynamic properties of these systems are appropriate. Since many of the processing steps, such as liquid-phase epitaxy and bulk crystal growth, involve contact of the liquid and solid phases of the material used, phase diagram data are important for providing equilibrium boundary conditions. Other processes, such as rapid thermal annealing and chemical vapor deposition involve contact of a vapor phase with the solid III-V material. Solid-vapor equilibrium is important in these processes, and a thermodynamic description of the solid phase can often be obtained from analysis of solid-liquid equilibrium data. As

the measurement of thermodynamic properties of all the possible III-V binaries, ternaries and quaternaries would be a monumental task, accurate prediction, extrapolation and interpolation of thermodynamic quantities are equally important.

In the present study, the technique of coulometric titration was used in conjunction with solid electrolyte galvanic cells to obtain thermodynamic data for two binary systems, Al-Sb and Al-In. These systems have been less well characterized than the other antimonides and III-III binaries, and were also well-suited to investigation by the proposed technique, since their melting points and vapor pressures are in an experimentally appropriate range.

The particular advantage of the proposed experimental technique was that it provided a means of studying the homogeneity region (range of solid solution) of the AlSb compound, heretofore not experimentally investigated. Since the electronic properties of semiconductor materials are highly sensitive to minute amounts of impurity or native defect, determination of the width of the homogeneity region and of the nature of the defects present would provide information critically important for the design of devices and their processing steps.

The thermodynamic data measured for the Al-In and Al-Sb systems were then used in the critical assessment and calculation of these systems. Careful evaluation of available thermodynamic data is critical to achieving a reliable calculated description of the system, as is the choice of a reasonable model.

The calculated descriptions of the binaries were then used in the calculation of the Al-In-Sb ternary system. The success of a calculated description of a ternary system is highly dependent on the quality of the binary descriptions which form the building blocks of the ternary description. For cases where the binary descriptions are very good and the ternary deviates somewhat from ideal behavior, accurate ternary descriptions can be obtained with only a few ternary data to fix the ternary parameters.

CHAPTER II

EXPERIMENTAL METHODS

Introduction

Along with calorimetric and vapor pressure methods, the use of galvanic cells is an important experimental method for obtaining thermodynamic quantities for metallurgical systems. In contrast to electromotive force (emf) cells employing fused salt or aqueous electrolytes, the use of solid electrolytes in galvanic cells is relatively new. It was promoted primarily by the publication of two articles in 1957 by Kiukkola and Wagner [57Kiu1, 57Kiu2]; in the first, they reviewed different types of galvanic cells, cited previous work on solid electrolytes and pointed out further applications. In the second paper, they demonstrated the usefulness of solid electrolytes in galvanic cells by reporting their emf determinations of the standard molar Gibbs energies of formation of several oxides, sulfides and tellurides. A plethora of thermodynamic investigations has since established the solid state galvanic cell as a major experimental tool, and numerous review articles on the subject are available [70Rap, 71Sch, 72Sch, 74Ram, 83Kom].

Beyond the general experimental problems in emf cells, such as obtaining reversible emf values and avoiding side reactions, mixed potentials and polarization, the use of solid state electrolytes requires a few extra precautions. In that a minimum conductivity of about $10^{-6}\ \Omega^{-1}cm^{-1}$ is necessary to operate a galvanic cell [72Sch], most solid electrolytes become useful only at elevated temperatures. Since ionic mobilities are much lower in solid

than in liquid electrolytes, the contribution of electronic conductivity can be significant in the former. The electrolyte and the experimental conditions must be selected so that the conductivity in the electrolyte remains almost wholly ionic (ionic transport number $t_i \geq 0.99$).

Among the various oxide and halide compounds employed in emf cells, CaF_2 has been well characterized and widely used. Ure [57Ure] studied the ionic defects in CaF_2 and found the dominant disorder type in CaF_2 to be anti-Frenkel on the F sublattice, *i.e.* equal concentrations of F^- vacancies and interstitials. The electrolyte conducts primarily by F^- ions over a wide temperature range and maintains an ionic transport number of essentially unity over a wide electrolytic domain. The limits of this domain have been investigated by a number of authors [68Wag, 73Hin, 75Bau, 78Del]. The results of Delcet *et al.* [78Del] recommend the use of CaF_2 at calcium activities below 10^{-3} for temperatures in the range 800 – 950 °C. Hinze and Patterson [73Hin] determined CaF_2 to be useful as a solid electrolyte at fluorine partial pressures down to 10^{-48} atm at 800 °C. It has also been determined that single-crystal CaF_2 is preferable to polycrystalline CaF_2 for use in long-term (longer than several hours) galvanic cell operation, since diffusion of electrode cations along grain boundaries can short the cell [83Kle]. Further information on the properties and use of CaF_2 solid electrolyte is available in the review papers of Tretyakov and Kaul [72Tre] and Kleykamp [83Kle].

The measurement of open-circuit emf values in galvanic cells can provide such thermodynamic quantities as component activity data, Gibbs energies of formation and enthalpy values, as well as phase diagram data, depending on the type of cell used and the system studied. In addition, the method of coulometric titration, introduced by Wagner [53Wag], allows accurate changes in composition to be made, whereby deviations from ideal stoichiometry and defect structures in binary compounds can be determined [30Wag, 71Wag].

In this study, galvanic cells containing single-crystal CaF_2 as the solid electrolyte were employed to investigate the Al-In and Al-Sb systems. Emf data in the temperature range 850 – 900 °C were measured for the following two types of cell:

Alloy: $Ca - Sn\ (l) \parallel CaF_2\ (s) \parallel AlF_3 - CaF_2\ (l/s)$, $Al - M\ (l \text{ or } s)$ (I)

where M = In or Sb, and:

Pure Al: $Ca - Sn\ (l) \parallel CaF_2\ (s) \parallel AlF_3 - CaF_2\ (l/s)$, $Al\ (l)$ (II)

The use of pure aluminum as the reference electrode was not satisfactory, due to the strong tendency of Al to react with container materials at elevated temperatures. Instead, the Ca-Sn (10 at.% Ca) alloy served as a reference electrode with very reproducible behavior. The difference $(E_I - E_{II})$ yielded the emf values used to determine Al component activities in the Al alloy systems:

$$\ln a_{Al} = -\frac{3F}{RT}(E_I - E_{II}) \qquad (2-1)$$

To change the composition of the working electrode in cell type I, coulometric titration was used. Al was titrated into (or out of) the Al-M system from the AlF_3-CaF_2 salt, producing F^- ions which crossed the CaF_2 solid electrolyte and combined with a minute amount of Ca in the Ca-Sn reference alloy. This process is represented by the following half-cell reactions:

$$AlF_3\ (\text{in } AlF_3 - CaF_2) + 3e^- \rightleftharpoons Al\ (\text{in } Al - M) + 3F^-$$

$$3F^- + \frac{3}{2}Ca\ (\text{in } Ca - Sn) \rightleftharpoons \frac{3}{2}CaF^2 + 3e^-$$

Since the Ca-Sn reference electrode contained 100 to 600 times the amount of Ca needed for the cell titrations, the Ca-Sn alloy composition remained essentially constant during cell operation.

Apparatus

The cell design, developed by Egan and coworkers [79Del, 83Alq, 85Ega] is depicted schematically in Figure 2-1 and was used for both cell types, I and II. A small amount (0.001 to 0.010 g) of the Al metal or alloy was placed in the working electrode (WE) cup, along with a small amount (*ca.* 0.020 g) of the AlF_3-CaF_2 salt mixture. The stacked electrode cups were pressed between stainless steel plates which were held together by four Ta rods. Upon heating the cell, the solid CaF_2 electrolyte softened somewhat at about 600 °C, and a tight seal between the electrolyte and electrode cups was effected by the greater expansion of the stainless steel plug as compared to the expansion of the Ta rods. The electrode salts and metals that were molten at 850 °C were thus kept from leaking out of the cell. The temperature of the cell was measured by means of a chromel-alumel thermocouple, which was positioned just under the molybdenum cap. Figure 2-2 shows a photograph of the galvanic cell.

To enable the cell to be placed under a vacuum or under inert atmosphere, a Vycor sleeve (Figure 2-3, right) was used to cover the galvanic cell. It was lined with a Ta foil getter to protect the Vycor from attack by fluoride or aluminum vapors. The sleeve was sealed with black wax to a glass base (Figure 2-3, left), which sat outside the furnace and provided passage for the lead wires from the cell and from the cell thermocouple. The laboratory equipment used to operate the galvanic cell is shown in Figure 2-4 and included (clockwise from top):

(a) the tubing leading to a high-vacuum system, which was able to achieve a vacuum of 10^{-6} torr by means of a diffusion pump

(b) a Lindberg 54341 furnace, controlled by a Leeds and Northrup Electromax IV temperature controller (not shown), capable of heating the cell up to

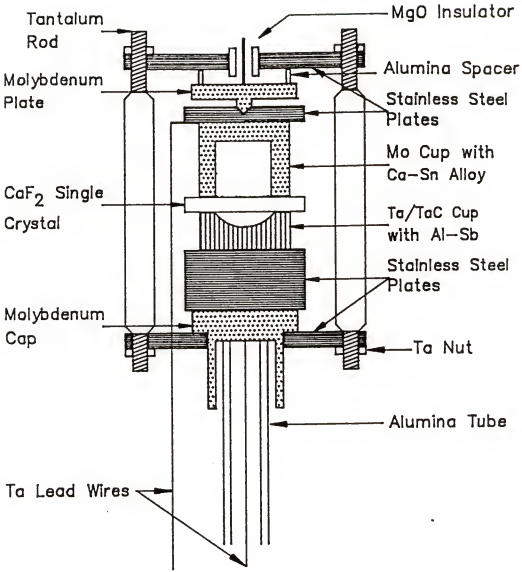

Figure 2-1

Schematic diagram of galvanic solid-electrolyte cell used to obtain emf data for the Al-In and Al-Sb systems.

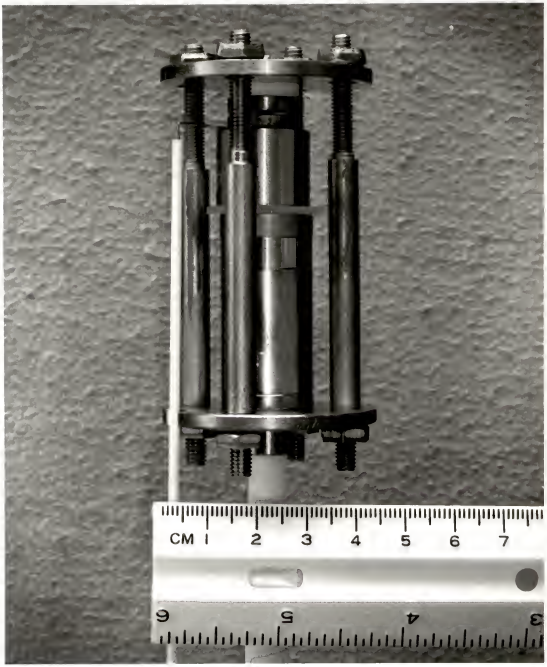

Figure 2-2

Photograph of galvanic solid-electrolyte cell used to obtain emf data for the Al-In and Al-Sb systems.

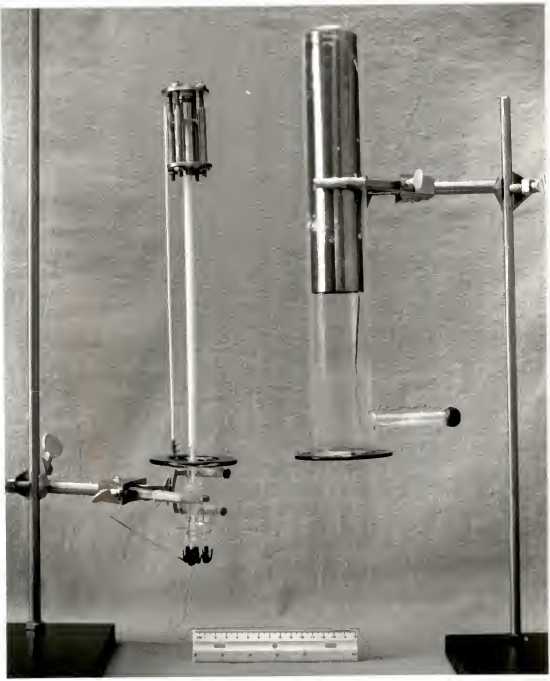

Figure 2-3

Photograph of galvanic solid-electrolyte cell with glass base (left) and Vycor sleeve with Ta liner (right).

1000 °C (however, at temperatures above 900 °C the Vycor sleeve began to soften)

(c) an HP 85 microcomputer which was used to run stepwise coulometric titrations automatically

(d) a Honeywell Electronik 19 continuous-strip chart recorder which was used to record the cell current and voltage

(e) a Princeton Applied Research model 173 potentiostat-galvanostat which also included a PAR model 179 coulometer with a precision of 10^{-4} C

(f) multimeters (Beckman 3010) for individual digital reading of the current and voltage

(g) an Omega 115 thermocouple thermometer providing digital readout in °C or K.

Materials

The electrodes and electrolyte are shown in Figures 2-5 and 2-6. The Ca-Sn reference electrode (10 at.% Ca) was contained in a molybdenum cup and made by melting *ca.* 0.3 g Ca (Ventron Corp., 0.994+ purity) and *ca.* 8 g Sn (Alfa Products, 0.99999 purity) under vacuum in an induction furnace. For each reference electrode used, emf vs. T values for pure Al versus the Ca-Sn alloy were measured (cell type II). Barring leakage during cell operation, a reference electrode generally lasted through twenty or more cells. After ten or fifteen cells using the same reference electrode, its emf vs. T behavior against pure Al (cell type II) was rechecked.

The single-crystal CaF_2 material was obtained from Harshaw. Crystals of *ca.* 0.1 cm thickness and *ca.* 2.5 cm in diameter were cut and polished with 600 SiC paper. The resulting crystals were almost transparent (Figure 2-5), and the smooth surfaces provided

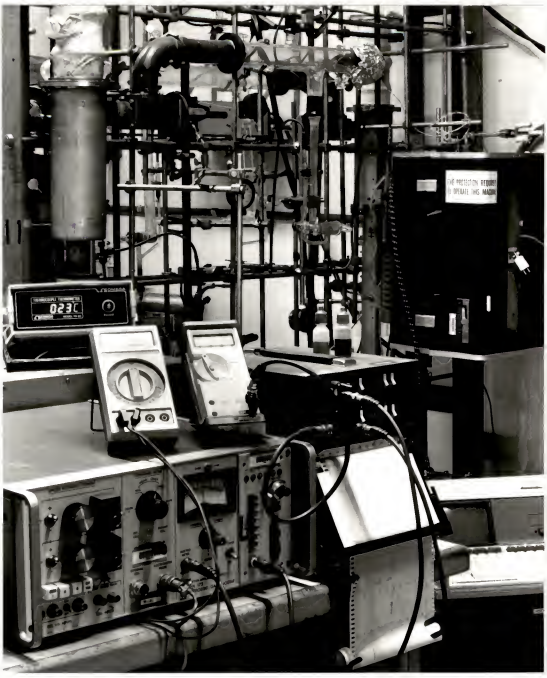

Figure 2-4

Photograph of laboratory equipment used
to operate the galvanic cells in this study.

Figure 2-5

Photograph of Ta/TaC working electrode cup (left), CaF_2 single-crystal electrolyte (center) and Ca-Sn reference electrode cup (right). Exploded view of their orientation in the galvanic cell.

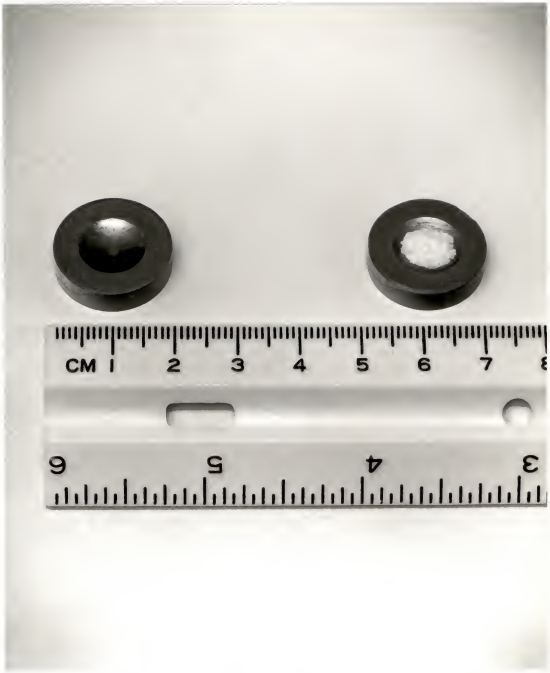

Figure 2-6

Photograph of two Ta/TaC working electrode cups, showing the dimple-shaped indentation (left) and the amount of AlF_3-CaF_2 salt used in assembling the cells (right).

a very flush contact to the lips of the electrode cups, which were also polished with 600 SiC paper. This was critical in avoiding fracture of the crystal under the pressure applied when assembling the galvanic cell.

The working electrode cup, shown in Figure 2-6, was machined from tantalum. Since Al reacts with Ta at elevated temperatures, a TaC coating was formed on the Ta cup by packing it in graphite powder and heating it under vacuum at 1650 – 1700 °C for several hours. In order to minimize the possibility of cracks in the TaC coating, the Ta cup was designed with a dimple-shaped indentation to hold the Al alloys; cups of this design, having no sharp corners, proved to be more resistant to Al attack than cups of the earlier design, which had cylindrical depressions counterbored in them.

High-purity metals were used in the working electrode. Aluminum (Aldrich, 99.999% pure) and indium (Asarco, 0.99999 purity) were obtained in the form of rods, from which small chunks were cut and weighed. Antimony shot of 0.999999 purity was obtained from Alfa Products. For the pure aluminum cells (type II), Al was either formed by titration from the AlF_3-CaF_2 salt mixture or added as a chunk to the working electrode cup before cell assembly. The cells for the Al-In system were assembled with small chunks of In or, in some cases, of each element (up to 0.02 g total) in the working electrode cup.

In the cells for the Al-Sb system, coulmetric titration of Al into the alloy led to the formation of the solid compound AlSb. In order to reduce the equilibration rates in the solid, a thin film configuration was desirable. To this end, antimony films were formed on the indentation of the working electrode cups by evaporation of Sb under vacuum in an induction furnace. The deposition area was controlled by a circular mask with a diameter of 0.6 to 0.8 cm. Films of 1 to 7 mg were deposited, corresponding to thicknesses of 3 to 21 μm. Aluminum was generally added to the antimony during cell operation by coulometric titration.

The AlF_3-CaF_2 salt mixture was used as the source for Al formation by coulometric titration. Pure AlF_3 salt alone would not have been compatible with the CaF_2 electrolyte since these two salts form several double salts, as shown in the CaF_2-AlF_3 phase diagram (Figure 2-7) taken from the work of Craig and Brown [77Cra]. The composition of the AlF_3-CaF_2 salt mixture was chosen at 25 at.% AlF_3, so that at cell operating temperatures the mixture existed as two phases, a liquid AlF_3-CaF_2 phase in equilibrium with a solid phase of pure CaF_2. This was important for two reasons: (a) since the liquid AlF_3-CaF_2 phase was already in equilibrium with solid CaF_2, active dissolution of the single-crystal CaF_2 constituting the cell electrolyte was precluded, and (b) depletion of the AlF_3 constituent by coulometric titration at constant temperature shifted the proportion of the two phases in the salt mixture but left their compositions unchanged. Therefore the activity of the salt phase was the same for both cell types (I and II), cancelling out in equation (2-1).

The AlF_3-CaF_2 (25 at.% AlF_3) salt mixture was made from the single salts. The CaF_2 salt was obtained in the form of optical-grade, single-crystal chunks from Alfa Products. Triple-distilled AlF_3 was generously contributed by the Laboratory of Industrial Electrochemistry at the Norwegian Technical Institute, Trondheim. Since AlF_3 is very hygroscopic, all preparative steps were performed in a glove box. The salt mixture was melted under argon in an induction furnace and returned to the glove box where it was crushed and stored.

Experimental Procedure

The following general procedure was followed for all the galvanic cells operated:

- Weigh out the appropriate amounts of AlF_3-CaF_2 and of any metals required for the working electrode
- Assemble the galvanic cell and seal Vycor cover over it

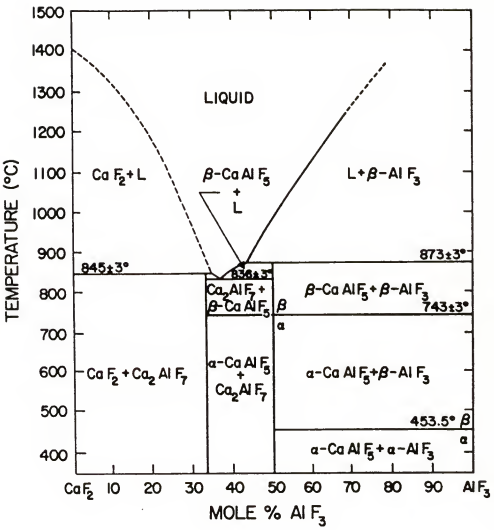

Figure 2-7

Phase diagram for the system CaF_2-AlF_3, taken from Craig and Brown [77Cra].

- Slide assembly into furnace and clamp into position
- Connect assembly to vacuum system via pyrex tubing and black wax and pump down to *ca.* 10^{-5} torr
- Turn on furnace and set temperature controller to *ca.* 120 °C
- Heat overnight under vacuum at *ca.* 120 °C to drive off water vapor from cell
- Backfill with purified argon and heat cell to 850 °C
- Measure emf; perform coulometric titrations
- Increase temperature and take further emf measurements; repeat at selected temperature increments up to 900 °C maximum
- Shut furnace off and allow cell to cool overnight
- Disassemble cell and examine electrodes

Note that only increases in temperature could be made, since dropping the temperature by more than 10 °C incurred the risk of leakage from the electrode cups. Further procedural details are described in the specific chapters on the alloy systems.

CHAPTER III

THE Al-In SYSTEM

Introduction

In the prediction and assessment of phase diagrams for higher-order III-V systems, information on the III-III and V-V as well as on the III-V component binary systems is needed. Among the III-III systems, the Al-In system has been the least well characterized and moreover is well suited to investigation in the solid electrolyte galvanic cells used in this study.

A thorough discussion of the Al-In literature is given in Chapter V. Emf studies of the Al-In system have been done previously by Massart *et al.* [66Mas, 71Mas] and by Yazawa and Lee [69Yaz], using chloride molten salt electrolytes. Their data agree well, but the use of a molten salt electrolyte has raised the question of whether Al^{+1} ions as well as Al^{+3} ions might not be present in the cell [72Tre]. The present study, using a solid electrolyte, provided an alternative emf method and avoided this possible problem. In addition, the coulometric titration technique was employed to obtain data at smaller x_{Al} values than those reported by Massart *et al.* and by Yazawa and Lee.

Experimental

Several preliminary experiments were performed at constant x_{Al} values to determine the useful range of the experimental technique. Emf measurements obtained in the range

$x_{Al} = 0$ to 0.2 yielded reliable net emf data, but at x_{Al} values above 0.2 the net emf values dropped to magnitudes equal to or smaller than the experimental error. Therefore, reliable data in the vicinity of the critical point of the miscibility gap could not be measured.

While the sensitivity and exactness of the coulometric titration technique allows the measurement of emf values at very small Al concentrations, it is at these small concentrations that the experimental Al-In cells have been found to be particularly susceptible to instabilities in the emf. These instabilities are characterized by a drift in the open-circuit potential; this drift is quite rapid at the smallest Al concentrations ($x_{Al} < 0.001$), and slows down with increasing x_{Al} until it becomes undetectable at concentrations above 0.01 or 0.02 mole fraction. The emf instabilities can also be lessened by increasing the amount of alloy material in the working electrode. Numerous attempts were made to eliminate this low-Al drift in the emf, but its cause could not be determined. Some systematic or impurity-related problem is suspected.

In order to obtain meaningful data for the Al-In system, a set of experiments was designed to minimize the effect of the emf drift on the data measured. In the first cell (Cell 57), a relatively large quantity of indium (14 mg) was employed, thus requiring substantial amounts of Al to be titrated for each incremental concentration change. The amount of alloy present was sufficient to allow titration through the low-Al region to proceed without significant interference from emf drift. However, titration to larger Al concentrations became very time-consuming, since galvanostatic titration using a maximum current of 300 μA was employed. Therefore the Al concentration in this cell was varied from 0 to only 0.05 mole fraction.

The second Al-In cell (Cell 59) was constructed using one quarter the amount of indium (3.5 mg) used in the first cell. In the same time frame as above, the Al concentration in this cell could be varied to 0.20 mole fraction; however, the low-Al region was markedly

affected by emf drift, particularly at the lowest temperature studied, 850 °C. In order to be able to make use of the data obtained at larger x_{Al} values, the titration curves from the first cell were used to adjust those from the second cell in the questionable x_{Al} regions. The adjustment procedure was simple and straightforward and is explained in detail in Appendix A.

For each Al-In cell, coulometric titrations were carried out at three temperatures: 850, 875 and 900 °C. In addition, emf vs. T data at constant x_{Al} were recorded when the temperature of the cell was raised between titrations or lowered at the very end. Between Cells 57 and 59, this yielded temperature-dependent Al activity data at four x_{Al} values.

For Cell 57, the data were obtained in the following sequence:

1. a_{Al} vs. x_{Al} at 850 °C, from $x_{Al} = 0$ to 0.05, ending at $x_{Al} = 0.05$
2. a_{Al} vs. T at $x_{Al} = 0.05$, from $T = 850$ to 875 °C
3. a_{Al} vs. x_{Al} at 875 °C, from $x_{Al} = 0$ to 0.05, ending at $x_{Al} = 0.05$
4. a_{Al} vs. T at $x_{Al} = 0.05$, from $T = 875$ to 900 °C
5. a_{Al} vs. x_{Al} at 900 °C, from $x_{Al} = 0$ to 0.05, ending at $x_{Al} = 0.03$
6. a_{Al} vs. T at $x_{Al} = 0.03$, from $T = 900$ to 850 °C (data were taken as cell cooled rapidly after shutting off furnace)

The sequence for data acquisition for Cell 59 was analogous, with $x_{Al} = 0.20$ being the constant x_{Al} value in steps 2 and 4, and $x_{Al} = 0.10$ in step 6. The x_{Al} range investigated for Cell 59 was 0 to 0.20 (steps 1, 3, and 5).

Results and Discussion

Emf data were obtained for the Al-In system over the temperature range 850 – 900 °C, using the following cell arrangement:

$$\text{Ca} - \text{Sn}\ (l) \parallel \text{CaF}_2\ (s) \parallel \text{AlF}_3 - \text{CaF}_2\ (l/s),\ \text{Al} - \text{In}\ (l) \qquad \text{(I)}$$

The results were combined with those from the Ca-Sn vs. pure Al cell:

$$\text{Ca} - \text{Sn}\ (l) \parallel \text{CaF}_2\ (s) \parallel \text{AlF}_3 - \text{CaF}_2\ (l/s), \text{Al}\ (l) \qquad \text{(II)}$$

to yield the Al activities in the alloy in terms of the emf difference, $(E_I - E_{II})$, as described in Chapter II:

$$\ln a_{Al} = -\frac{3F}{RT}(E_I - E_{II}) \qquad (3-1)$$

Reference electrode number 40 (RE40) was the Ca-Sn electrode used for the Al-In cells (Cells 57 and 59). Its behavior vs. pure Al (cell type II), shown in Figure 3-1, is linear within experimental error over the temperature range investigated. The line fitted to the E_{II} vs. T data, determined by linear least squares regression, is given by

$$E_{II} = (-0.3215 \pm 0.0089)\ T + (698.9 \pm 7.8) \qquad (3-2)$$

where E_{II} is in millivolts and T is the temperature in °C.

The small deviations of the data from the line in Figure 3-1 are due primarily to limitations in the precision of the measuring instruments used (1 °C for the temperature and 1 mV for the potential). Therefore the E_{II} values used in subsequent calculations were calculated from Equation (3-2). For the subsequent Al-In cells, a multimeter with greater precision was employed to measure the emf values; measurements to 0.1 mV were obtained.

As mentioned in the previous section and explained in Appendix A, the Al-In emf data from Cell 57 were used to adjust the data from Cell 59. Both data sets (Cell 57 and Cell 59, unadjusted) are tabulated in Appendix A. This treatment yielded an adjusted, consistent set of data over the composition range studied (0 to 0.2 mole fraction Al). The adjusted emf vs. x_{Al} data for Cell 59 are shown in Tables 3-1 to 3-3, for T = 850, 875 and 900 °C, respectively. Included are the net cell potential values, E, determined from the difference

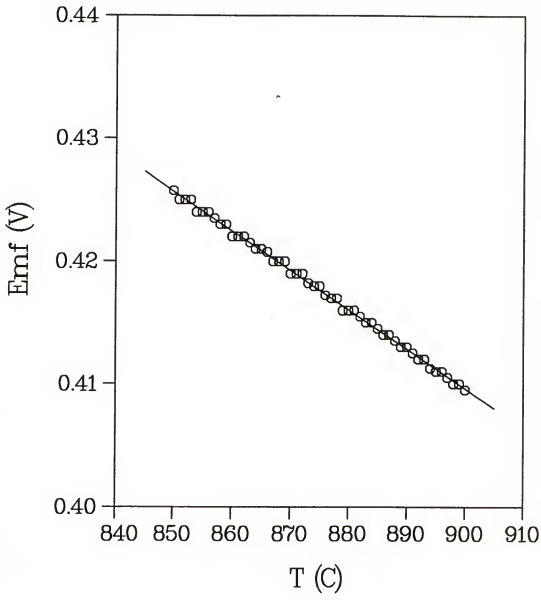

Figure 3-1

Emf vs. T data for pure Al vs. Ca-Sn Reference Electrode 40. The straight line was fitted to the data by linear least squares regression.

$(E_I - E_{II})$. Figure 3-2 shows the titration curve, E_I vs. x_{Al}, at $T = 900$ °C; the curves at 850 and 875 °C have essentially the same shape.

From the Al-In emf data, partial molar thermodynamic properties for Al were backed out. The relative partial molar Gibbs energy of Al in the Al-In alloy is related directly to the net cell potential, E:

$$g_{Al}^{M} = -3FE \qquad (3-3)$$

where F is the Faraday constant.

The excess partial molar Gibbs energy, g_{Al}^{E}, the activity, a_{Al}, and the activity coefficient, γ_{Al}, of Al in the alloy were all determined from thermodynamic relations involving g_{Al}^{M}:

$$g_{Al}^{M} = g_{Al}^{E} + RT \ln x_{Al} \qquad (3-4)$$

$$g_{Al}^{M} = RT \ln a_{Al} \qquad (3-5)$$

$$g_{Al}^{E} = RT \ln \gamma_{Al} \qquad (3-6)$$

where R is the gas constant. The four thermodynamic quantities, g_{Al}^{M}, g_{Al}^{E}, a_{Al} and γ_{Al}, were calculated from the adjusted Cell 59 data for each temperature, 850, 875 and 900 °C, and are listed in Tables 3-4 to 3-6. The Al activity values at 900 °C are plotted in Figure 3-3 as a function of x_{Al} and show a strong positive deviation from ideality. Also shown in the figure are Al activity data at 900 °C from the literature. It can be seen that the data from the current study are in excellent agreement with those of Massart *et al.* [66Mas] and of Yazawa and Lee [69Yaz].

The use of the Gibbs-Duhem relations allows calculation of partial thermodynamic quantities for the indium component and of molar quantities for the Al-In alloy. The following equations, involving integration of the partial excess Gibbs energy of Al, were

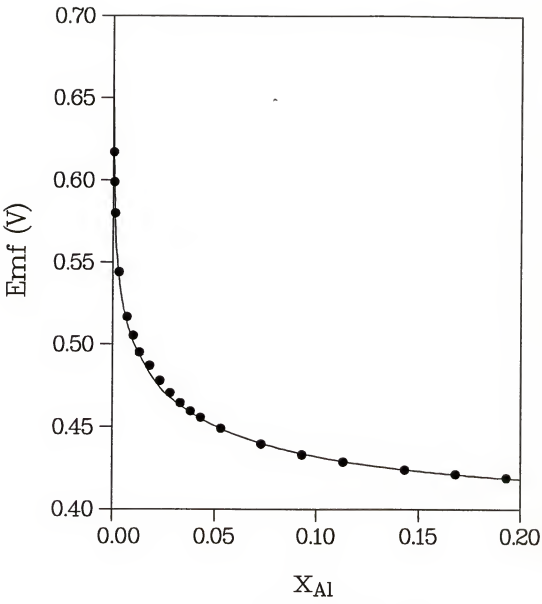

Figure 3-2

Titration curve for liquid Al-In at 900 °C (Cell 59). Line represents fit to data using straight-line approximation for g^E_{Al} vs. x_{Al} (Equation 3-11).

Table 3-1

Emf vs. x_{Al} data for the Al-In system at 850 °C (Cell 59, adjusted). E is the net cell emf, $E_I - E_{II}$.

$E_{II} = 0.4257$ V

x_{Al}	E_I(V)	E(V)
0.0006	0.6095	0.1838
0.0010	0.5922	0.1665
0.0030	0.5579	0.1322
0.0070	0.5302	0.1045
0.0100	0.5214	0.0957
0.0200	0.4940	0.0683
0.0250	0.4878	0.0621
0.0300	0.4821	0.0564
0.0400	0.4730	0.0473
0.0600	0.4601	0.0344
0.0800	0.4524	0.0267
0.1000	0.4465	0.0208
0.1300	0.4407	0.0150
0.1550	0.4375	0.0118
0.1800	0.4355	0.0098

Table 3-2

Emf vs. x_{Al} data for the Al-In system at 875 °C (Cell 59, adjusted). E is the net cell emf, $E_I - E_{II}$.

$E_{II} = 0.4176$ V

x_{Al}	E_I(V)	E(V)
0.0006	0.5989	0.1813
0.0010	0.5812	0.1636
0.0030	0.5476	0.1300
0.0070	0.5205	0.1029
0.0100	0.5108	0.0932
0.0177	0.4949	0.0773
0.0227	0.4875	0.0699
0.0277	0.4803	0.0627
0.0327	0.4744	0.0568
0.0377	0.4690	0.0514
0.0427	0.4648	0.0472
0.0527	0.4578	0.0402
0.0727	0.4484	0.0308
0.0927	0.4420	0.0244
0.1127	0.4375	0.0199
0.1427	0.4324	0.0148
0.1677	0.4299	0.0123
0.1927	0.4284	0.0108

Table 3-3
Emf vs. x_{Al} data for the Al-In system at 900 °C
(Cell 59, adjusted). E is the net cell emf, $E_I - E_{II}$.

$E_{II} = 0.4096$ V

x_{Al}	E_I(V)	E(V)
0.0003	0.6170	0.2074
0.0006	0.5988	0.1892
0.0010	0.5799	0.1703
0.0030	0.5441	0.1345
0.0070	0.5166	0.1070
0.0100	0.5052	0.0956
0.0130	0.4950	0.0854
0.0180	0.4870	0.0774
0.0230	0.4780	0.0684
0.0280	0.4706	0.0610
0.0330	0.4646	0.0550
0.0380	0.4596	0.0500
0.0430	0.4557	0.0461
0.0530	0.4491	0.0395
0.0730	0.4397	0.0301
0.0930	0.4332	0.0236
0.1130	0.4289	0.0193
0.1430	0.4240	0.0144
0.1680	0.4213	0.0117
0.1930	0.4191	0.0095

used to calculate G^E, the excess molar Gibbs energy, G^M, the integral molar Gibbs energy, and g^E_{In}, the excess partial Gibbs energy of indium [52Wag]:

$$G^E = (1 - x_{Al}) \int_0^{x_{Al}} \frac{g^E_{Al}}{(1 - x_{Al})^2} dx_{Al} \qquad (3-7)$$

$$G^M = G^E + RT\left[x_{Al} \ln x_{Al} + x_{In} \ln x_{In}\right] \qquad (3-8)$$

$$g^E_{In} = \frac{G^E - x_{Al}\, g^E_{Al}}{(1 - x_{Al})} = \int_0^{x_{Al}} \frac{g^E_{Al}}{(1 - x_{Al})^2} dx_{Al} - \frac{x_{Al}\, g^E_{Al}}{(1 - x_{Al})} \qquad (3-9)$$

The g^E_{In} values obtained from Equation (3-9) were then used in equations analogous to Equations (3-4) to (3-6) above, yielding the relative partial Gibbs energy, the activity and the activity coefficient of In in Al-In.

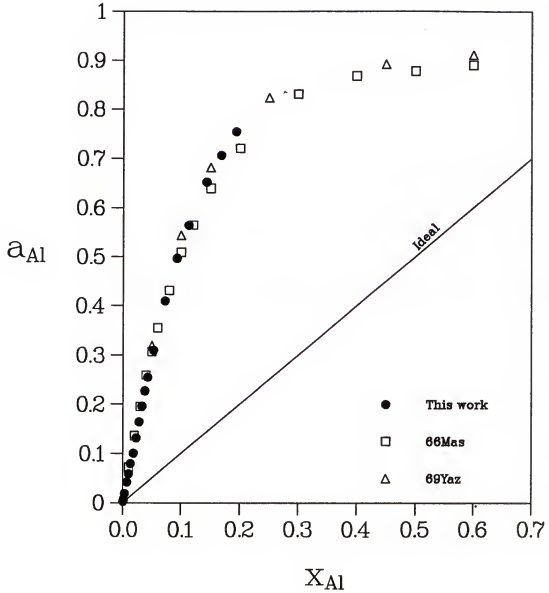

Figure 3-3

Aluminum activity vs. Al mole fraction for the Al-In system at 900 °C. Data from the present study are plotted together with literature values.

Table 3-4
Partial thermodynamic quantities for the Al-In system at 850 °C, calculated from Cell 59 emf vs. x_{Al} data (adjusted).

x_{Al}	g^M_{Al} (J/mol)	g^E_{Al} (J/mol)	a_{Al}	γ_{Al}
0.0006	-53200	16540	0.0034	5.882
0.0010	-48200	16210	0.0057	5.675
0.0030	-38270	16130	0.0166	5.627
0.0070	-30250	16080	0.0392	5.597
0.0100	-27700	15300	0.0515	5.147
0.0200	-19770	16760	0.1203	6.017
0.0250	-17980	16470	0.1458	5.834
0.0300	-16330	16420	0.1740	5.801
0.0400	-13690	16360	0.2308	5.769
0.0600	-9957	16310	0.3442	5.737
0.0800	-7729	15850	0.4370	5.463
0.1000	-6021	15480	0.5248	5.248
0.1300	-4342	14710	0.6281	4.832
0.1550	-3416	13990	0.6936	4.475
0.1800	-2837	13170	0.7380	4.100

Table 3-5
Partial thermodynamic quantities for the Al-In system at 875 °C, calculated from Cell 59 emf vs. x_{Al} data (adjusted).

x_{Al}	g^M_{Al} (J/mol)	g^E_{Al} (J/mol)	a_{Al}	γ_{Al}
0.0006	-52480	18690	0.0041	7.086
0.0010	-47360	18380	0.0070	6.859
0.0030	-37630	17820	0.0194	6.469
0.0070	-29790	17580	0.0441	6.305
0.0100	-26980	16980	0.0592	5.923
0.0177	-22380	16130	0.0959	5.419
0.0227	-20230	15900	0.1201	5.289
0.0277	-18150	16080	0.1494	5.392
0.0327	-16440	16210	0.1786	5.462
0.0377	-14880	16410	0.2104	5.581
0.0427	-13660	16440	0.2390	5.597
0.0527	-11640	16460	0.2955	5.607
0.0727	-8915	16110	0.3930	5.405
0.0927	-7063	15640	0.4771	5.147
0.1127	-5760	15080	0.5469	4.853
0.1427	-4284	14300	0.6384	4.474
0.1677	-3560	13480	0.6887	4.107
0.1927	-3126	12590	0.7207	3.740

Table 3-6
Partial thermodynamic quantities for the Al-In system at 900 °C, calculated from Cell 59 emf vs. x_{Al} data (adjusted).

x_{Al}	g^M_{Al} (J/mol)	g^E_{Al} (J/mol)	a_{Al}	γ_{Al}
0.0003	-60030	17880	0.0021	6.253
0.0006	-54770	17900	0.0036	6.266
0.0010	-49300	17940	0.0064	6.293
0.0030	-38930	17720	0.0185	6.150
0.0070	-30970	17420	0.0418	5.968
0.0100	-27670	17240	0.0586	5.858
0.0130	-24720	17630	0.0793	6.099
0.0180	-22400	16780	0.1005	5.585
0.0230	-19800	16990	0.1313	5.710
0.0280	-17660	17210	0.1636	5.842
0.0330	-15920	17350	0.1955	5.923
0.0380	-14470	17420	0.2267	5.967
0.0430	-13340	17340	0.2546	5.920
0.0530	-11430	17220	0.3096	5.842
0.0730	-8713	16810	0.4093	5.607
0.0930	-6831	16330	0.4964	5.337
0.1130	-5587	15680	0.5639	4.991
0.1430	-4168	14800	0.6522	4.561
0.1680	-3387	14010	0.7066	4.206
0.1930	-2750	13290	0.7543	3.908

Table 3-7
Straight-line equations fitted to g^E_{Al} vs. x_{Al} data (Cell 59, adjusted) for the Al-In system.

T (°C)	g^E_{Al} (kJ/mol) vs. x_{Al} equation
850	$g^E_{Al} = (-23.5 \pm 1.2)\,x_{Al} + (17.6 \pm 0.1)$
875	$g^E_{Al} = (-26.1 \pm 1.0)\,x_{Al} + (17.9 \pm 0.1)$
900	$g^E_{Al} = (-27.8 \pm 1.1)\,x_{Al} + (18.7 \pm 0.1)$

The integrations in Equations (3-7) and (3-9) were accomplished by fitting the g^E_{Al} vs. x_{Al} data to a straight line, substituting the equation for the line into Equations (3-7) and (3-9), and integrating. This was done for the adjusted Cell 59 data at each temperature. The three g^E_{Al} straight-line equations are listed in Table 3-7, and the thermodynamic quantities derived from them are shown in Tables 3-8 to 3-13.

Table 3-8

Integral Gibbs energies for the Al-In system at 850 °C, derived from the g_A^E data (Cell 59, adjusted).

x_{Al}	G^M (J/mol)	G^E (J/mol)
0.0006	-35.03	10.04
0.0010	-56.68	17.79
0.0030	-136.1	51.90
0.0070	-266.6	122.8
0.0100	-347.8	175.1
0.0200	-567.6	347.8
0.0250	-658.3	433.3
0.0300	-740.0	518.1
0.0400	-882.1	686.0
0.0600	-1105	1014
0.0800	-1270	1333
0.1000	-1394	1641
0.1300	-1524	2084
0.1550	-1594	2434
0.1800	-1634	2767

Table 3-9

Integral Gibbs energies for the Al-In system at 875 °C, derived from the g_A^E data (Cell 59, adjusted).

x_{Al}	G^M (J/mol)	G^E (J/mol)
0.0006	-36.31	10.32
0.0010	-58.62	18.24
0.0030	-141.4	53.48
0.0070	-273.6	124.5
0.0100	-357.1	177.4
0.0177	-536.8	312.2
0.0227	-635.4	398.9
0.0277	-723.9	485.0
0.0327	-804.2	570.3
0.0377	-877.6	655.0
0.0427	-945.0	739.0
0.0527	-1065	905.0
0.0727	-1259	1229
0.0927	-1406	1541
0.1127	-1519	1842
0.1427	-1641	2271
0.1677	-1709	2608
0.1927	-1754	2925

Table 3-10
Integral Gibbs energies for the Al-In system at 900 °C, derived from the g_A^E data (Cell 59, adjusted).

x_{Al}	$G^M\ (J/mol)$	$G^E\ (J/mol)$
0.0003	-23.39	6.357
0.0006	-37.01	10.88
0.0010	-59.08	18.99
0.0030	-143.2	56.12
0.0070	-276.2	130.4
0.0100	-360.2	186.0
0.0130	-435.4	241.2
0.0180	-546.5	332.7
0.0230	-644.4	423.5
0.0280	-732.0	513.6
0.0330	-811.3	603.0
0.0380	-883.7	691.7
0.0430	-950.2	779.6
0.0530	-1068	953.3
0.0730	-1257	1292
0.0930	-1399	1619
0.1130	-1507	1933
0.1430	-1621	2381
0.1680	-1683	2732
0.1930	-1722	3062

Table 3-11
Partial indium thermodynamic quantities for the Al-In system at 850 °C, derived from the g_{Al}^E data (Cell 59, adjusted).

x_{Al}	x_{In}	$g_{In}^M\ (J/mol)$	$g_{In}^E\ (J/mol)$	a_{In}	γ_{In}
0.0006	0.9994	-5.319	0.0051	0.9994	1.000
0.0010	0.9990	-9.423	0.0116	0.9990	1.000
0.0030	0.9971	-27.48	0.1027	0.9971	1.000
0.0070	0.9930	-65.01	0.5802	0.9931	1.000
0.0100	0.9900	-92.66	1.183	0.9901	1.000
0.0200	0.9800	-183.9	4.762	0.9805	1.001
0.0250	0.9750	-228.9	7.465	0.9758	1.001
0.0300	0.9700	-273.6	10.79	0.9711	1.001
0.0400	0.9600	-361.9	19.31	0.9620	1.002
0.0600	0.9400	-533.7	44.05	0.9445	1.005
0.0800	0.9200	-699.1	79.43	0.9279	1.009
0.1000	0.9000	-857.8	125.9	0.9122	1.014
0.1300	0.8700	-1083	217.6	0.8905	1.024
0.1550	0.8450	-1257	315.2	0.8740	1.034
0.1800	0.8200	-1420	433.4	0.8590	1.048

It should be noted that the g^E_{Al} vs. x_{Al} data exhibited excellent straight-line behavior above $x_{Al} = 0.03$, but deviated at the smaller Al concentrations, first to lower g^E_{Al} values, then to steeper linear behavior as x_{Al} approached zero. The data for $x_{Al} < 0.03$ were therefore omitted in fitting the straight lines by least squares. While the g^E_{Al} data seem to be susceptible to uneven behavior at low x_{Al} values, due perhaps to x_{Al} errors which though low in absolute magnitude would increase in percent as x_{Al} approaches zero, use of the straight-line approximation for g^E_{Al} vs. x_{Al} to calculate fitted curves for other Al-In thermodynamic data is nevertheless very successful. For example, substituting the relation:

$$g^E_{Al} = M x_{Al} + B \qquad (3-10)$$

where M is the slope and B the y-intercept for a given temperature, into the equation for E_I:

$$E_I = -\frac{1}{3F}\left[g^E_{Al} + RT \ln x_{Al}\right] + E_{II} \qquad (3-11)$$

a very good fit to the emf data is obtained, as shown by the solid line in Figure 3-2.

Further thermodynamic quantities for the Al-In system were determined from the E versus T data from Cells 57 and 59. These were measured over the temperature range 850 to 900 °C at constant x_{Al} values of 0.03, 0.05, 0.093, and 0.18. The experimental data, tabulated in Appendix A, are shown in Figure 3-4 and exhibit excellent straight-line behavior. The lines fitted to the E vs. T data in the figure were obtained by least-squares regression. Their equations are listed in Table 3-14 and are represented generally by

$$E\,(\text{in V}) = m\,T\,(\text{in °C}) + b \qquad (3-12)$$

where m is the slope and b the y-intercept for a given x_{Al} value. The slope, m, represents the temperature coefficient, $\delta E/\delta T$, and is shown plotted against x_{Al} in Figure 3-5. It can be

Table 3-12
Partial indium thermodynamic quantities for the Al-In system at 875 °C, derived from the g^E_{Al} data (Cell 59, adjusted).

x_{Al}	x_{In}	g^M_{In} (J/mol)	g^E_{In} (J/mol)	a_{In}	γ_{In}
0.0006	0.9994	-5.512	0.0051	0.9994	1.000
0.0010	0.9990	-9.736	0.0140	0.9990	1.000
0.0030	0.9970	-28.55	0.1184	0.9970	1.000
0.0070	0.9930	-66.40	0.6427	0.9931	1.000
0.0100	0.9900	-94.61	1.315	0.9901	1.000
0.0177	0.9823	-166.3	4.141	0.9827	1.000
0.0227	0.9773	-212.3	6.834	0.9780	1.001
0.0277	0.9723	-257.9	10.21	0.9733	1.001
0.0327	0.9673	-303.1	14.28	0.9688	1.001
0.0377	0.9623	-347.8	19.04	0.9642	1.002
0.0427	0.9573	-392.0	24.51	0.9598	1.003
0.0527	0.9473	-479.2	37.60	0.9510	1.004
0.0727	0.9273	-647.9	72.57	0.9344	1.008
0.0927	0.9073	-808.9	119.7	0.9188	1.013
0.1127	0.8873	-961.8	179.5	0.9041	1.019
0.1427	0.8573	-1175	294.3	0.8842	1.031
0.1677	0.8323	-1338	414.3	0.8692	1.044
0.1927	0.8073	-1485	557.9	0.8559	1.060

seen that the slope determined for the largest x_{Al} value, 0.18, deviates significantly from the trend established by the first three slopes. This is not surprising, since the E vs. T slopes become flatter as x_{Al} increases, and their determination becomes therefore less reliable. Therefore, the E vs. T data for $x_{Al} = 0.18$ were not used for further thermodynamic calculations.

The derivative of the function for E (Equation 3-12) was used to calculate the partial molar entropy of Al, s^M_{Al}:

$$s^M_{Al} = -\frac{\delta g^M_{Al}}{\delta T} = -\frac{\delta\left(-3FE\right)}{\delta T} = 3Fm \qquad (3-13)$$

From the s^M_{Al} values, the excess partial entropy and partial molar enthalpy of Al, s^E_{Al} and h^M_{Al}, were backed out:

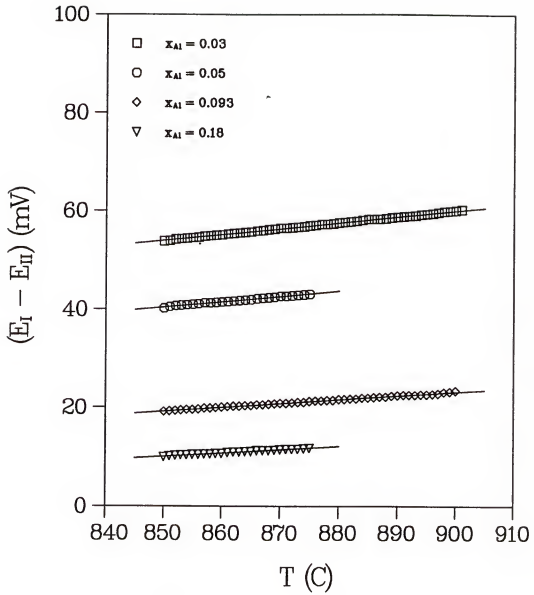

Figure 3-4

E vs. *T* data for the Al-In system at four values of constant mole fraction (Cells 57 and 59-adjusted). The net cell emf, $E_I - E_{II}$, is represented.

Table 3-13
Partial indium thermodynamic quantities for the Al-In system at 900 °C, derived from the g^E_{Al} data (Cell 59, adjusted).

x_{Al}	x_{In}	$g^M_{In}\,(J/mol)$	$g^E_{In}\,(J/mol)$	a_{In}	γ_{In}
0.0003	0.9997	-3.307	0.0030	0.9997	1.000
0.0006	0.9994	-5.663	0.0063	0.9994	1.000
0.0010	0.9990	-9.879	0.0154	0.9990	1.000
0.0030	0.9970	-29.20	0.1271	0.9970	1.000
0.0070	0.9930	-67.81	0.6848	0.9931	1.000
0.0100	0.9900	-96.62	1.398	0.9901	1.000
0.0130	0.9870	-125.3	2.366	0.9872	1.000
0.0180	0.9820	-172.6	4.551	0.9825	1.000
0.0230	0.9770	-219.5	7.456	0.9778	1.001
0.0280	0.9720	-265.9	11.09	0.9731	1.001
0.0330	0.9670	-311.8	15.45	0.9685	1.002
0.0380	0.9620	-357.3	20.56	0.9640	1.002
0.0430	0.9570	-402.2	26.42	0.9596	1.003
0.0530	0.9470	-490.7	40.42	0.9509	1.004
0.0730	0.9270	-661.5	77.77	0.9344	1.008
0.0930	0.9070	-824.0	128.0	0.9190	1.013
0.1130	0.8870	-977.6	191.8	0.9046	1.020
0.1430	0.8570	-1191	314.1	0.8851	1.033
0.1680	0.8320	-1352	442.0	0.8706	1.046
0.1930	0.8070	-1496	594.9	0.8578	1.063

Table 3-14
Straight-line equations fitted to E vs. T data (Cells 57 and 59-adjusted) for the Al-In system.

x_{Al}	E vs. T equation
0.0300	$E\,(mV) = (0.1209 \pm 0.0020)\,T\,(°C) \;+\; (-48.8 \pm 1.8)$
0.0500	$E\,(mV) = (0.1090 \pm 0.0058)\,T\,(°C) \;+\; (-52.2 \pm 5.0)$
0.0930	$E\,(mV) = (0.0797 \pm 0.0021)\,T\,(°C) \;+\; (-48.6 \pm 1.8)$
0.1800	$E\,(mV) = (0.0675 \pm 0.0058)\,T\,(°C) \;+\; (-47.4 \pm 5.0)$

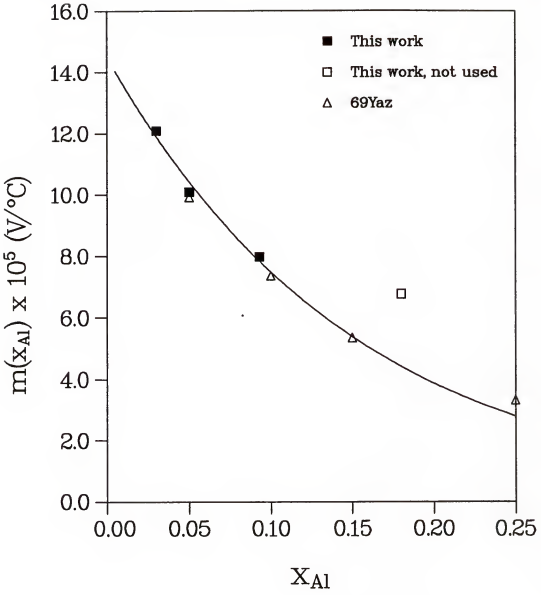

Figure 3-5

Slopes of E vs. T data plotted versus x_{Al}. The line represents the exponential function fitted to the upper three points in the figure.

Table 3-15
Partial entropy and enthalpy values for the Al-In system at 900 °C, derived from E vs. T data (Cells 57 and 59-adjusted).

x_{Al}	$s^M_{Al}\,(J/K\ mol)$	$s^E_{Al}\,(J/K\ mol)$	$h^M_{Al}\,(J/mol)$
0.0300	34.99	5.838	24750
0.0500	29.21	4.299	22400
0.0930	23.08	3.334	20240

$$s^E_{Al} = s^M_{Al} + R\ln x_{Al} \qquad (3-14)$$

$$h^M_{Al} = g^M_{Al} + Ts^M_{Al} \qquad (3-15)$$

Since the adjusted Cell 59 data for g^M_{Al} at 900 °C did not include values at $x_{Al} = 0.03$ or 0.05, these were calculated using the 900 °C straight-line fit of the g^E_{Al} data (Eq. 3-10) in Equation (3-4):

$$g^M_{Al} = (Mx_{Al} + B) + RT\ln x_{Al} \qquad (3-16)$$

and then used in Equation (3-15) above. The quantities, s^M_{Al}, s^E_{Al} and h^M_{Al}, were calculated at 900 °C for each of the constant x_{Al} values (except $x_{Al} = 0.18$) and are shown in Table 3-15.

By integrating the partial molar entropy of Al, the integral molar entropy could be obtained:

$$S^M = (1-x_{Al})\int_0^{x_{Al}} \frac{s^M_{Al}}{(1-x_{Al})^2}dx_{Al} \qquad (3-17)$$

Substitution of Equation (3-13) for s^M_{Al} gives

$$S^M = 3F(1-x_{Al})\int_0^{x_{Al}} \frac{m(x_{Al})}{(1-x_{Al})^2}dx_{Al} \qquad (3-18)$$

where $m(x_{Al})$ is the E vs. T slope, as discussed above. Integration of Equation (3-18) required the parameter m to be described as a function of x_{Al}. This was done by fitting the function, $m = C\ \exp(D\ x_{Al})$ to the m values. The following equation was obtained:

$$m(x_{Al})\ \ (\mathrm{V/^\circ C}) = (0.145 \pm 0.004) \exp\left[(-6.62 \pm 0.22)\, x_{Al}\right] \qquad (3-19)$$

which is shown as the solid curve in Figure 3-5 and exhibits reasonable behavior even above the largest x_{Al} value fitted, 0.093. Also shown in the figure are the temperature coefficient values (m values) reported by Yazawa and Lee [69Yaz], which were determined from their E vs. T data over the temperature range 700 to 900 °C. Their values agree very well with the m values determined in the present study, except for the mistrusted value, at $x_{Al} = 0.18$. They are also in excellent agreement with the fitted curve (Equation 3-19) obtained in this study, even well beyond the x_{Al} range of the values used to fit the curve. The decision to omit the value at $x_{Al} = 0.18$ in fitting the curve is thereby supported.

The integration of equation (3-18), using expression (3-19), was performed numerically for each of the constant x_{Al} values. The resulting S^M values were then used to back out the corresponding excess molar entropies, S^E, and integral heats of mixing, H^M:

$$S^E = S^M + R\left[x_{Al} \ln x_{Al} + (1 - x_{Al}) \ln (1 - x_{Al})\right] \qquad (3-20)$$

$$H^M = G^M + TS^M \qquad (3-21)$$

The S^M, S^E and H^M values are given in Table 3-16. The H^M values are also shown in Table 3-17 with enthalpy of mixing values reported for the Al-In system by Wittig and Keil [63Wit], by Predel and Sandig [69Pre1] and by Girard *et al.* [77Gir]. Although some of the literature data are reported for much lower temperatures (715 and 717 °C), a comparison is nevertheless valid, since the temperature dependence of H^M is very small. The H^M values derived in the present study compare well to the data available in the literature.

Table 3-16
Integral entropy and enthalpy values for the Al-In system at 900 °C, derived from E vs. T data (Cells 57 and 59-adjusted).

x_{Al}	$S^M\,(J/K\ mol)$	$S^E\,(J/K\ mol)$	$H^M\,(J/mol)$
0.0300	1.138	0.0178	547.9
0.0500	1.777	0.1269	1050
0.0930	2.880	0.3069	1979

Table 3-17
Comparison of derived H^M values with literature values.

	H^M (J/mol)			
	This work	[63Wit]	[69Pre1]	[77Gir]
x_{Al}	(900 °C)	(715 °C)	(*ca.* 850 °C)	(717 °C)
0.030	547.8	–	–	–
0.050	1050	–	–	–
0.057	–	1133	–	–
0.061	–	–	–	1150
0.093	1979	–	–	–
0.100	–	2000	–	–
0.108	–	–	–	2018
0.101	–	–	2278	–

Experimental errors for the variables measured in this study of the Al-In system are reported in Table B-1 of Appendix B. Errors for the thermodynamic quantities calculated from the measured variables are given in Table B-2.

CHAPTER IV

THE Al-Sb SYSTEM

Introduction

Although the Al-Sb system has been studied by a number of authors, it is the least well characterized of the binary antimonides. A thorough discussion of the literature is presented in Chapter V, where inconsistencies between various reported data sets are pointed out. Three emf studies on the Al-Sb system have been published; these are in qualitative agreement. In the first two papers [65Vec, 68Sam], data for the AlSb solid are presented, and the third study, by Predel and Schallner [69Pre2], focusses on the Al-Sb liquid.

The goal of the present investigation was to use the technique of coulometric titration to obtain emf vs. x_{Al} data through the Sb-rich liquid region, through the two-phase region and, for the first time, through the very narrow homogeneity region of the AlSb compound. The challenge of obtaining data in the solid phase was met by using thin films to minimize equilibration times.

Experimental

Emf data for the Al-Sb liquid were readily obtained using an approach similar to that used for the Al-In system. Cells were assembled with pure antimony in the working electrode,

$$Ca - Sn\ (l) \parallel CaF_2\ (s) \parallel AlF_3\text{-}CaF_2\ (l/s),\ Sb\ (l) \qquad (I)$$

and aluminum was added by stepwise coulometric titration. Again, the net cell emf, E_I - E_{II}, was obtained by running additionally a cell with pure Al versus the Ca-Sn reference electrode:

$$\mathrm{Ca - Sn}\ (l) \parallel \mathrm{CaF_2}\ (s) \parallel \mathrm{AlF_3\text{-}CaF_2}\ (l/s) \qquad \text{(II)}$$

The same cell used to obtain liquid-phase emf data (type I) was also used to investigate the AlSb solid, by titrating in sufficient quantites of Al to form the compound at $x_{Al} = 0.5$. Once at the compound, titrations through the very narrow homogeneity region were attempted. The success of the solid-phase titrations depended on a number of factors. The first of these was the stability of the cell itself. By the time the amount of Al to reach the compound had been titrated in, it was often discovered that a defect in the protective TaC coating had allowed Al to react with the Ta working electrode (WE) cup.

For cells in which attack of the Ta WE cup by Al did not occur, the achievement of thin film geometry of the AlSb compound in the cell became the critical factor. Since the diffusion coefficient of Al in AlSb is reported by Pines and Chaikovskii to be $0.51 \times 10^{-10}\mathrm{cm^2/sec}$ at 620 °C [59Pin], it was estimated that an equilibration time of ten minutes for each titration step would require a maximum film thickness of about 20 μm. Thin AlSb film formation was first attempted by depositing thin films of Sb on the WE surface. However, since at the temperatures of cell operation (800 – 900 °C) antimony is molten and has a significant surface tension, the liquid Sb could easily coalesce into large droplets which, when reacting with Al to form the AlSb compound, would result in crystalline chunks of solid. Among the cells assembled with an Sb film, it was found that some yielded reasonable titration curves through the solid, while many did not.

Because of the impossibility of controlling the size of Sb droplet formation and thereby the AlSb particle size in the cells, a number of cells were assembled using the AlSb solid directly. Several forms of AlSb solid were tried, but without success; they are the following:

1. Evaporated Al film on top of evaporated Sb film. Since it was impossible to control the amounts of material deposited by evaporation, one element was usually in excess. At cell operation temperatures, the excess element would melt, coalesce into droplets, and lead to the same kinds of diffusion problems encountered with the Sb films alone.
2. Sputtered Al film on top of evaporated Sb film. The sputtering process allowed a controlled amount of Al to be deposited, but unfortunately the process also removed some of the Sb film, producing non-stoichiometric ratios.
3. AlSb powder of very fine particle size. The large surface area of the powder seemed to have enhanced the tendency of AlSb to oxidize slowly over time, since the cells using the powder gave no titration results whatsoever, and subsequent investigation of the powder strongly suggested the presence of a significant amount of oxide.
4. AlSb film formed by chemical vapor deposition in the laboratory of Dr. Georges J. Bougnot, at the Centre d'Electronique de Montpellier, Université des Sciences et Techniques du Langvedoc, France. The films upon arrival had the matte black appearance of oxidized AlSb, and cells assembled with them were totally unsuccessful.

Experimental difficulties notwithstanding, a number of titrations through the AlSb solid were obtained from the cells assembled with the Sb films alone.

Table 4-1
Emf vs. x_{Al} data for liquid Al-Sb at 806 °C
(Cell 12). E is the net cell emf, $E_I - E_{II}$.

$E_{II} = 0.439$ V

x_{Al}	E_I(V)	E(V)
0.0170	0.596	0.157
0.0363	0.569	0.130
0.0654	0.551	0.112
0.0750	0.546	0.107
0.0094	0.538	0.099
2-phase:		
0.1130	0.542	0.103

Results and Discussion

Liquid Al-Sb Results

Coulometric titrations through the Al-Sb liquid phase were done at three different temperatures: 806 °C, 846 °C and 875 °C. A number of cells were run at 846 °C and the titration curves agree very well. The liquid-phase emf data from all of these cells are shown in Tables 4-1 to 4-6. Since several Ca-Sn reference electrodes were used over the course of the investigation, the E_{II} value of the reference electrode used is reported in each table, along with the resulting net emf values, E. The titration curve for liquid Al-Sb at 846 °C (Cell 14 data) is shown in Figure 4-1. The shape of the other Al-Sb titration curves is very similar, and resembles as well the titration curves for the liquid Al-In system (see Figure 3-2).

The thermodynamic quantities calculated from the emf vs. x_{Al} data were obtained in the same manner as described for the liquid Al-In system in Chapter III. Tables 4-7 to 4-9 show the values of g^M_{Al}, g^E_{Al}, a_{Al} and γ_{Al}. For the calculations at 846 °C, the data of Cell 14 were used (Table 4-8). The a_{Al} vs. x_{Al} values for the Al-Sb system, as shown in Figure 4-2 for Cell 14, exhibit negative deviation from ideality. Across the two-phase region (liquid-solid), the activity of aluminum is, of course, constant.

Table 4-2
Emf vs. x_{Al} data for liquid Al-Sb at 846 °C
(Cell 10). E is the net cell emf, $E_I - E_{II}$.

$E_{II} = 0.426$ V

x_{Al}	E_I(V)	E(V)
0.0100	0.603	0.177
0.0200	0.581	0.155
0.0400	0.558	0.132
0.0600	0.541	0.115
0.0800	0.531	0.105
0.1000	0.521	0.095
0.1200	0.516	0.090
2-phase:		
0.1409	0.517	0.091

Table 4-3
Emf vs. x_{Al} data for liquid Al-Sb at 846 °C
(Cell 11). E is the net cell emf, $E_I - E_{II}$.

$E_{II} = 0.426$ V

x_{Al}	E_I(V)	E(V)
0.0100	0.613	0.187
0.0200	0.591	0.165
0.0400	0.568	0.142
0.0600	0.554	0.128
0.0800	0.545	0.119
0.1000	0.537	0.111
0.1100	0.534	0.108
0.1200	0.530	0.104
0.1300	0.528	0.102
2-phase:		
0.14	0.525	0.099
0.15	0.525	0.099

Straight-line fits were made to the g^E_{Al} vs. x_{Al} data; the equations are listed in Table 4-10. The thermodynamic quantities derived from these functions, namely the integral Gibbs energies, G^M and G^E, and the partial antimony functions, g^M_{Sb}, g^E_{Sb}, a_{Sb} and γ_{Sb}, are shown in Tables 4-11 to 4-16.

Titration into the liquid-solid, two-phase region yielded liquidus data for the phase diagram. The liquidus composition at each temperature investigated was determined by

Table 4-4
Emf vs. x_{Al} data for liquid Al-Sb at 846 °C
(Cell 14). E is the net cell emf, $E_I - E_{II}$.

$E_{II} = 0.427$ V

x_{Al}	E_I(V)	E(V)
0.0100	0.611	0.184
0.0200	0.588	0.161
0.0300	0.574	0.147
0.0400	0.564	0.137
0.0600	0.550	0.123
0.0800	0.539	0.112
0.1000	0.530	0.103
0.1200	0.523	0.096
0.1300	0.519	0.092
2-phase:		
0.1400	0.517	0.090
0.1590	0.517	0.090

Table 4-5
Emf vs. x_{Al} data for liquid Al-Sb at 846 °C
(Cell 15). E is the net cell emf, $E_I - E_{II}$.

$E_{II} = 0.427$ V

x_{Al}	E_I(V)	E(V)
0.0009	0.690	0.263
0.0157	0.593	0.166
0.0208	0.584	0.157
0.0411	0.562	0.135
0.0608	0.549	0.122
0.0807	0.538	0.111
0.1023	0.529	0.102
0.1206	0.522	0.095
0.1306	0.518	0.092
2-phase:		
0.1406	0.517	0.090
0.1512	0.517	0.090

observing, during coulometric titration, the transition in the emf data to a constant (*i.e.* 2-phase) value. The three liquidus compositions thus obtained are listed in Table 4-17. As discussed in Chapter V, they are in excellent agreement with the phase diagram data of other authors (see Figure 5-7).

Table 4-6
Emf vs. x_{Al} data for liquid Al-Sb at 875 °C
(Cell 11). E is the net cell emf, $E_I - E_{II}$.

$E_{II} = 0.418$ V

x_{Al}	E_I(V)	E(V)
0.0525	0.550	0.132
0.0625	0.543	0.125
0.0729	0.536	0.118
0.0924	0.527	0.109
0.1086	0.520	0.102
0.1312	0.512	0.094
0.1488	0.506	0.088
2-phase:		
0.1588	0.503	0.085
0.1688	0.503	0.085
0.1989	0.503	0.085

In addition to the calculation of thermodynamic quantities for the liquid phase, the Gibbs energy of formation of the AlSb solid phase was able to be calculated from the liquid-phase emf data. Integration of the following relation to $x_{Al} = 0.5$:

$$G^M = (1 - x_{Al}) \int_0^{x_{Al}} \frac{g^M_{Al}}{(1 - x_{Al})^2} dx_{Al} \qquad (4-1)$$

was accomplished by breaking it up into two parts. The first integration, from $x_{Al} = 0$ to $x_{Al} = 0.14$, represents the integration across the single-phase liquid region. The straight-line function for g^E_{Al} vs. x_{Al} was used to obtain an expression for g^M_{Al} which could be integrated exactly:

$$g^M_{Al} = g^E_{Al} + RT \ln x_{Al} = Mx_{Al} + B + RT \ln x_{Al} \qquad (4-2)$$

The second part of the integration, from $x_{Al} = 0.14$ to 0.50, represents the part through the two-phase region. It used the constant g^M_{Al} value at $x_{Al} = 0.14$, and could also be integrated exactly.

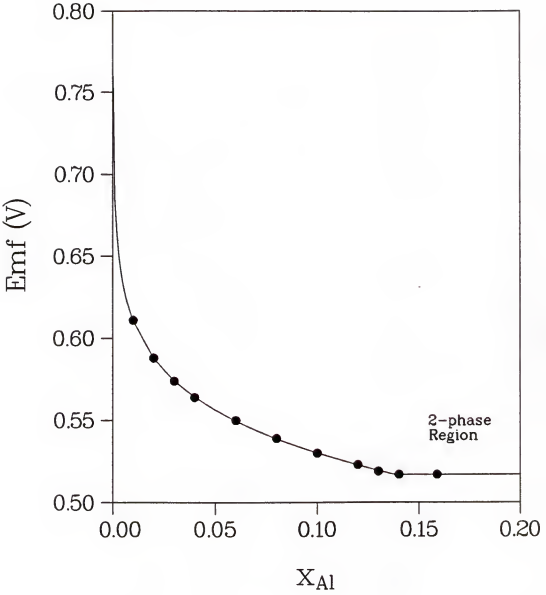

Figure 4-1

Titration curve for liquid Al-Sb at 846 °C (Cell 14). Line represents fit to data using straight-line approximation for g^E_{Al} vs. x_{Al} (Equation 3-11).

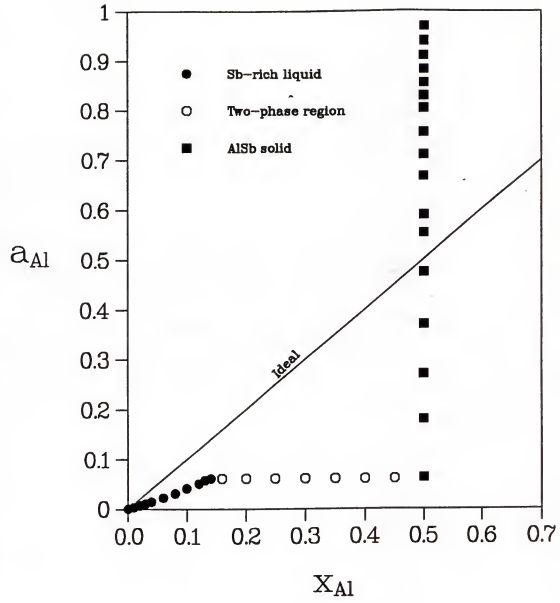

Figure 4-2

Aluminum activity vs. Al mole fraction for the Al-Sb system at 846 – 848 °C. The circles represent liquid- and two-phase data from Cell 14 (846 °C), and the squares represent solid-phase data from titration 4 of Cell 11 (848 °C).

Table 4-7
Partial thermodynamic quantities for liquid Al-Sb
at 806 °C, calculated from Cell 12 emf vs. x_{Al} data.

x_{Al}	$g^M_{Al}(J/mol)$	$g^E_{Al}(J/mol)$	a_{Al}	γ_{Al}
0.0170	-45400	-8890	0.00631	0.371
0.0363	-37600	-7880	0.0151	0.415
0.0654	-32400	-7950	0.0270	0.412
0.0750	-31000	-7730	0.0317	0.422
0.0944	-28700	-7480	0.0410	0.434

Table 4-8
Partial thermodynamic quantities for liquid Al-Sb
at 846 °C, calculated from Cell 14 emf vs. x_{Al} data.

x_{Al}	$g^M_{Al}(J/mol)$	$g^E_{Al}(J/mol)$	a_{Al}	γ_{Al}
0.0100	-53300	-10400	0.00326	0.326
0.0200	-46600	-10200	0.00668	0.334
0.0300	-42600	-9930	0.0103	0.344
0.0400	-39700	-9710	0.0141	0.352
0.0600	-35600	-9430	0.0218	0.363
0.0800	-32400	-8920	0.0307	0.383
0.1000	-29800	-8390	0.0406	0.406
0.1200	-27800	-8060	0.0505	0.420
0.1300	-26600	-7650	0.0571	0.440
0.1400	-26100	-7760	0.0608	0.434

Table 4-9
Partial thermodynamic quantities for liquid Al-Sb
at 875 °C, calculated from Cell 11 emf vs. x_{Al} data.

x_{Al}	$g^M_{Al}(J/mol)$	$g^E_{Al}(J/mol)$	a_{Al}	γ_{Al}
0.0525	-38200	-10100	0.0183	0.348
0.0625	-36200	-9720	0.0226	0.361
0.0729	-34200	-9160	0.0279	0.383
0.0924	-31600	-8820	0.0367	0.397
0.1086	-29500	-8330	0.0454	0.418
0.1312	-27200	-7820	0.0578	0.441
0.1488	-25500	-7290	0.0693	0.466
0.1588	-24600	-7040	0.0759	0.478

Table 4-10
Straight-line equations fitted to g^E_{Al} vs. x_{Al} data
(Cells 12, 14, and 11) for the Al-Sb system.

T (°C)	g^E_{Al} (kJ/mol) vs. x_{Al} equation
806	$g^E_{Al} = (19.8 \pm 1.9)\,x_{Al} + (-9.52 \pm 0.12)$
846	$g^E_{Al} = (22.3 \pm 0.8)\,x_{Al} + (-10.65 \pm 0.07)$
875	$g^E_{Al} = (27.8 \pm 1.0)\,x_{Al} + (-11.40 \pm 0.10)$

Table 4-11
Integral Gibbs energies for liquid Al-Sb at
806 °C, derived from the g^E_{Al} data (Cell 12).

x_{Al}	G^M (J/mol)	G^E (J/mol)
0.0170	-932	-159
0.0363	-1730	-332
0.0654	-2750	-579
0.0750	-3050	-657
0.0944	-3610	-808

Table 4-12
Integral Gibbs energies for liquid Al-Sb at
846 °C, derived from the g^E_{Al} data (Cell 14).

x_{Al}	G^M (J/mol)	G^E (J/mol)
0.0100	-626	-105
0.0200	-1120	-209
0.0300	-1560	-309
0.0400	-1970	-408
0.0600	-2710	-598
0.0800	-3370	-779
0.1000	-3970	-950
0.1200	-4520	-1110
0.1300	-4780	-1190
0.1400	-5030	-1260

In addition to calculating $G^M = G^{form}_{AlSb}$ for each of the three temperatures investigated, G^{form}_{AlSb} at 527 °C (800 K) was calculated by adjusting the G^{form}_{AlSb} value at 846 °C down to 527 °C using the $(H_T - H_{298})$ and $(S_T - S_{298})$ values reported by Lichter and Sommelet [69Lic]. The four G^{form}_{AlSb} values from this study are shown in Table 4-18 along with the 800 K value reported by Samokhval and Vecher [68Sam]. The agreement with Samokhval and Vecher, within 3%, is excellent.

Table 4-13
Integral Gibbs energies for liquid Al-Sb at
875 °C, derived from the g^E_{Al} data (Cell 11).

x_{Al}	$G^M\ (J/mol)$	$G^E\ (J/mol)$
0.0525	-2520	-560
0.0625	-2890	-657
0.0729	-3250	-755
0.0924	-3870	-931
0.1086	-4350	-1070
0.1312	-4960	-1250
0.1488	-5390	-1370
0.1588	-5620	-1440

Table 4-14
Partial antimony thermodynamic quantities for liquid
Al-Sb at 806 °C, derived from the g^E_{Al} data (Cell 12).

x_{Al}	x_{Sb}	$g^M_{Sb}\ (J/mol)$	$g^E_{Sb}\ (J/mol)$	a_{Sb}	γ_{Sb}
0.0170	0.9830	-157	-2.90	0.983	1.00
0.0363	0.9637	-345	-13.4	0.962	0.999
0.0654	0.9346	-651	-44.4	0.930	0.995
0.0750	0.9250	-758	-58.7	0.919	0.993
0.0944	0.9056	-984	-94.4	0.896	0.990

Table 4-15
Partial antimony thermodynamic quantities for liquid
Al-Sb at 846 °C, derived from the g^E_{Al} data (Cell 14).

x_{Al}	x_{Sb}	$g^M_{Sb}\ (J/mol)$	$g^E_{Sb}\ (J/mol)$	a_{Sb}	γ_{Sb}
0.0100	0.9900	-94.6	-1.12	0.990	1.00
0.0200	0.9800	-192	-4.52	0.980	1.00
0.0300	0.9700	-294	-10.2	0.969	0.999
0.0400	0.9600	-398	-18.3	0.958	0.998
0.0600	0.9400	-617	-41.8	0.936	0.996
0.0800	0.9200	-851	-75.3	0.913	0.992
0.1000	0.9000	-1100	-119	0.889	0.987
0.1200	0.8800	-1360	-175	0.864	0.981
0.1300	0.8700	-1500	-206	0.851	0.978
0.1400	0.8600	-1640	-241	0.838	0.974

Table 4-16
Partial antimony thermodynamic quantities for liquid Al-Sb at 875 °C, derived from the g^E_{Al} data (Cell 11).

x_{Al}	x_{Sb}	g^M_{Sb} (J/mol)	g^E_{Sb} (J/mol)	a_{Sb}	γ_{Sb}
0.0525	0.9475	-554	-39.7	0.944	0.996
0.0625	0.9375	-673	-56.7	0.932	0.994
0.0729	0.9271	-800	-77.7	0.920	0.992
0.0924	0.9076	-1050	-127	0.896	0.987
0.1086	0.8914	-1270	-177	0.875	0.982
0.1312	0.8688	-1600	-262	0.845	0.973
0.1488	0.8512	-1880	-342	0.821	0.965
0.1588	0.8412	-2040	-393	0.807	0.960

Table 4-17
Sb-rich liquidus data for the Al-Sb system, determined from the emf vs. x_{Al} data (Cells 12, 14, 11).

T (°C)	x_{Al}
806	0.094
846	0.137
875	0.158

Table 4-18
Gibbs energy of formation of the AlSb compound.

Reference	T (°C)	G^{form}_{AlSb} $(J/g\text{-}atom)$
This work	806	-14.9
This work	846	-13.7
This work	875	-13.3
This work	527	-20.5
[68Sam]	527	-21.1

Solid AlSb Results

Coulometric titrations through the AlSb compound were successfully obtained in three cells. All of these were assembled with an Sb film deposited onto the Ta/TaC WE cup, and Al was supplied by titration from the AlF_3 salt. Cell 1 was operated at 800 °C, while the results from Cells 11 and 17 were obtained at 847 – 848 °C. Cell 11 was an exceptionally stable cell, and a series of six titrations through the solid, adding Al and then removing it each time, was possible.

All of the solid-phase titration curves exhibited a similar shape. As Al was added to the compound, the emf value dropped off steeply at first and then tailed off toward the constant Al-rich emf value. A typical curve is shown in Figure 4-3, which presents the results for the fourth titration of Cell 11. The titration data obtained for the AlSb solid are presented in Tables 4-19 to 4-23. For Cell 11, the shape of the titration curves steepened somewhat as the titrations were repeated. The emf vs. x_{Al} data for titrations 1, 4 and 6 represent the variations encountered for Cell 11, and these are the data included in the tables.

The width of the homogeneity region for the AlSb compound indicated by the titration curves ranged from *ca.* 0.001 to 0.0028 mole fraction. In Figure 4-3, for example, the width is under 0.002 mole fraction. This is an intermediate value of the Cell 11 results and matches the results of Cell 17 quite well. The Cell 1 data indicate a larger width, *ca.* 0.0028 mole fraction.

In order to determine the position of the stoichiometric composition, the method of Wagner [71Wag] was used. According to Wagner's theory for point defects arising from small deviations from the stoichiometric composition in binary compounds, coulometric titrations across the compound should yield an antisymmetrical hyperbolic sine curve with the inflection point at the exact stoichiometric composition. Since the shape of all of the titration curves in the present study corresponded to only one half of the theoretical shape, it was inferred that deviations in the stoichiometry of AlSb occur primarily on the Al-rich side. Therefore the value of $x_{Al} = 0.5000$ was assigned to the initial composition of each titration curve, as the inflection point. The x_{Al} values reported in Tables 4-19 to 4-23 are all derived from this assumption. Direct comparison of the solid-phase emf data to Wagner's model is made in Chapter V (see Figure 5-17).

The data from titration 4 of Cell 11 were selected to represent the solid-phase emf behavior, and, again using the standard thermodynamic relations presented in Chapter III,

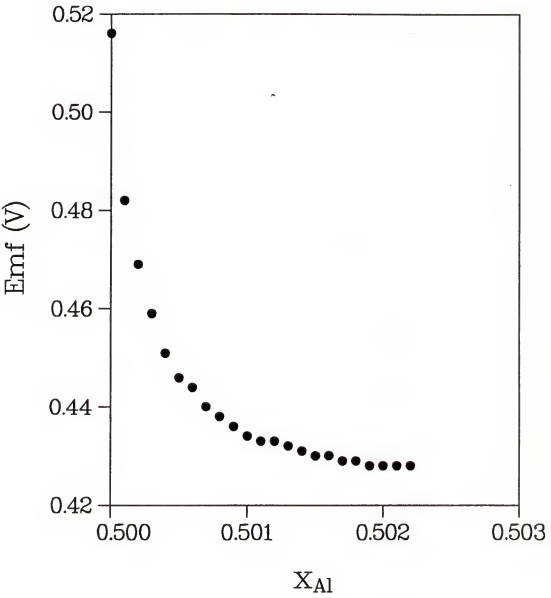

Figure 4-3

Titration curve through the AlSb compound at 848 °C (titration 4, Cell 11).

Table 4-19
Emf vs. x_{Al} data for the AlSb solid at 800 °C
(Cell 1). E is the net cell emf, $E_I - E_{II}$.

$E_{II} = 0.409$ V

x_{Al}	E_I(V)	E(V)
0.5000	0.470	0.061
0.5002	0.464	0.055
0.5004	0.453	0.044
0.5006	0.443	0.034
0.5008	0.436	0.027
0.5010	0.431	0.022
0.5012	0.427	0.018
0.5014	0.424	0.015
0.5016	0.422	0.013
0.5018	0.419	0.010
0.5020	0.417	0.008
0.5022	0.416	0.007
0.5024	0.414	0.005
0.5026	0.413	0.004
0.5028	0.412	0.003
0.5030	0.410	0.001

calculation of partial thermodynamic quantities for the solid phase was carried out. The values obtained for g^M_{Al}, g^E_{Al}, a_{Al} and γ_{Al} are presented in Table 4-24. The a_{Al} values, shown in Figure 4-2, span an enormous range. This is expected, since the solid phase must change from being in equilibrium with an Sb-rich liquid (low a_{Al} values) to being in equilibrium with an Al-rich liquid ($a_{Al} \simeq 1$).

Despite the experimental challenges to studying the emf behavior in the AlSb compound, the homogeneity region of AlSb has been successfully measured for the first time. The region has also been shown to be primarily Al-rich in the 800 – 850 °C range. This agrees with the results of Jordan *et al.* [74Jor] for another III-V system, GaP; they report data which indicate that the GaP compound deviates from stoichiometry primarily on the Ga-rich (Group III element) side.

Table 4-20

Emf vs. x_{Al} data for the AlSb solid at 847 °C (Cell 11, titration 1). E is the net cell emf, $E_I - E_{II}$.

$E_{II} = 0.426$ V

x_{Al}	E_I(V)	E(V)
0.5000	0.497	0.071
0.5002	0.471	0.045
0.5004	0.459	0.033
0.5006	0.450	0.024
0.5008	0.443	0.017
0.5010	0.437	0.011
0.5012	0.434	0.008
0.5014	0.432	0.006
0.5016	0.432	0.006
0.5018	0.431	0.005
0.5020	0.430	0.004
0.5022	0.429	0.003
0.5024	0.429	0.003
0.5026	0.428	0.002
0.5028	0.428	0.002
0.5030	0.427	0.001
0.5032	0.427	0.001
0.5034	0.427	0.001
0.5036	0.427	0.001
0.5038	0.426	0.000
0.5040	0.426	0.000

Table 4-21

Emf vs. x_{Al} data for the AlSb solid at 848 °C (Cell 11, titration 4). E is the net cell emf, $E_I - E_{II}$.

$E_{II} = 0.426$ V

x_{Al}	E_I(V)	E(V)
0.5001	0.482	0.056
0.5002	0.469	0.043
0.5003	0.459	0.033
0.5004	0.451	0.025
0.5005	0.446	0.020
0.5006	0.444	0.018
0.5007	0.440	0.014
0.5008	0.438	0.012
0.5009	0.436	0.010
0.5010	0.434	0.008
0.5011	0.433	0.007
0.5012	0.433	0.007
0.5013	0.432	0.006
0.5014	0.431	0.005
0.5015	0.430	0.004
0.5016	0.430	0.004
0.5017	0.429	0.003
0.5018	0.429	0.003
0.5019	0.428	0.002
0.5020	0.428	0.002
0.5021	0.428	0.002
0.5022	0.428	0.002

Table 4-22

Emf vs. x_{Al} data for the AlSb solid at 848 °C (Cell 11, titration 6). E is the net cell emf, $E_I - E_{II}$.

$E_{II} = 0.426$ V

x_{Al}	E_I(V)	E(V)
0.5001	0.468	0.042
0.5002	0.457	0.031
0.5003	0.446	0.020
0.5004	0.443	0.017
0.5005	0.438	0.012
0.5006	0.435	0.009
0.5007	0.433	0.007
0.5008	0.432	0.006
0.5009	0.430	0.004
0.5010	0.429	0.003
0.5012	0.430	0.004

Table 4-23
Emf vs. x_{Al} data for the AlSb solid at 847 °C
(Cell 17). E is the net cell emf, $E_I - E_{II}$.

$E_{II} = 0.427$ V

x_{Al}	E_I(V)	E(V)
0.5002	0.462	0.035
0.5004	0.451	0.024
0.5006	0.444	0.017
0.5008	0.438	0.011
0.5010	0.436	0.009
0.5012	0.435	0.008
0.5014	0.433	0.006
0.5016	0.431	0.004
0.5018	0.430	0.003
0.5020	0.428	0.001

Table 4-24
Partial thermodynamic quantities for the Al-Sb solid at
848 °C, calculated from emf vs. x_{Al} data of Cell 11, titration 4.

x_{Al}	$g^M_{Al}(J/mol)$	$g^E_{Al}(J/mol)$	a_{Al}	γ_{Al}
0.5001	-16200	-9750	0.176	0.351
0.5002	-12400	-5990	0.263	0.526
0.5003	-9550	-3100	0.359	0.717
0.5004	-7240	-784	0.460	0.919
0.5005	-5790	662	0.537	1.07
0.5006	-5210	1240	0.572	1.14
0.5007	-4050	2390	0.647	1.29
0.5008	-3470	2970	0.689	1.38
0.5009	-2890	3550	0.733	1.46
0.5010	-2320	4130	0.780	1.56
0.5011	-2030	4410	0.805	1.61
0.5012	-2030	4410	0.805	1.61
0.5013	-1740	4700	0.830	1.66
0.5014	-1450	4990	0.856	1.71
0.5015	-1160	5270	0.883	1.76
0.5016	-1160	5270	0.883	1.76
0.5017	-868	5560	0.911	1.82
0.5018	-868	5560	0.911	1.82
0.5019	-579	5850	0.940	1.87
0.5020	-579	5840	0.940	1.87
0.5021	-579	5840	0.940	1.87
0.5022	-579	5840	0.940	1.87

CHAPTER V

ASSESSMENT AND CALCULATION OF THE THERMOCHEMICAL PROPERTIES AND PHASE DIAGRAMS FOR THE Al-In AND Al-Sb SYSTEMS

The Al-In System

Introduction

While an abundance of experimental data on the Al-In system is available in the literature, discrepancies among these data are almost as abundant. In particular, different phase diagram data for the large miscibility gap in the system indicate critical temperature values ranging over one hundred degrees, from 830 °C [65Pre] to 945 °C [66Cam]. Several assessments and calculations of the Al-In system have been made, all reasonable in the face of the conflicting data, but all differing significantly in the representation of the miscibility gap.

In the current study, an attempt is made to reconcile the conflicting miscibility gap representations by optimizing a regular-solution-type model to obtain a good fit of all the types of experimental data available. These include phase diagram data, liquid-phase enthalpies of mixing, and partial Gibbs energies of aluminum in the liquid, including the emf results of this study reported in Chapter III. The following section addresses the first step in the assessment of the Al-In system, which is the evaluation of the available experimental data.

Experimental Data

Phase diagram data

Phase diagram data for the miscibility gap in the Al-In system have been obtained by three different methods: differential thermal analysis (DTA), sampling followed by density measurements, and emf measurements. Predel [65Pre], using DTA, proposed a miscibility gap with a flat shape at the top and a critical temperature of 830 °C. Campbell and coworkers have published two articles [52Cam, 66Cam] on the miscibility gap of Al-In; both determinations were made by sampling the two liquid layers and determining the composition of each by density measurements. In the first article, Campbell *et al.* [52Cam] proposed a miscibility gap with a critical temperature of 875 °C, substantially higher than Predel's observation. However, in the subsequent investigation of Campbell and Wagemann [66Cam], a more sophisticated sampling technique was used, which employed a baffled pipette and allowed measurements to be made up to 950 °C; the resulting miscibility gap suggests an even higher critical temperature of 945 °C. In the interest of impartiality, the data above 800 °C for each of these authors was not used in the computer optimization. Data below 800 °C were substantially in agreement.

Miscibility gap data were also obtained in emf studies of Al-In by Massart *et al.* [66Mas, 71Mas] and by Yazawa and Lee [69Yaz]. In both investigations, the boundary of the miscibility gap is determined for a given composition by the temperature at which the slope of emf vs. T is found to change suddenly, from the 1-phase to the 2-phase slope. This slope change is relatively dramatic for high-In compositions, but becomes very slight at lower In concentrations, so that the inaccuracy of the temperature obtained from the intersection of the two lines becomes very large, possibly up to ±30 °C. Therefore, only the points for the miscibility gap obtained at or above $x_{In} = 0.70$ (equivalently, at or below 810 °C) were deemed reliable.

A number of authors have reported on the Al-rich region, all in reasonable agreement. However the data from two investigations have not been used: Raub and Engel [46Rau], who used crucibles made of silica-rich glass (with which Al is now well-known for reacting), obtained phase diagram values consistently lower than most of the other reported values. The data of Valentiner and Puzicha [47Val] have also been omitted, since they report a melting temperature of 658 °C for pure Al. This is 2 °C lower than the generally accepted value [83Mur] and suggests that the rest of their data is also too low, possibly due to calibration errors or impurities. The thermal analysis (TA) data of Klemm *et al.* [48Kle] and the DTA data of Predel [65Pre] and of Campbell *et al.* [52Cam] were all retained. Note that the TA data of Campbell *et al.* [52Cam] did not match their DTA data, and, since DTA is a significantly more sensitive technique, the TA data for the liquidus were omitted.

In the In-rich solid-liquid region, the data from two of the investigations show excellent agreement (see Figure 5-1). These were the DTA data of Predel [65Pre] and the emf data of Massart *et al.* [66Mas]. In the latter study, the liquidus points were derived (again, for given compositions) from the temperatures at which the emf reached zero, indicating the onset of solid Al formation. The data of Campbell *et al.* [52Cam] for this region fall significantly to the In-rich side of those obtained by Predel and by Massart *et al.* It is possible that Campbell *et al.* quenched the liquid phase before equilibrium with the solid aluminum phase had been reached. In the end, these data were not used. Likewise, the single datum of Klemm *et al.* [48Kle] was very far off from the other data and was omitted.

For the temperature of the monotectic reaction, $L_1 \Rightarrow Al(s) + L_2$, the datum of Campbell *et al.* [52Cam] was selected. They report the temperature at this point as 638.6 °C. This seemed a reasonable choice, since it lies in the middle of the range of temperatures reported, 634 – 640 °C [46Rau, 47Val, 48Kle, 52Cam]. The temperature of 634 °C reported both by Raub and Engel [46Rau] and by Valentiner and Puzicha [47Val] is suspected of

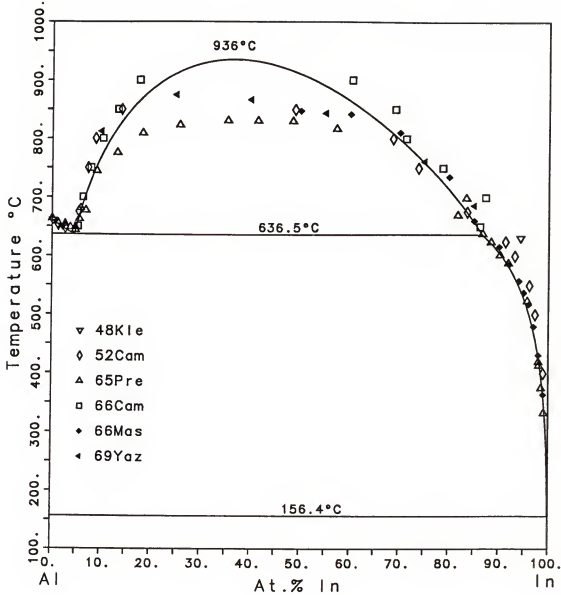

Figure 5-1

Calculated phase diagram for the Al-In system,
with all available experimental phase diagram data.

being at least 2 °C too low, based on their low values in the Al-rich region as discussed above. The value of Klemm *et al.* [48Kle] at 640 °C, though not unreasonable, lies at the high end of the range. It was therefore concluded that the monotectic temperature must lie in the range 636 – 640 °C.

Values for the eutectic temperature, representing the reaction $L_2 \Rightarrow Al(s) + In(s)$, have been reported by a number of authors [46Rau, 47Val, 48Kle, 52Cam] and are in excellent agreement at 156 °C, as summarized by Murray [83Mur]. As the solubility of In in Al was found by Samuels [55Sam] to be less than 0.045 at.% at 638 °C, the solid Al phase was assumed to be pure for calculational purposes. The same assumption was made for the solid In phase, since the solubility of Al in In-rich liquid was determined by Campbell *et al.* [52Cam] to be less than 0.2 at. % at temperatures below 300 °C, and since the eutectic temperature (156 °C) is essentially equal to the melting point of pure In (156.6 °C), which also indicates that the solubility of Al in solid In is negligible.

All of the phase diagram data sources are listed in Table 5-1 along with the estimated errors used in the computer optimization. Note that for data which had to be read off of a plot (digitized), the errors are generally estimated a little higher. Accuracies reported in the literature were generally retained.

Thermodynamic data

While the enthalpy of mixing data of Wittig and Keil [63Wit] and of Girard *et al.* [77Gir] show an excellent match, (see Figure 5-6), those of Predel and Sandig [69Pre1] are substantially more endothermic. In addition, they show significant scatter among themselves, and therefore they were not used. For the first two references, only single-phase values of the enthalpy of mixing were used. In the case of the data reported by Girard *et al.* [77Gir], some of the values reported as single-phase were later omitted when preliminary

Table 5-1
Phase diagram data sources and estimated errors for the Al-In system.

Reference	Method	Range x_{In}	Accuracy ΔT(K)	Δx	Remarks
–miscibility gap–					
[65Pre]	DTA	0.0003-0.991	5	0.005	digitized; no exptl. details; data at $T > 1073$ K not used
[52Cam]	sampling	0.055-0.836	3	0.005-0.008	data at $T > 1073$ K not used
[66Cam]	sampling	0.053-0.873	3	0.005-0.008	digitized; data at $T > 1073$ K not used
[66Mas]	emf	0.5-0.85	4-13	0.002	data at $x_{In} < 0.70$ not used
[69Yaz]	emf	0.1-0.85	4-20	0.002	data at $x_{In} < 0.75$ not used
–Al-rich solid-liquid–					
[46Rau]	TA	0.006-0.902	–	–	not used
[47Val]	TA/DTA	0-0.979	–	–	not used
[48Kle]	TA	0.002-0.022	5	0.005	digitized
[65Pre]	DTA	0-0.05	5	0.005	digitized
[52Cam]	TA	0-0.027	–	–	not used
[52Cam]	DTA	0.011-0.027	3	0.002	
–In-rich solid-liquid–					
[48Kle]	TA	0.943	5	0.005	not used
[52Cam]	quench	0.913-0.990	3	0.002	not used
[65Pre]	DTA	0.867-0.991	5	0.005	digitized
[66Mas]	emf	0.90-0.99	5	0.002	
–monotectic (Al-L_1-L_2)–					
[52Cam]	TA	0-0.048	1	0.003	
–eutectic (Al-L-In)–					
[83Mur]	evaluated	0-1	3	0.005	

results of the computer optimization suggested that they might in fact be two-phase values (see Results and Discussion section below).

As discussed earlier in Chapter III, the partial Gibbs energy values of aluminum in the liquid obtained in this study for the Al-In system agree very well with the data reported in previous emf studies of Al-In by Massart *et al.* [66Mas] and by Yazawa and Lee [69Yaz]. Examining the data plotted together as g_{Al}^{M} vs. composition (at.% In) in Figure 5-4, one observes that the data of Yazawa and Lee [69Yaz] are generally a bit higher than the rest, and some of the data from the present study are a bit lower. Since a calibration error of a mere 0.01 mV would account for these discrepancies, none of the data was omitted. Table 5-2 lists the available thermodynamic data for Al-In and their estimated errors.

Method of Calculation

To model the Al-In system, the program written by Lukas *et al.* [77Luk], which uses a least-squares method to optimize phase diagrams, was employed. All of the selected experimental data for the Al-In system, with their estimated errors, were utilized in the program to obtain an optimal set of coefficients for the temperature and concentration dependence of the excess Gibbs energy of the liquid. The Redlich-Kister polynomial was chosen to represent the liquid phase:

$$G^{E} = x_i \, x_j \sum_{\nu=0}^{n} (x_i - x_j)^{\nu} \, L_{ij}^{(\nu)} \qquad (5-1)$$

where the coefficients $L_{ij}^{(\nu)}$ are linear functions of temperature, which can be represented by

$$L_{ij}^{(\nu)} = A_{ij}^{(\nu)} - B_{ij}^{(\nu)} T \qquad (5-2)$$

Table 5-2
Thermodynamic data sources and estimated errors for the Al-In system.

Reference	Method	Ranges T (K) x_{In}	Accuracy ΔT (K) Δx ΔV (J/mol)	Remarks V = value
–enthalpy of mixing of liquid–				
[69Pre1]	high-T cal.	*ca.* 0.1123	10	digitized;
		0.01-0.90	0.005	not used
			150	
[63Wit]	high-T cal.	988	3	
		0.05-0.95	0.002	
			40	
[77Gir]	high-T cal.	990-1182	3	digitized;
		0.05-0.94	0.002	data suspected
			7%	2-phase not used
–partial Gibbs energy of Al in liquid–				
[66Mas]	emf/molt.salt	933-1223	3	
		0.40-0.99	0.002(0.005, 2-ph)	
			100 + 3%	
[69Yaz]	emf/molt.salt	963-1210	3	digitized
		0.10-0.95	0.002(0.005, 2-ph)	
			100 + 5%	
This work	emf/CaF_2	1123-1173	3	
		0.80-1.00	0.002-0.005	
			(100-200) + 2%	

Note: – Temp is not cited by Predel and Sandig [69Pre1]

The coefficients A_{ij} and B_{ij} correspond to the temperature-independent contributions to the enthalpy and excess entropy of mixing, and these are the parameters which are obtained from the optimization program.

The solid pure elements were chosen as the reference state of the system. Since Al(s) and In(s) reveal negligible mutual solubility, they were modeled as stoichiometric compounds.

To model the pure liquid elements, Al(l) and In(l), mixing to form the Al-In liquid phases, the Gibbs energy of transformation of each solid element to the liquid state was taken from the recent evaluation and compilation of Saunders *et al.* [88Sau]:

$$\{G_0^{liq} - G_0^{fcc}\}_{Al} \ (J/mol) = 10711 - 11.473\ T\,(K) \qquad (5-3)$$

$$\{G_0^{liq} - G_0^{bct}\}_{In} \ (J/mol) = 3283 - 7.639\ T\,(K) \qquad (5-4)$$

The overall Gibbs energy in the liquid, in J/mol, is then

$$\begin{aligned} G = {} & x_{Al}\,(10711 - 11.473\ T) + x_{In}\,(3283 - 7.639\ T) \\ & + RT\,(x_{Al} \ln x_{Al} + x_{In} \ln x_{In}) \\ & + x_{Al} x_{In} \sum_{\nu=0}^{n} \left(A_{Al-In}^{(\nu)} - B_{Al-In}^{(\nu)} T\right) (x_{Al} - x_{In})^{\nu} \end{aligned} \qquad (5-5)$$

where T is in K and where the third term represents the ideal configurational entropy.

Results and Discussion

To describe the Al-In system with the Redlich-Kister expression, it was first determined that limiting the polynomial expansion to two terms ($\nu = 0$ and $\nu = 1$) gave poor convergence in the optimization. Three terms were then used, with satisfactory convergence. In optimizing the six coefficients corresponding to these three terms, the following procedure was used:

1. Use only the selected enthalpy of mixing data to optimize the three enthalpy coefficients.
2. Fix the three enthalpy coefficients at the values obtained in step 1, allow the three entropy coefficients to float, and use the phase diagram data and the partial Gibbs energy data to optimize the entropy coefficients.

3. Allow all six coefficients to float, and run the optimization program using all the selected data. Steps 1 and 2 thus provide a reasonable set of initial values for the final optimization.

In practice, steps 1 and 2 also allow evaluation of various sets of experimental data. For example, in step 2, optimizations were run with and without the In-rich solid- liquid phase diagram data of Campbell *et al.* [52Cam]. Although these data do not appear drastically different from those of the other two authors, their inclusion yields coefficients which model the phase diagram and the partial Gibbs energies poorly. These data were therefore omitted. In step 3, multiple sets of the phase diagram data (6x) and of the enthalpy of mixing data (7x) were used in order to give these kinds of data a weight equivalent to that of the partial Gibbs energy data, which numbered 340 points. Similarly, the datum for the monotectic point provided by Campbell *et al.* [52Cam] was entered 31 times.

When steps 1-3 were first followed, coefficients were obtained which fit all the data reasonably well, but which yielded a miscibility gap in the phase diagram with a very high critical temperature of 970 °C. This tendency to a high T_{crit} was evident even when only the phase diagram data were used in step 2. If the assumption is made that the critical temperature in the Al-In system does in fact occur at a temperature above 900 °C, then a second look at the enthalpy of mixing data provided by Girard *et al.* [77Gir] is warranted. Their data, as reported, suggest a very low T_{crit} value, below 839 °C. A substantial number of points which were reported as single-phase could be re-evaluated as two-phase, and thereby omitted from the optimization. This was carried out, steps 1-3 were repeated, and the resulting coefficients gave a significantly improved fit to the selected experimental data.

The final set of coefficients for the Al-In system is listed in Table 5-3. The six coefficients that were optimized in the program are underlined. The calculated phase diagram is shown in Figure 5-1 along with all the experimental data. A calculated critical temperature of

936 °C was obtained, which fits in well with the observations of Campbell and Wagemann [66Cam]. They obtained data for two liquid phases up to 900 °C, but found the Al-In liquid to be single-phase at 950 °C. Figure 5-2 shows a blow-up of the Al-rich region and the satisfactory calculated fit of the monotectic point.

The calculated partial Gibbs energies of aluminum in the liquid fit the experimental data very well, as shown plotted as g_{Al}^{M} vs. composition (at.% In) in Figures 5-3 and 5-4, where all the data have been adjusted to T = 900 °C. The calculated temperature dependence of the partial Gibbs energies is also satisfactory, as demonstrated more clearly in Figure 5-4.

Particularly striking is the comparison of Figures 5-5 and 5-6, both of which show ΔH_{mix} vs. at.% In. Figure 5-5 includes only the final set of experimental data used in the optimization and shows an excellent fit of the calculated curve to the selected data. Figure 5-6, however, includes all of the available experimental data; the data of Girard *et al.* [77Gir] that were suspected of being two-phase are designated by the half-filled circles. In addition, the dashed lines in the figure represent two-phase tie lines at T = 909 °C and at T = 839 °C, which are the two highest temperatures at which Girard *et al.* reported their data. Their suspected two-phase data fall almost entirely between the two tie lines. Moreover, some of the data of Predel and Sandig [69Pre1], primarily the high-In and low-In values, are seen to match quite well the calculated curve. Note that in both figures, the solid line was calculated at 950 °C. No temperature dependence of the enthalpy of mixing was used in the analytical description, corresponding to the behavior of the experimental results reported in the literature; therefore the experimental points in Figures 5-5 and 5-6 were plotted without adjustment to 950 °C.

A number of phase diagram calculations for the Al-In system have been reported previously. They are compared with the present study in Table 5-4. The first two authors have

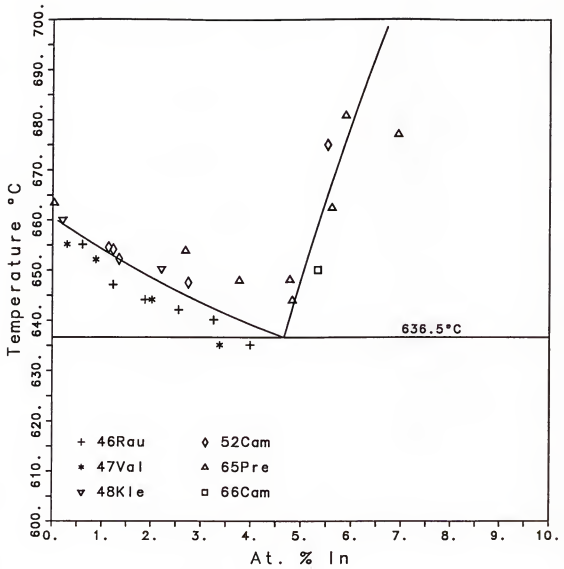

Figure 5-2

Enlargement of the Al-In phase diagram in the Al-rich monotectic region. Lines represent calculated phase diagram.

Table 5-3
Thermodynamic description of the Al-In system,
using the polynomial model for the liquid phase.

Phase stabilities of the elements (from [88Sau]):

		Multipliers	
Phase	Element	1	$-T$
liquid	Al	10711	11.473
liquid	In	3283	7.639
solid	Al	0	0
solid	In	0	0

Excess terms of the liquid phase (Redlich-Kister polynomial):

	T-Multipliers	
x-Multipliers	1	$-T$
$x_{In}\ (1\text{-}x_{In})$	21259.6	0.48737
$x_{In}\ (1\text{-}x_{In})\ (1\text{-}2x_{In})$	3850.3	1.20564
$x_{In}\ (1\text{-}x_{In})\ (1\text{-}2x_{In})^2$	5479.2	3.16805

Notes:

- All values are in J/mol and K
- The given multipliers belong to the integral Gibbs energy
- The values adjusted by the least squares method are underlined

based their calculations on phase diagram data only, from which Gokcen and Chang [72Gok] arrive at low values (853 °C, 3900 J/mol) for the critical temperature and the maximum ΔH_{mix}, while Peres and Campos [74Per] report very high values (975 °C, 6200 J/mol). The analysis of Hultgren *et al.* [73Hul] relies on thermodynamic and phase diagram data available at the time [65Pre, 66Cam, 66Mas, 63Wit] and provides a low T_{crit} (854 °C) and a rather high maximum ΔH_{mix} value (5800 J/mol).

The calculational technique of Kaufman *et al.* [81Kau] allows a maximum of only two polynomial terms in the expression for the liquid-phase excess Gibbs energy; although a higher T_{crit} (902 °C) was obtained, the very low value they calculated for T_{mono} (619 °C) suggests that more terms are needed to adequately model the Al-In system. Chang [85Cha] also employed only two excess terms, using the Non-Random Two-Liquid model developed by Renon and Prausnitz [68Ren], and obtained an overly symmetric liquidus curve. His

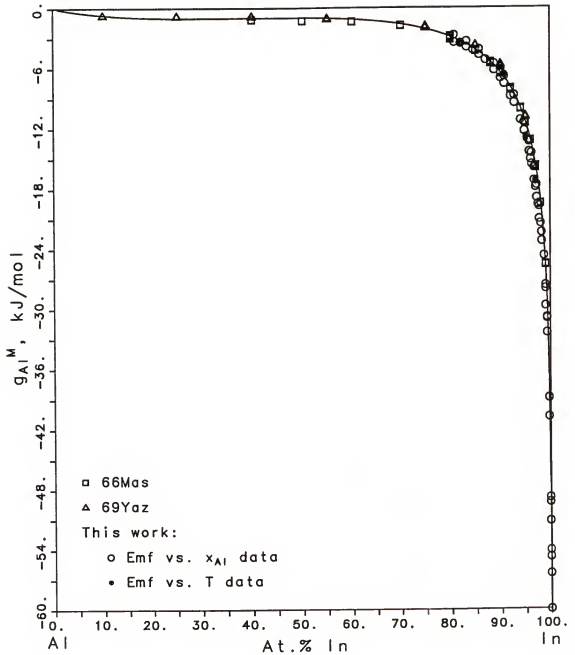

Figure 5-3

Calculated partial Al Gibbs energy vs. composition for the Al-In system at 900 °C. All of the experimental data have been adjusted to 900 °C, using the temperature dependence for g_{Al}^{M} determined by the calculated Al-In description.

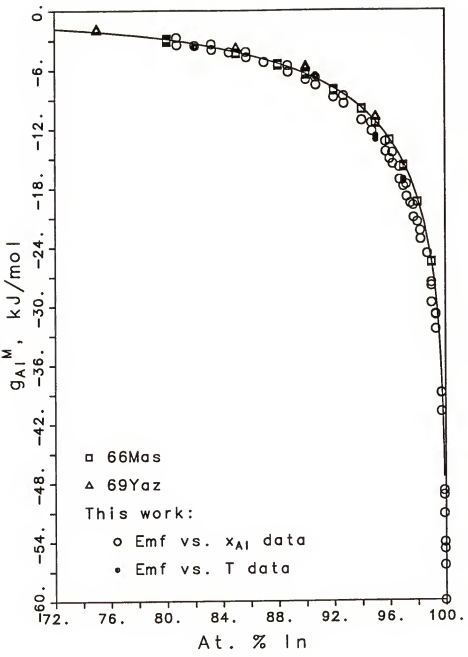

Figure 5-4

Enlargement of the In-rich region of Figure 5-3, for g_{Al}^{M} versus at.% In for the Al-In system at 900 °C.

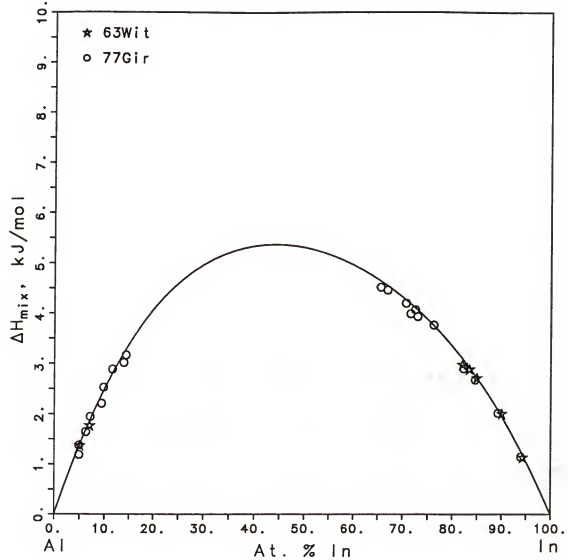

Figure 5-5

Calculated enthalpy of mixing vs. composition for the Al-In system. The experimental data shown are those in the final selected data set used in the optimization calculation.

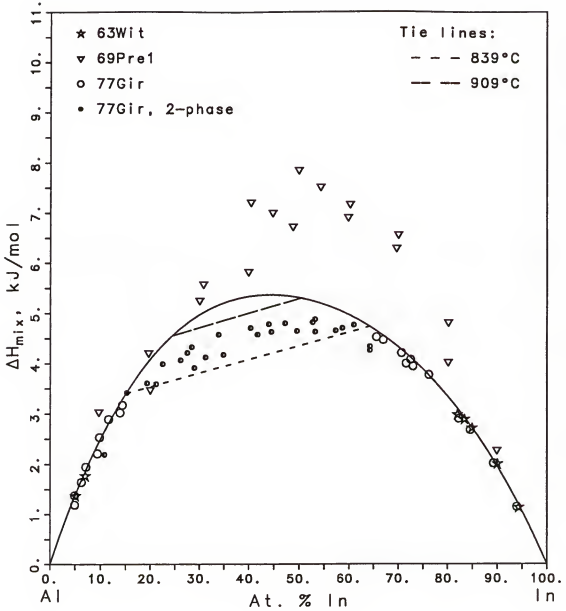

Figure 5-6

Calculated enthalpy of mixing vs. composition for the Al-In system. The dashed lines represent calculated tie lines for the miscibility gap. All of the literature values for ΔH_{mix} are included in the figure.

Table 5-4
Comparison of calculated descriptions of the Al-In system.

Reference	# terms	T_{crit} (°C)	T_{mono} (°C)	Max. ΔH_{mix} (J/mol)
[72Gok]	2	853	—	*ca.* 3900
[74Per]	2	975	635	6200
[73Hul]	–	854	637	5800
[81Kau]	2	902	619	–
[78Ans]	4	854	634	4833
[83Mur]	3	902/875[a]	638	4740
[85Cha]	2	921	—	5870
[89Rug]	4	908	638	4700
This work	3	934	636.5	5300

[a]The first temperature was obtained from the model calculation; the second was adjusted from the first by extrapolation into the critical region.

T_{crit} value, at 921 °C, is similar to the value obtained in the current study, but his value for the maximum ΔH_{mix} is much larger (5870 J/mol).

Calculation of the Al-In system using four terms in the excess Gibbs energy expression was first presented by Ansara *et al.* [78Ans]. They included most of the available thermodynamic data in the optimization [63Wit, 77Gir, 66Mas, 69Yaz] and obtained reasonable fits for the phase diagram data and for the enthalpies of mixing, but the values for T_{crit} (854 °C), for the maximum ΔH_{mix} (4833 J/mol), and even for T_{mono} (634 °C) are all low. Murray's analysis [83Mur], using the Mathieu (surrounded-atom) model with four parameters, yields a similarly low value for the maximum ΔH_{mix} (4740 J/mol), a somewhat higher T_{crit} (875 °C), and a very reasonable T_{mono} (638 °C). In the recent work of Rugg and Chart [89Rug], again four terms were used to model the Al-In system. They obtained a relatively high T_{crit} value (908 °C), but calculate ΔH_{mix} to fit all of the data of Girard *et al.* [77Gir] and thereby obtain a low value for the maximum ΔH_{mix} (4700 J/mol).

While the experimental phase diagram data for the Al-In system leave the true critical temperature difficult to pinpoint, the enthalpy of mixing data are far less contradictory. In the present work, a critical evaluation of the data of Girard *et al.* [77Gir] has led to

the calculated curve in Figure 5-6, where the data at high- and low-In values are fitted best. This, and the maximum calculated ΔH_{mix} value of 5300 J/mol are in sharp contrast with the results of the calculations of Murray, of Ansara *et al.*, and of Rugg and Chart, all of whom present a generally better fit of all of the data of Girard *et al.*, with maximum ΔH_{mix} values well below 5000 J/mol. However, close inspection of their calculated curves shows that they fit more poorly the high- and low-In experimental data, which are the most reliable data with respect to the possibility of falling within the two-phase region. Their closer fit of the middle-x_{In} data does not then seem appropriate.

In the current study, three terms in the Redlich-Kister expression for the excess Gibbs energy of the liquid have been used. Close evaluation of all the available experimental data has yielded a very consistent set of data for the Al-In system, and the coefficients obtained from the optimization of this selected data set provide an excellent fit to all three types of data for the system.

The Al-Sb System

Introduction

Unlike in the Al-In system, inconsistencies in the phase diagram data for the Al-Sb system were ironed out almost a century ago. However, the liquid-phase enthalpies of mixing reported for the Al-Sb system differ drastically from author to author. Resolution of this problem was attempted in the current study by using the Lukas optimization program to find out which enthalpy of mixing data set was most consistent with the phase diagram and thermodynamic data available for the Al-Sb system.

As in the previous section, the Redlich-Kister polynomial was employed to model the Al-Sb liquid. Since a number of semiconductor systems have been successfully described

using the associated solution model, this model was also used in the current study to fit the Al-Sb liquid solution. A comparison of the two descriptions was then made. In addition, the Wagner-Schottky model was introduced to describe the homogeneity region in the AlSb compound and to fit the results of the emf studies in this work.

Experimental Data

Phase diagram data

In the very first two studies of the Al-Sb system, by Gautier [96Gau] and by Campbell and Mathews [02Cam], the liquidus curves obtained by solidification experiments exhibited two peaks, one at the AlSb compound and one at another composition (*ca.* 10 at.% Sb). Since the extra peak was subsequently shown to be anomalous [06Tam], the liquidus data from these two authors were not used. Using thermal analysis, Urazova [19Ura], Loofs-Rassow [31Loo] and Guertler and Bergmann [33Gue] obtained liquidus data which are generally in good agreement. With the exception of some of the Sb-rich values of Guertler and Bergmann, about which the authors themselves express uncertainty, the data from the above three studies were retained in the selected data set for the Al-Sb system. The data of Veszelka [31Ves] were not used, since the very low temperature reported (555 °C) for the Sb-AlSb eutectic suggests major contamination problems in the study.

Several authors have since contributed a few more points to the Al-Sb liquidus curve. Also using thermal analysis, Glazov and Petrov [58Gla] studied the region around the melting point of AlSb. Their data exhibit a sharp peak at the melting point, which implies a substantial degree of association in the melt. However, this implication is tempered by the fact that the other reported values in this region suggest a lower, flatter maximum in the liquidus curve (see Figure 5-7). Nevertheless, the data of Glazov and Petrov were included in the selected data set.

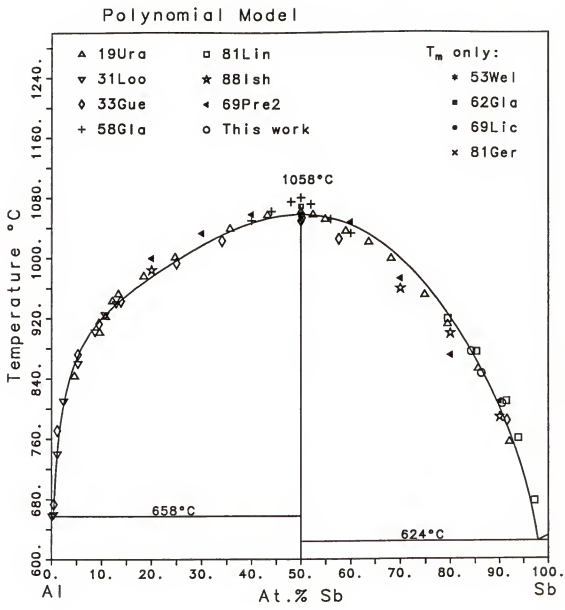

Figure 5-7

Calculated phase diagram for the Al-Sb system, with experimental phase diagram data. Redlich-Kister polynomial used in the calculation.

Linnebach and Benz [81Lin] obtained a few liquidus points in the Sb-rich region by direct observation of crystallization. Although their data fall a bit higher than the other reported values, they continue to higher x_{Sb} values and so were retained in the selected data set. Most recently, Ishida *et al.* [88Ish] determined a few values for the liquidus by differential thermal analysis. Only one point was in significant disagreement with the other authors, and this value was not used in the calculation.

From their emf studies of the Al-Sb system, Predel and Schallner [69Pre2] backed out points on the liquidus curve; these were derived from slope changes in the emf vs. T data. Since the slopes themselves are highly subject to interpretation and the resulting accuracy of their liquidus data was unsatisfactory, they were omitted from the selected data set. In the current study, liquidus data for the Al-Sb system were obtained from coulometric titration measurements (emf vs. x_{Al}). They agree very well with the other reported values and were used in the calculation.

In addition to values for the melting point of AlSb reported by Urazova [19Ura], by Guertler and Bergmann [33Gue] and by Glazov and Petrov [58Gla], T_m data for AlSb have been published by several other authors. Woolley and Smith [58Woo] used thermal analysis to determine the AlSb melting point, while Welker [53Wel] and Glazov and Chizhevskaya [62Gla] obtained T_m values by means of conductivity measurements. From their calorimetric studies of the Al-Sb system, Lichter and Sommelet [69Lic] also determined the melting point of AlSb. Finally, Gerdes and Predel [81Ger] used differential thermal analysis to obtain the AlSb melting point. All of these T_m values, listed in Table 5-5, span a range of 30 °C, from 1050 to 1080 °C. In general, they were all included in the selected Al-Sb data set, since omission of the few extreme values had no significant effect on the calculated description of the Al-Sb system.

Table 5-5
AlSb melting point values.

Reference	Method	T_m Value (°C)	Reported Accuracy (°C)
[19Ura]	TA	1062	-
[33Gue]	TA	1050	-
[58Gla]	TA	1080	-
[58Woo]	TA	*ca.* 1050	-
[53Wel]	conductivity	1060	-
[62Gla]	conductivity	1069	-
[69Lic]	calorimetry	1057	5
[81Ger]	DTA	1052	-

Table 5-6
Eutectic temperatures and compositions for the Al-Sb system.

Reference	Method	Eutectic	$T_{eut.}$(°C)	x_{Sb}(eut.)
[19Ura]	TA	Al-AlSb	655	*ca.* 0.001
		Sb-AlSb	631	*ca.* 0.999
[33Gue]	TA	Al-AlSb	656	0.002
		Sb-AlSb	624	0.956
[31Loo]	TA	Al-AlSb	651	0.002
[31Dix]	metallography	Al-AlSb	657	0.0025

The thermal analysis studies of Urazova [19Ura] and of Guertler and Bergmann [33Gue] also yielded temperatures for the Al-AlSb and Sb-AlSb eutectics; these are listed in Table 5-6. Additional data for the Al-AlSb eutectic are provided by Loofs-Rassow [31Loo] and by Dix *et al.* [31Dix], who each report the eutectic composition as well as the temperature (see Table 5-6). The data of Dix *et al.*, which were obtained by metallographic methods, are generally held to be the most reliable [84McA]. All of the reported eutectic data were nevertheless used in the calculation.

For the purpose of running the optimization program, errors for all of the values in the selected AlSb data set were assigned or, where available, taken from the literature sources. The sources and estimated errors for the phase diagram data discussed above are listed in Table 5-7.

Table 5-7
Phase diagram data sources and estimated errors for the Al-Sb system.

Reference	Method	Range x_{Sb}	Accuracy ΔT (K)	Δx	Remarks
–liquidus–					
[19Ura]	TA	0.046-0.921	5	0.005	
[31Loo]	TA	0.001-0.129	3	0.005	
[33Gue]	TA	0.005-0.916	3	0.005	some Sb-rich data not used
[58Gla]	TA	0.4-0.6	5	0.005	
[81Lin]	direct obs.	0.795-0.973	7	0.005	digitized
[88Ish]	TA	0.2-0.9	3	0.002	datum at $x_{Sb} = 0.70$ not used
[70Pre]	emf	0.2-0.9	5	0.002	digitized; not used
This work	emf	0.842-0.906	3	0.003	
–AlSb melting point–					
[19Ura]	TA		3	0.001	
[33Gue]	TA		3	0.001	
[58Gla]	TA		5	0.001	
[58Woo]	TA		–	–	not used
[53Wel]	conductivity		3	0.001	
[62Gla]	conductivity		7	0.001	
[69Lic]	calorimetry		5	0.001	
[81Ger]	DTA		3	0.001	
–eutectics–					
[19Ura]	TA	0.046-0.921	5	0.003	
[33Gue]	TA	0.005-0.956	3	0.005	
[31Loo]	TA	0.001-0.129	3	0.005	
[31Dix]	metallography	0.0010-0.0316	2	0.001	

Enthalpy data

Values for the enthalpy of mixing of liquid Al-Sb have been measured by three groups [71Bat, 85Lee, 87Gir]. Batalin *et al.* [71Bat] report very negative ΔH_{mix} values for the Al-Sb liquid at 1000 °C. Lee and Sommer [85Lee] obtained data for very Al-rich liquids at 925 °C by high-temperature solution calorimetry, from which they report only the derived

partial enthalpies of mixing, h_{Sb}^{M}, for the alloy compositions studied. The molar enthalpies of mixing were therefore recalculated in the present study; these values are all negative, but exhibit a less steep trend than the data of Batalin *et al.* (see Figure 5-8).

Girard *et al.* [87Gir] have used both direct and indirect drop calorimetric techniques to determine mixing enthalpies for liquid Al-Sb in the temperature range 846 to 952 °C. Due to the volatility of antimony, they were able to obtain data only in Al-rich and Sb-rich composition ranges. Their ΔH_{mix} data contrast sharply with those of the preceding two authors: most of the values are negative and an order of magnitude smaller than the values of Batalin *et al.*, and in the very Al-rich region the data of Girard *et al.* have positive values.

To assist in determining which of these three very different data sets for the liquid Al-Sb enthalpy of mixing might be the most correct, the values for ΔH_{mix} derived by Predel and Schallner [69Pre2] from their emf data were also added to the data set used in the optimization program. These values are negative and roughly twice the magnitude of Girard's values, but since they are derived from the emf data via differentiation followed by integration, they were used only as a guideline.

Martosudirdjo and Pratt [74Mar] have determined the heat of formation of the AlSb compound by means of precipitation calorimetry. Both the value obtained experimentally at 254 °C and the standard heat of formation derived from it were included in the selected data set. These values match the corresponding ones reported by Hultgren *et al.* [73Hul] well within the uncertainties listed.

The heat content data for AlSb measured by Lichter and Sommelet [69Lic] over the temperature range 400 to 1450 K (127 to 1177 °C) were included in the Al-Sb data set, along with the value they determined for the enthalpy of fusion of AlSb. The data from previous studies by Piesbergen [63Pie] and by Cox and Pool [67Cox] were not used, since

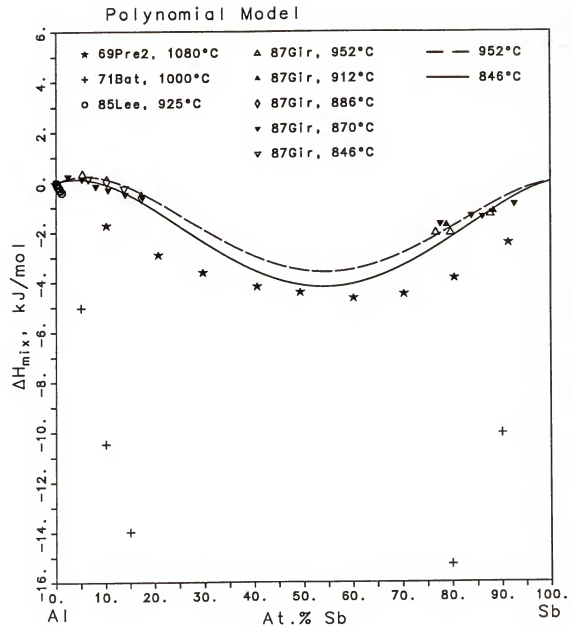

Figure 5-8

Calculated liquid-phase enthalpy of mixing vs. composition for the Al-Sb system, for two temperatures, with experimental ΔH_{mix} data. Redlich-Kister polynomial used in the calculation.

Piesbergen reports only low-temperature C_p values (below 0 °C), and Cox and Pool present only the straight-line equation fitted to their heat content data for the temperature range 298 to 1150 K.

Partial molar Gibbs energy data

Vecher and coworkers have done two emf studies on solid AlSb. The data from the earlier study [65Vec] were measured in a molten electrolyte cell, while the second set of measurements [68Sam] were obtained with a CaF_2 solid electrolyte cell. While there is more scatter in the first set of data, the two sets coincide reasonably well and were both retained in the selected data set.

Predel and Schallner [69Pre2], using molten electrolyte galvanic cells, measured a very large number of emf values both in the single-phase Al-Sb liquid and in the solid-liquid two-phase region. The data span the entire Al-Sb composition range and the temperature range 725 – 1120 °C. They were initially used in the calculation of the Al-Sb system, but in the end had to be omitted from the final Al-Sb data set, as is discussed further on.

The liquid-phase emf data obtained for the Al-Sb system in the present study was entered into the selected data set with separate codes for each cell. Since some variation in the data was encountered among the results obtained at 846 °C, two representative sets of data were used for this temperature. Though all of the data sets worked reasonably well in the optimization, only the data from Cell 11 at 846 °C was kept in the final Al-Sb data set.

The emf data obtained for solid AlSb in this study were also included in the selected data set, but they were not used in the optimization until the Al-Sb system had been satisfactorily fitted using the rest of the data set. As in the case of the liquid-phase data, variations among the titrations were entered as separate data sets. The low-temperature (806 °C) titration

data and the data from the narrowest titration from Cell 11 were eventually omitted from the selected data set.

The thermodynamic data sources discussed above and the errors estimated for the data are listed in Table 5-8. Note that all of the data which were omitted from the final selected Al-Sb data set are designated as "not used" under the remarks.

Method of Calculation

The optimization program of Lukas *et al.* [77Luk] was used to obtain the optimal parameter sets for the models chosen to describe the Al-Sb system. The Redlich-Kister polynomial was first selected to represent the liquid phase; this model has been described above for the Al-In system calculations. The second model used to describe the liquid phase is the associated solution model, first introduced by Jordan [70Jor]. It has been used successfully by a number of authors to model such semiconductor systems as In-Sb [80Ros, 80Sza], Ga-Sb [81Lel, 80Sza] and Pb-Te [86Kat]. At the same time, it should be noted that successful descriptions of semiconductor systems have also been achieved using the polynomial model, for example by Sharma *et al.* for the In-Sb and Ga-Sb systems [87Sha]. Therefore both models have been used and compared in this study of the Al-Sb system.

For both models, the pure solid elements were chosen as the reference state of the system. Negligible solubility of Al in Sb and of Sb in Al was assumed. The Gibbs energy of transformation of each solid element to the liquid state was taken from Saunders *et al.* [86Sau, 88Sau]:

$$\{G_0^{liq} - G_0^{fcc}\}_{Al} \ (J/mol) = 10711 - 11.473\ T\,(K) \qquad (5-6)$$

$$\{G_0^{liq} - G_0^{rho}\}_{Sb} \ (J/mol) = 19874 - 21.985\ T\,(K) \qquad (5-7)$$

Table 5-8

Thermodynamic data sources and estimated errors for the Al-Sb system.

Reference	Method	Ranges T (K) x_{In}	Accuracy ΔT (K) Δx ΔV (J/mol)	Remarks V = value
–enthalpy of mixing of liquid–				
[71Bat]	not reported	1273 0.05-0.90	5 0.005 209	not used
[85Lee]	solution calorimetry	1198 0.0006-0.0114	3 0.0003 5%	not used
[87Gir]	drop cal.	1119-1225 0.07-0.23, 0.83-0.98	3 0.003-0.007 10%	
[70Pre]	emf	*ca.* 1353 0.1-0.9	10 0.003 10%	not used
–enthalpy of formation of AlSb–				
[74Mar]	precipitation calorimetry	527 0.5	3 0.001 377	
–heat content of AlSb, stoichiometric Al-Sb liquid–				
[69Lic]	drop cal.	300-1450 0.5	3 0.001-0.002 1%	
–enthalpy of fusion of AlSb–				
[69Lic]	drop cal.	1330 0.5	5 0.001 1%	
–partial Gibbs energy of Al in AlSb-Sb two-phase equilibria–				
[65Vec]	emf/molt.salt	663-889 0.5	3 0.001 5%	
[68Sam]	emf/CaF_2	778-895 0.5	7 0.001 5%	digitized
–partial Gibbs energy of Al in liquid–				
[70Pre]	emf/molt.salt	998-1392 0.10-0.90	5 0.002 2-6%	not used
This work	emf/CaF_2	1079-1148 0.841-1.00	3 0.002-0.005 100 + 2%	used only data of Cell 11 at 1119 K
–partial Gibbs energy of Al in AlSb homogeneity gap–				
This work	emf/CaF_2	1073-1121 0.498-0.500	3 0.0002-0.0004 200 + 2%	omitted data of Cell 1 & Cell 11, #4

where the Gibbs energy units are J/mol.

The associate model assumes the formation of one or more types of molecular associate from the atomic components in the liquid. For the case of one associate species, A, forming from atomic components 1 and 2 in the binary, the excess Gibbs energy:

$$G^E = H^E - TS^E \tag{5-8}$$

is calculated from its components, H^E and S^E:

$$H^E = n_A H^f + n_A n_1 H_{A1} + n_A n_2 H_{A2} \tag{5-9}$$

$$S^E = n_A S^f + n_A n_1 S_{A1} + n_A n_2 S_{A2} \tag{5-10}$$

where n_i is the number of moles of species i in one mole of atoms in the liquid, H^f is the enthalpy of formation of the associate, H_{A1} and H_{A2} are the enthalpies of interaction between the associate and each atomic species, and S^f, S_{A1} and S_{A2} are the corresponding entropies. These last six quantities are the parameters for the liquid phase which are fitted by the optimization program.

The configurational entropy for the associate model is given by

$$S^{conf} = -R\left[n_A \ln \frac{n_A}{n_T} + n_1 \ln \frac{n_1}{n_T} + n_2 \ln \frac{n_2}{n_T}\right] \tag{5-11}$$

where $n_T = n_A + n_1 + n_2$. The overall Gibbs energy in the Al-Sb liquid, as described by the associate model, is then

$$G = x_{Al}\{G_0^{liq} - G_0^{fcc}\}_{Al} + x_{Sb}\{G_0^{liq} - G_0^{rho}\}_{Sb} + S^{conf} + H^E - TS^E \tag{5-12}$$

To describe the solid intermetallic phase, AlSb, a stoichiometric line compound was first assumed. Once a reasonable description of the overall system had been obtained, the solid was then described by the Wagner-Schottky model [30Wag], in which deviations from stoichiometry are modeled via the formation of defects on the sublattices of the compound. A combination of two primary defects is assumed, where the defects may be antistructure atoms, interstitials or vacancies. Here the antistructure defect, Al_{Sb}, and the Al vacancy, V_{Al}, were selected as the primary defects, based on the modeling work on GaSb by Edelin and Mathiot [80Ede], who successfully fitted experimental Hall data from previous authors using the analogous defects, Ga_{Sb} and V_{Ga}.

In the Wagner-Schottky model as used in the present study, the excess enthalpy includes terms for the enthalpy of formation of the ideal cell, H^I, and for the enthalpies of formation of the antistructures and vacancies, H_{21} and H_{10}:

$$H^E = (1 + n_{10})\, H^I + n_{21} H_{21} + n_{10} H_{10} \qquad (5-13)$$

where

$(1 + n_{10})$ = number of moles of all lattice sites in 1 mole of atoms

n_{21} = number of moles of antistructure atoms on the Sb sublattice

n_{10} = number of moles of vacancies on the Al sublattice

Note that truncation after the first term, *i.e.* for no defects present and $n_{10} = 0$, gives an H^E which is equivalent to that obtained assuming a stoichiometric line compound.

The vibrational entropy of formation is given by the analogous equation:

$$S^{vib} = (1 + n_{10})\, S^I + n_{21} S_{21} + n_{10} S_{10} \qquad (5-14)$$

The configurational entropy from the ideal mixing of the species present on each sublattice is represented by

$$S^{conf} = -R\left[x \ln \frac{x}{n_t} + n_{10} \ln \frac{n_{10}}{n_t} + n_{21} \ln \frac{n_{21}}{n_t} + (1 - x - n_{21}) \ln \frac{(1 - x - n_{21})}{n_t}\right] \quad (5-15)$$

where, on the basis of one mole total of atoms,

x = number of moles of Sb atoms on Sb sublattice

$(1 - x - n_{21})$ = number of moles of Al atoms on Al sublattice, and

$n_t = (1 + n_{10})/2$

= number of moles of lattice sites on either sublattice

The expression for the overall Gibbs energy of the AlSb solid is then

$$G = H^E - T\left(S^{vib} + S^{conf}\right) \quad (5-16)$$

The quantities H^I, S^I, H_{21}, H_{10}, S_{21} and S_{10} are the parameters which are optimized by the Lukas program. The first two are the parameters optimized for the "ideal cell", or when the AlSb phase is assumed to be a line compound.

Results and Discussion

Results using the Redlich-Kister model

Description of the Al-Sb liquid by the Redlich-Kister polynomial (Equation 5-1) was found to require a large number of parameters to model the significant degree of asymmetry in the system, as evident, for example, in the shape of the liquidus (see Figure 5-7). The final number of Redlich-Kister parameters needed was seven. These include a coefficient, $C_{ij}^{(0)}$, corresponding to the excess heat capacity, C_p^E, to describe the temperature dependence of

the enthalpy of mixing. Therefore, instead of Equation (5-2) as the temperature function, an extended temperature function was used:

$$L_{ij}^{(\nu)} = A_{ij}^{(\nu)} - B_{ij}^{(\nu)}T + C_{ij}^{(\nu)}T\,(1 - \ln T) \qquad (5-17)$$

The concurrent modeling of the AlSb solid phase as a stoichiometric line compound was successfully accomplished using four parameters for the temperature dependence of the Gibbs energy of formation:

$$G^{I} = A^{I} - B^{I}T + C^{I}T\,(1 - \ln T) + D^{I}\frac{T^2}{2} \qquad (5-18)$$

The fourth parameter, D^{I}, was required by the nonlinear temperature dependence of the solid-phase C_p data, presented by Lichter and Sommelet [69Lic].

The severe discrepancies in the enthalpy of mixing data for the Al-Sb system made the initial optimization attempts very difficult. Omission of all of the liquid-phase enthalpy of mixing data was an unsuccessful strategy, since without any ΔH_{mix} data at all it was difficult to obtain a reasonable fit of the phase diagram. This is probably related to the large number of parameters to be optimized and to the relatively small set of reliable data for the system. Finally, the following procedure was used to obtain a reasonable set of Redlich-Kister coefficients for the liquid phase:

1. Take the liquid C_p value of 8.90 cal/K g-at reported by Lichter and Sommelet [69Lic], reduce it to the excess heat capacity, C_p^E, by subtracting the C_p contributions of the pure liquid elements, and calculate the coefficient, $C_{ij}^{(0)}$ (see Equation 5-17), via

$$C_{ij}^{(0)} = (4)\,(4.184\ J/cal)\,C_p^E = 22.6773\ J/molK \qquad (5-19)$$

where C_p^E is multiplied here by 4 to account for later multiplication in the model by $x_{Sb}(1 - x_{Sb})$, at $x_{Sb} = 0.5$. This value for the coefficient is the one to be expected if the optimization were to match the data of Lichter and Sommelet exactly. Fix the coefficient at this value.

2. Use a subset of the selected data set, containing only the thermodynamic (enthalpy and partial molar Gibbs energy) data, and look at the Al-Sb description calculated from optimizing these data. Determine which of the data in the subset yield lower values for the mean square error in the optimization and predict curves closest to the data. Weed out the obviously inconsistant data.

3. Use the entire selected data set and continue to test variations on the data set. Come up with the best overall data set to calculate the optimum fit of all the types of data available for the Al-Sb system.

4. Take the parameters obtained in step 3 and unfix the coefficient whose value was fixed in step 1. Run the optimization again, and see whether the coefficient set changes significantly.

In step 2, omission of the ΔH_{mix} data of Batalin [71Bat] and of Lee and Sommer [85Lee] caused the mean square error of the optimization to drop sharply; inclusion of the data was found to worsen the shape of the liquidus. In step 3, it was finally determined that the emf data of Predel and Schallner [69Pre2], while qualitatively reasonable, had the effect of shifting the calculated curve for the liquidus unacceptably lower than the phase diagram data on the Al-rich side. The derived ΔH_{mix} data of Predel and Schallner [69Pre2] were also shown to be inconsistant with the phase diagram and heat content data. However, use of the ΔH_{mix} data of Girard *et al.* [87Gir] allowed a good match of all the types of data in

the Al-Sb system; they are the only authors whose liquid ΔH_{mix} values seem to be at all consistent with the other types of data.

Finally, omission of some of the emf data from the current work gave a slight improvement in the calculated fit of the heat content data of Lichter and Sommelet [69Lic] and of the solid-phase data for the partial Gibbs energy of aluminum. By omitting from the selected data set all the data shown to be inconsistent, a set of parameters was obtained which described the Al-Sb system very well. When, in step 4, the $C_{ij}^{(0)}$ coefficient was optimized along with the rest of the coefficients, they did not change at all.

The final, successful parameter set for the Al-Sb system, as described using the Redlich-Kister model, is listed in Table 5-9. The calculated phase diagram is shown in Figure 5-7, along with the experimental data from the literature, including those omitted from the selected data set. The fit to the data is very good, as are the calculated T_m (1058 °C) and eutectic temperatures (658, 624 °C). In Figure 5-8, which shows the enthalpy of mixing as a function of composition (at.% Sb), the calculated curve fits the data of Girard *et al.* [87Gir] quite well, and also indicates that the derived ΔH_{mix} data of Predel and Schallner [69Pre2] are at least of the right order of magnitude. Moreover, the calculated minimum ΔH_{mix} value, at about -4 kJ/mol, seems reasonable compared to the minimum values of about -1 kJ/mol [71Pre, 75Gam] and -3 kJ/mol [80Ros] obtained experimentally for the analogous systems, GaSb and InSb, respectively. The fit of the calculated curves to the excess heat content data of Lichter and Sommelet [69Lic] is excellent, as shown in Figure 5-9. The representation of their solid- and liquid-phase data in the plot was accomplished by subtracting out the heat content contributions from the pure elements.

Figure 5-10 shows the calculated g_{Al}^{M} vs. composition (at.% Sb) curve at 850 °C. The experimental data in the plot have all been adjusted to this temperature as well. The fit seems less than perfect, even to the data from the present work, but it must be kept in mind

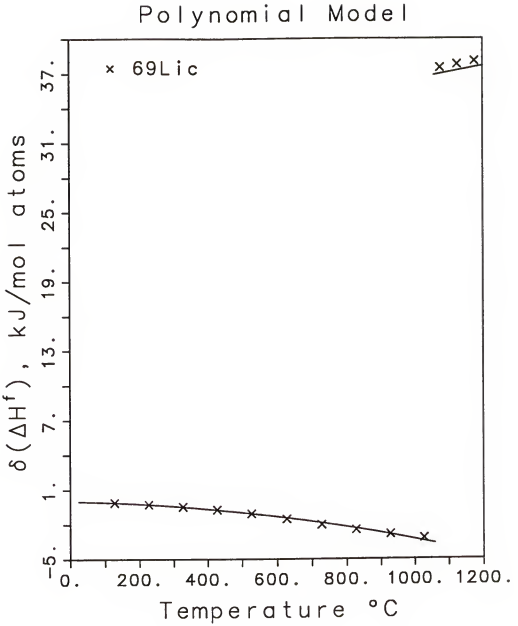

Figure 5-9

Plot of (ΔH_T^f - ΔH_{298}^f) vs. T, showing the calculated lines for solid AlSb and for liquid Al-Sb at $x_{Al} = 0.5$, with experimental data. Redlich-Kister polynomial used in the calculation.

Table 5-9
Thermodynamic description of the Al-Sb system,
using the polynomial model for the liquid phase.

Phase stabilities of the elements (from [86Sau, 88Sau]):

		Multipliers	
Phase	Element	1	$-T$
liquid	Al	10711	11.473
liquid	Sb	19874	21.985
solid	Al	0	0
solid	Sb	0	0

Excess terms of the liquid phase (Redlich-Kister polynomial):

	T-Multipliers		
x-Multipliers	1	$-T$	$T(1-\ln T)$
$x_{Sb}\ (1-x_{Sb})$	−41894.5	−162.9441	22.67728
$x_{Sb}\ (1-x_{Sb})\ (1-2x_{Sb})$	5685.8	−1.93333	0
$x_{Sb}\ (1-x_{Sb})\ (1-2x_{Sb})^2$	17158.5	9.54781	0

Excess terms of the AlSb phase (as a stoichiometric line compound),
referred to the pure solid elements:

	T-Multipliers			
x-Multipliers	1	$-T$	$T(1-\ln T)$	$-T^2/2$
1	−24486.0	−6.70061	0.827827	−0.0053594

Notes:

- All values are in J/g-at and K
- The given multipliers belong to the integral Gibbs energy
- The values adjusted by the least squares method are underlined

that a change of a few mV will shift the partial Gibbs energy by a few thousand J/mol. The effect of the emf data on the calculated description of the other thermodynamic properties is ultimately more critical. The plot of g^M_{Al} vs. T for the two-phase equilibria (Figure 5-11) shows a reasonable fit to the AlSb-Sb (solid-solid) data, matching best those of Samokhval and Vecher [68Sam], and a qualitatively acceptable match of the liquid-AlSb two-phase data.

Results using the associated solution model

Convergence of the optimization program was even more difficult using the associate model. However, when the final Al-Sb data set obtained in the previous section was used,

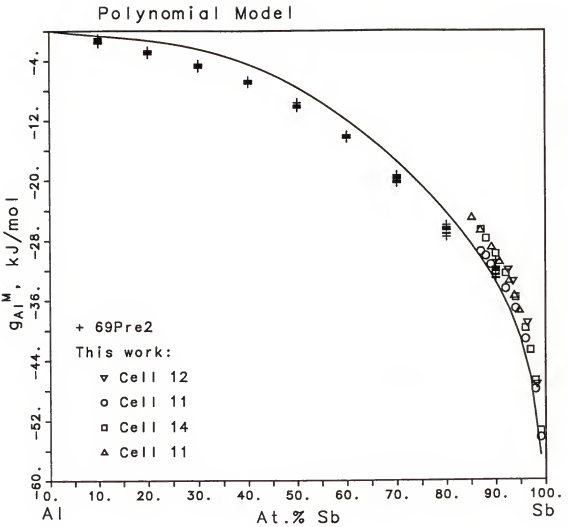

Figure 5-10

Calculated partial Al Gibbs energy vs. composition for the Al-Sb system at 850 °C. All of the experimental data have been adjusted to 850 °C, using the temperature dependence for g_{Al}^{M} determined by the calculated Al-Sb description. Redlich-Kister polynomial used in the calculation.

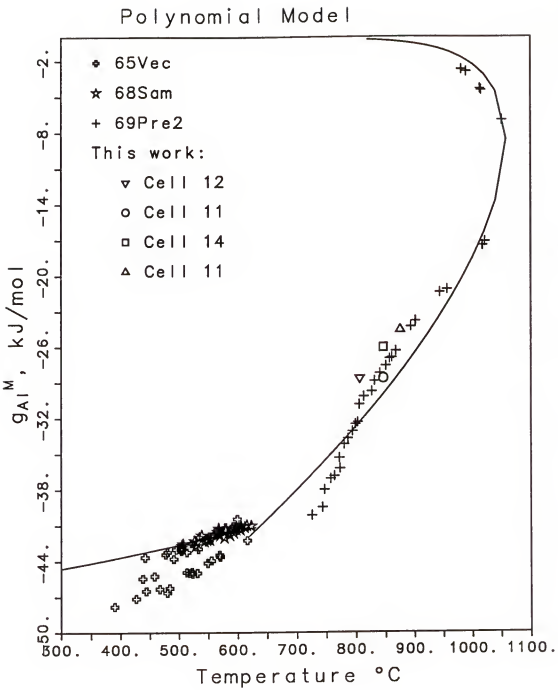

Figure 5-11

Figure 5-11. Plot of g_{Al}^{M} vs. T for two-phase equilibria in the Al-Sb system. Lines calculated from Redlich-Kister polynomial description.

reasonable results were obtained. To adequately describe the Al-Sb liquid, with its asymmetrical behavior, all of the interaction terms between the elements and the Al-Sb associate were used in the model (see Equations 5-9 and 5-10). Attempts to improve the match of the calculated curves and the experimental data by adding terms for the element-element interactions in the liquid or for asymmetry in the element-associate interactions were not successful.

The final parameter set for the Al-Sb system, described using the associate model for the liquid phase and using, again, the stoichiometric line compound approximation for the solid, is listed in Table 5-10. The curves calculated for the phase diagram and thermodynamic quantities of the system are all reasonable, but differ slightly from those obtained from the polynomial model. The calculated liquidus, shown in Figure 5-12, fits the experimental data a little more closely on the Sb-rich side than does the polynomial curve (Figure 5-7), but falls short of the data in the Al-rich region. The T_m (1060 °C) and the Al-AlSb eutectic temperature (655 °C) differ by a few degrees from the polynomial calculation, but are all still within the experimental scatter.

As with the Redlich-Kister results, the associate model curve calculated for the liquid-phase enthalpy of mixing as a function of x_{Sb}, shown in Figure 5-13, matches the data of Girard *et al.* [87Gir] reasonably well, but the shape of the curve is distinctly different from the polynomial curve (Figure 5-8). The sharp minimum near 50 at.% Sb in Figure 5-13 is directly related to the model's assumption of the formation of the 1:1 Al:Sb associate in the liquid. The degree of association calculated by the model is moderate, about 25% associated at the melting point. The ΔH_{mix} vs. composition curve exhibits a stronger temperature dependence in the region of the minimum than was calculated by the polynomial model; this is also related to the formation of the associate. Meanwhile, the curves calculated by

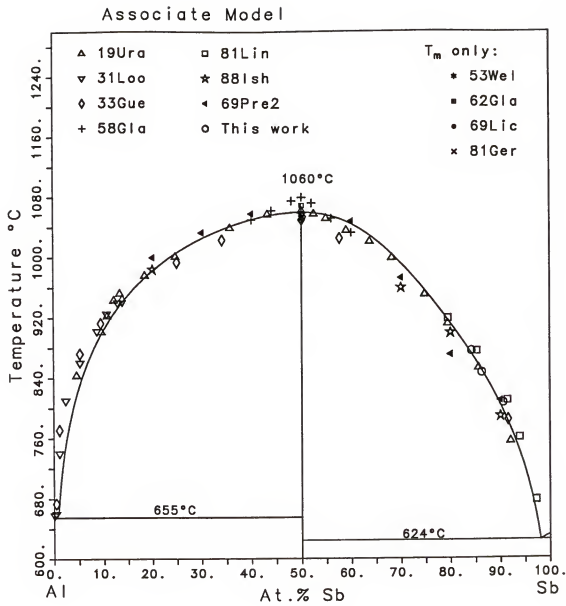

Figure 5-12

Calculated phase diagram for the Al-Sb system, with experimental phase diagram data. Associate model used in the calculation.

Table 5-10
Thermodynamic description of the Al-Sb system,
using the associate model for the liquid phase.

Phase stabilities of the elements (from [86Sau, 88Sau]):

		Multipliers	
Phase	Element	1	$-T$
liquid	Al	10711	11.473
liquid	Sb	19874	21.985
solid	Al	0	0
solid	Sb	0	0

Excess terms of the liquid phase (associate model):

	T-Multipliers	
n-Multipliers	1	$-T$
n_A	-52039.0	-34.79354
$n_1\ n_A$	39440.1	18.01410
$n_2\ n_A$	27957.3	21.06015

Excess terms of the AlSb phase (as a stoichiometric line compound), referred to the pure solid elements:

	T-Multipliers			
x-Multipliers	1	$-T$	$T(1-\ln T)$	$-T^2/2$
1	-24796.6	-6.62585	0.829373	-0.0053633

Notes:

- All values are in J/g-at and K
- The given multipliers belong to the integral Gibbs energy
- n_i represents the moles of species i in one mole of atoms
- The values adjusted by the least squares method are underlined

each model for the heat content vs. temperature appear identical (compare Figures 5-14 and 5-9).

In Figure 5-15, which shows g_{Al}^{M} vs. composition (at.% Sb) for the liquid, a bend is observed in the calculated curve. This is again related to the formation of the associate species assumed by the model. The curve thereby fits the data of Predel and Schallner [69Pre2] more closely than does the polynomial curve in Figure 5-10, but inclusion of these data in the selected data set resulted in a much worse overall description of the Al-Sb system. The g_{Al}^{M} vs. T calculation yields a curve for the liquid phase (Figure 5-16) which is similar to the polynomial one, while the solid-phase curve is shifted down by *ca.* 1 kJ/mol.

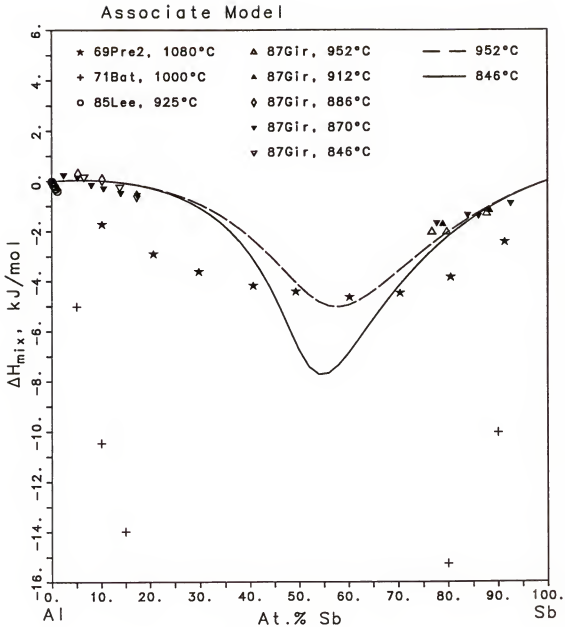

Figure 5-13

Calculated liquid-phase enthalpy of mixing vs. composition for the Al-Sb system, for two temperatures, with experimental ΔH_{mix} data. Associate model used in the calculation.

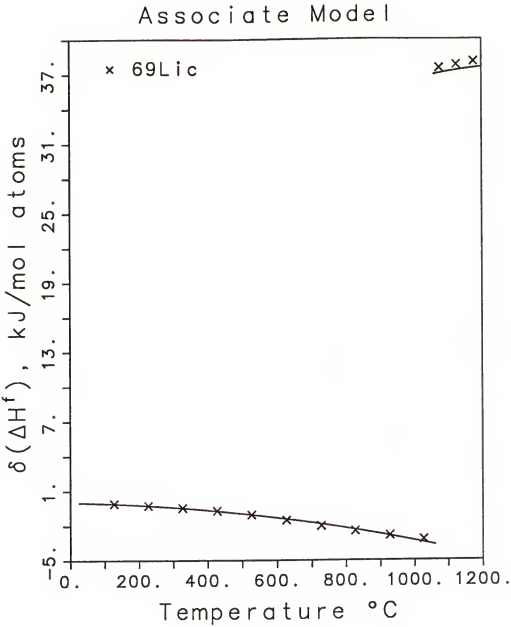

Figure 5-14

Plot of $(\Delta H_T^f - \Delta H_{298}^f)$ vs. T, showing the calculated lines for solid AlSb and for liquid Al-Sb at $x_{Al} = 0.5$, with experimental data. Associate model used in the calculation.

This gives an intersection with the liquid-phase curve at a lower g_{Al}^{M} value, yielding the 2 °C higher Sb-AlSb eutectic temperature of the associate model.

While the descriptions of the Al-Sb liquid by the polynomial and the associate models are generally similar, and each successful, preference is given to the polynomial description, since it gives slightly better calculated fits to the various experimental data. Therefore, the Redlich-Kister polynomial was used for further modeling purposes, such as in the following section.

Results using the Wagner-Schottky model

The description of the Al-Sb system using the Redlich-Kister polynomial to model the liquid phase, obtained above, was modified by employing the Wagner-Schottky model to describe the solid AlSb phase. As discussed earlier, the antistructure defect, Al_{Sb}, and the Al vacancy, V_{Al}, were the two primary defects assumed for this system. In the emf data of this work, the titration curves indicated deviations from stoichiometry only on the Al-rich side. This corresponds to the assumption that the concentration of the V_{Al} defect must be very small. Lacking any data on how small these concentrations might be, they were fixed at a negligible magnitude in the model by setting the H_{10} coefficient (Eq. 5-13) at a fixed, large number; 200,000 was sufficient to effectively pin the vacancy concentration at zero. The coefficient for the V_{Al} entropy contribution, S_{10}, was set at zero.

Preliminary optimizations were run on the system in order to evaluate the utility of the temperature-dependent term, $-n_{21}TS_{21}$, in the model description. This was accomplished by keeping fixed the coefficients obtained previously for the liquid phase and for the "ideal cell" (stoichiometric) AlSb solid, and optimizing only the H_{21} and S_{21} coefficients. The inclusion of the S_{21} parameter to describe the temperature dependence of the Al_{Sb} defect behavior was unable to bridge the disparity between the Cell 1 data (at 800 °C) and the

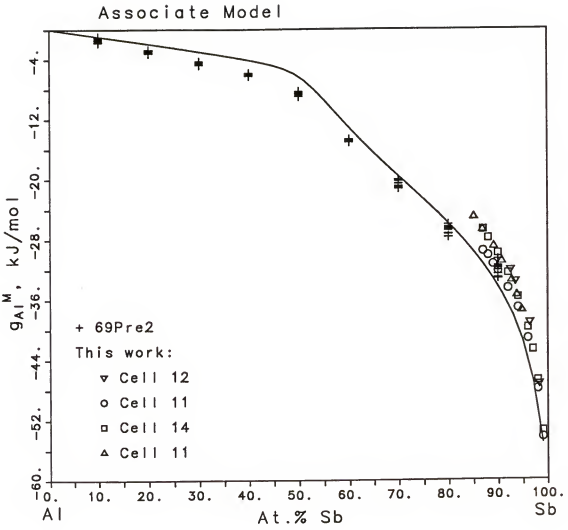

Figure 5-15

Calculated partial Al Gibbs energy vs. composition for the Al-Sb system at 850 °C. All of the experimental data have been adjusted to 850 °C, using the temperature dependence for g_{Al}^{M} determined by the calculated Al-Sb description. Associate model used in the calculation.

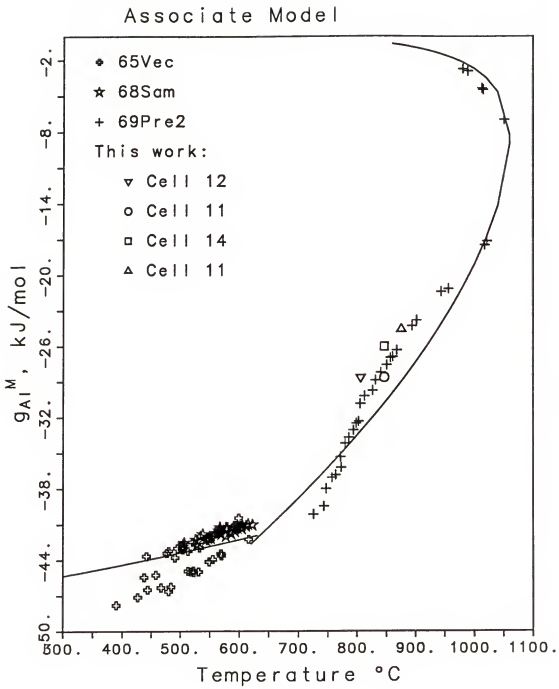

Figure 5-16

Plot of g_{Al}^{M} vs. T for two-phase equilibria in the Al-Sb system. Lines calculated from associate model description.

other data (at 848 °C). Therefore the Cell 1 data were omitted from the data set, and the S_{21} coefficient was dropped as well, since the rest of the data for the homogeneity range had all been taken at the same temperature.

The AlSb melting point predicted from optimizing only the H_{21} coefficient was too high (1067 °C). However, when the rest of the coefficients were optimized along with H_{21}, the T_m value dropped to the previously obtained value of 1058 °C. The other coefficients changed slightly, but their description of the Al-Sb system did not. It was then determined that the narrowest titration (Cell 11, #6) obtained for AlSb in this study gave a much larger mean square error for the optimization than did either of the other two titration data sets (Cell 11, titrations 1 and 4). Of these, the data from Cell 11, titration 4, seem slightly better, but as the differences are within the experimental error, both sets were retained for the final calculation, whereas the titration 6 data were omitted.

The final parameter set, including the optimized coefficients for the polynomial model and for the Wagner-Schottky model, is listed in Table 5-11. The calculated fit to the solid AlSb g^M_{Al} data, shown in Figure 5-17, matches the data from titrations 1 and 4 (Cell 11) quite well. The predicted solidus line (Figure 5-18) gives a homogeneity width of 0.0018 mole fraction at 848 °C, which is within the range of 0.0014 to 0.0020 mole fraction obtained from the various data sets in this study. Further modeling of the AlSb phase will require more extensive data for the homogeneity region.

Comparison with previous calculations

Several calculated descriptions of the Al-Sb system have been reported previously in the literature. Most of these have employed regular-solution type polynomial models. The authors, along with some of their phase diagram results, are listed in Table 5-12. The first three calculations [72Pan, 79Jou, 81Kau] yielded a T_m value of 1065 °C, as first estimated by

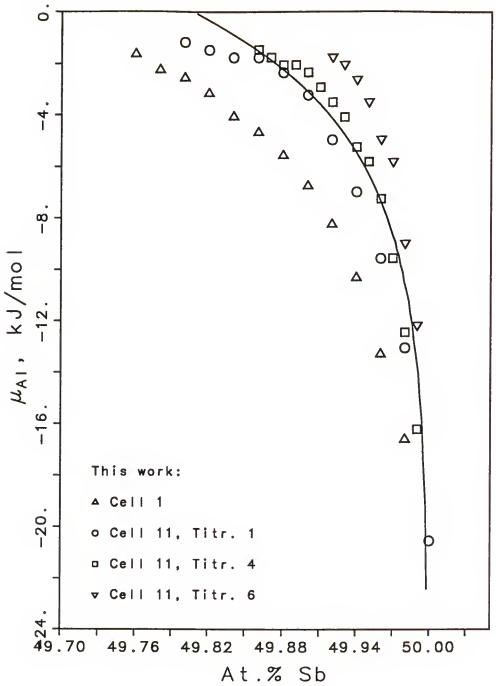

Figure 5-17

Calculated g_{Al}^{M} vs. composition for the AlSb compound at 848 °C. The experimental data have been adjusted to 848 °C, using the temperature dependence for g_{Al}^{M} determined by the calculation. Wagner-Schottky and Redlich-Kister polynomial models used in the calculation.

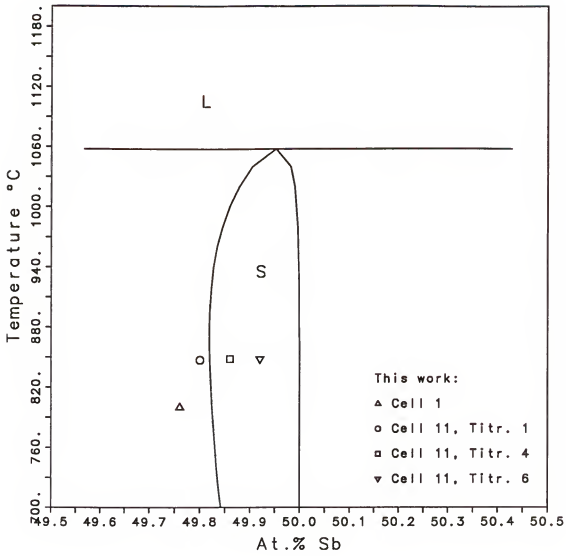

Figure 5-18

Enlargement of the Al-Sb phase diagram in the AlSb solid region, showing the solidus line calculated from the Wagner-Schottky model and the experimental solidus data.

Table 5-11
Thermodynamic description of the Al-Sb system, using the Wagner-Schottky model for the AlSb solid and the polynomial model for the liquid.

Phase stabilities of the elements (from [86Sau, 88Sau]):

		Multipliers	
Phase	Element	1	$-T$
liquid	Al	10711	11.473
liquid	Sb	19874	21.985
solid	Al	0	0
solid	Sb	0	0

Excess terms of the liquid phase (Redlich-Kister polynomial):

	T-Multipliers		
x-Multipliers	1	$-T$	$T(1-\ln T)$
$x_{Sb}\ (1-x_{Sb})$	-41544.6	-162.6317	22.67726
$x_{Sb}\ (1-x_{Sb})\ (1-2x_{Sb})$	5847.6	-1.78843	0
$x_{Sb}\ (1-x_{Sb})\ (1-2x_{Sb})^2$	16435.4	8.87467	0

Excess terms of the AlSb phase (Wagner-Schottky model), referred to the pure solid elements:

	T-Multipliers			
n-Multipliers	1	$-T$	$T(1-\ln T)$	$-T^2/2$
$(1+n_{10})$	-24533.6	-6.72908	0.826012	-0.0053560
n_{10}	200000.0	0	0	0
n_{21}	85893.1	0	0	0

Notes:

- All values are in J/g-at and K
- The given multipliers belong to the integral Gibbs energy
- n_{ij} represents the moles of defect species j on sublattice i, in one mole of atoms
- The values adjusted by the least squares method are underlined

Hansen and Anderko [58Han], and in each case one of the calculated eutectic temperatures is too low. Joullie *et al.* [79Jou] had some success in fitting the high degree of asymmetry in the liquidus by using the ideal solution model on the Al side and the regular solution model on the Sb side.

McAlister's description of the Al-Sb system [84McA] was the first to invoke the use of available thermodynamic data in addition to phase diagram data in the calculation. He used the Legendre polynomial to describe the liquid phase and obtained an excellent fit to

Table 5-12
Comparison of calculated descriptions of the Al-Sb system.

Reference	Model	# of excess terms	T_m (°C)	T_{cut} (°C) Al-AlSb	Sb-AlSb
[72Pan]	quasi-reg.	1	1065	*ca.* 625	–
[79Jou]	reg./ideal	1/0	1065	650	624
[81Kau]	polynomial	2	1065	660	612
[84McA]	polynomial	4	1058	657	627
[85Cha]	NRTL	2	> 1065	–	–
This work	polynomial	3	1058	658	624
This work	associate	3	1060	655	624

the phase diagram data. Unfortunately, no liquid-phase ΔH_{mix} or emf data were available to be assessed or fitted at that time.

In the work of Chang [85Cha], seven different models were used to describe the Al-Sb system. While the Non-Random Two-Liquid model [68Ren] was found to best fit the various types of data, even this description was unable to fit the asymmetry of the liquidus. The most probable source of difficulty in the study is the fact that the data of Predel and Schallner [69Pre2] were chosen to represent the ΔH_{mix} and g^M_{Al} values in the selected data set; these values, as has been shown above, are not consistent with the phase diagram data.

In the present work, the Redlich-Kister polynomial has been used successfully to fit a more complete data set for the Al-Sb system. In addition, the system has been described for the first time using the associate model, with similar success. Modeling of the homogeneity region with the Wagner-Schottky model gave results that were consistent with the AlSb solid data and with the description of the rest of the Al-Sb system.

CHAPTER VI

EXTRAPOLATION AND OPTIMIZATION OF THE Al-In-Sb SYSTEM

Introduction

The calculation of ternary phase diagrams and thermodynamic properties starts with the descriptions for the component binary systems. For ternary systems which exhibit non-ideal behavior, ternary parameters are often needed to adequately describe the system; these can be fitted to experimental data where available.

In the present work, two calculated descriptions of the Al-In-Sb ternary have been obtained. The first was derived from extrapolation of the three binary systems, Al-In, Al-Sb and In-Sb. The descriptions of the Al-In and Al-Sb systems presented in Chapter V were used, and for the In-Sb system, the polynomial description was taken from the work of Sharma *et al.* [87Sha]. The second ternary calculation was obtained by starting with the binaries and optimizing the available ternary data to obtain two ternary parameters.

Experimental Data

Most of the experimental data available for the Al-In-Sb system are solidus and liquidus data for the AlSb-InSb quasibinary section of the phase diagram. Liquidus data are reported by Koster and Thoma [55Kos], solidus data by Woolley and Smith [58Woo], and Goryunova [65Gor] and Ishida *et al.* [88Ish] report both liquidus and solidus data for the quasibinary. These data are generally in good agreement. Ishida *et al.* [88Ish] have also measured a large

number of liquidus data across the composition range in the ternary. Enthalpy of mixing data in the liquid phase have been obtained by Gerdes and Predel [79Ger].

Results and Discussion

Extrapolation from the Binary Subsystems

The In-Sb system has been thoroughly studied, and the description of the In-Sb system given by Sharma *et al.* [87Sha] matches the experimental data very well. They used the quasi sub-subregular solution model, which is equivalent to a three-term form of the Redlich-Kister polynomial. In order to use this description in the Lukas program, the parameters were merely transformed algebraically to match the Redlich-Kister formalism. The resulting parameter set yielded plots identical to those reported by Sharma *et al.* [87Sha]. Figure 6-1 shows the calculated phase diagram for the In-Sb system. Plots of ΔH_{mix} vs. composition (at.% Sb) and g_{In}^{M} vs. composition are given in Figures 6-2 and 6-3, respectively. Experimental data from the selected data set of Sharma *et al.* are included in the figures.

The transformed In-Sb parameters of Sharma *et al.* [87Sha] were combined with the Redlich-Kister parameters obtained in the present study for the Al-In and Al-Sb systems to give the ternary parameter set. For the extrapolation of the liquid phase, Muggianu's formula was used:

$$G = \sum_{i=1}^{3}\{x_i G_i^0 + RT\, x_i \ln x_i + x_i\, x_j \sum_{\nu=0}^{n_{ij}} L_{ij}^{(\nu)} (x_i - x_j)^{\nu}\} \qquad (6-1)$$

The continuous solid solution of the semistoichiometric (Al,In)Sb compound was assumed to be ideal:

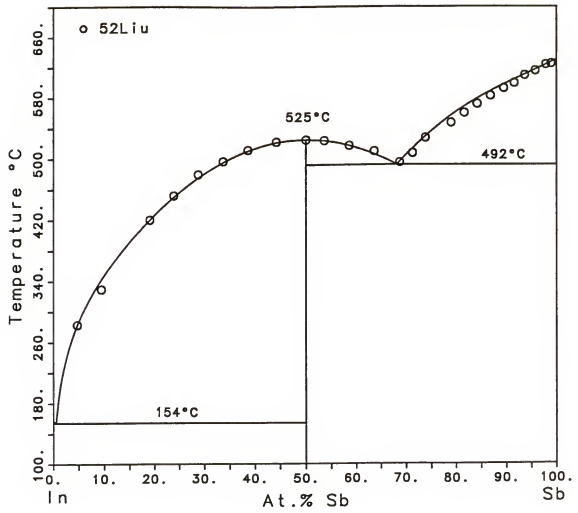

Figure 6-1

Calculated phase diagram for the In-Sb system, using polynomial description from assessment work of Sharma *et al.* [87Sha].

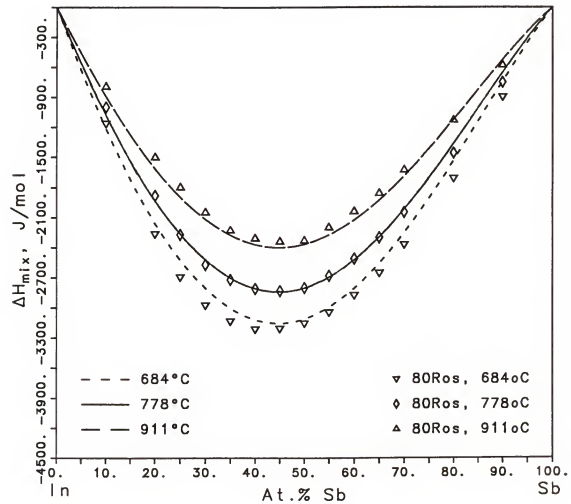

Figure 6-2

Calculated enthalpy of mixing vs. composition for the In-Sb system, using polynomial description from assessment work of Sharma *et al.* [87Sha].

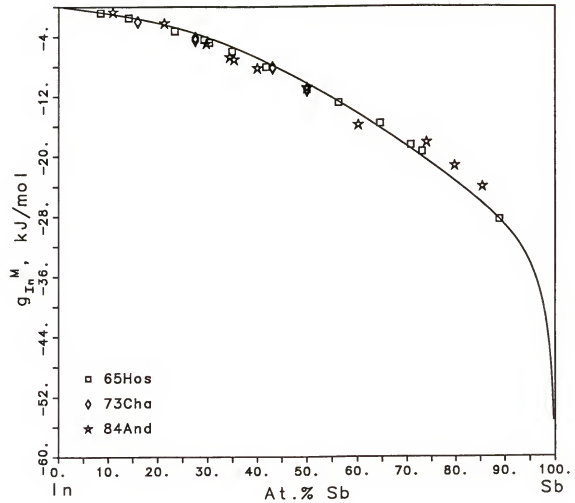

Figure 6-3

Calculated partial In Gibbs energy vs. composition for the In-Sb system, using polynomial description from assessment work of Sharma *et al.* [87Sha].

$$G = \sum_{i=1}^{3} (x_i G_i^0) \; + \; RT\{x_{Al} \ln(2x_{Al}) + x_{In} \ln(2x_{In})\} + 2x_{Al} G'_{AlSb} + 2x_{In} G'_{InSb} \qquad (6-2)$$

Calculation of the Al-In-Sb ternary using only the component binary parameters gave a very reasonable match to the experimental ternary data. The quasibinary section is shown in Figure 6-4, and the calculated lines match the data very well; only the calculated liquidus is a bit high on the InSb-rich side. The ternary liquidus data of Ishida *et al.* [88Ish] are shown in Figure 6-5, along with calculated liquidus lines at 700, 800, 900 and 1000 °C. The lines fall somewhat to the right of the experimental data, but the general agreement is good.

The calculated isothermal sections for 800 °C and 700 °C are shown individually in Figures 6-6 and 6-7, respectively. Included are tie lines within the two-phase regions. The isothermal section at 700 °C (Figure 6-7) also shows a three-phase region, outlined by the small triangle, which represents two liquid phases in equilibrium with the (Al,In)Sb solid phase.

The liquid-phase enthalpy of mixing curve calculated for the quasibinary liquid is less exothermic than the data of Gerdes and Predel [79Ger], but it manifests a similar shape and shows the same positive deviation from ideality as do the experimental data (see Figure 6-8). Note that the representation of the data in Figure 6-8 was accomplished by adding the linearly interpolated mixing enthalpies of the binary melts. This was necessary since Gerdes and Predel reported only the difference in mixing enthalpy, $\delta(\Delta H_{mix})$, between the ternary ΔH_{mix} and the ΔH_{mix} interpolated linearly between the binary ΔH_{mix} values.

Ternary Optimization

To fit parameters to the ternary Al-In-Sb data, the Lukas optimization program [77Luk] was used. The Redlich-Kister polynomial was again used to describe the liquid phase and was also employed to model the continuous solution of the semistoichiometric solid phase.

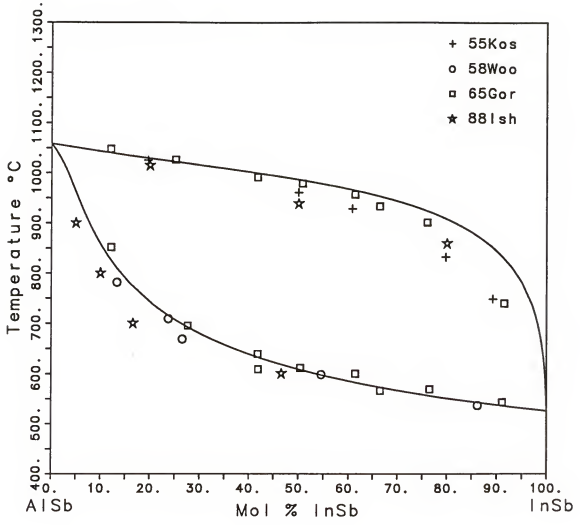

Figure 6-4

Calculated liquidus and solidus curves for the AlSb-InSb quasibinary system, with experimental quasibinary data. Calculated description obtained from extrapolation of the binary subsystems.

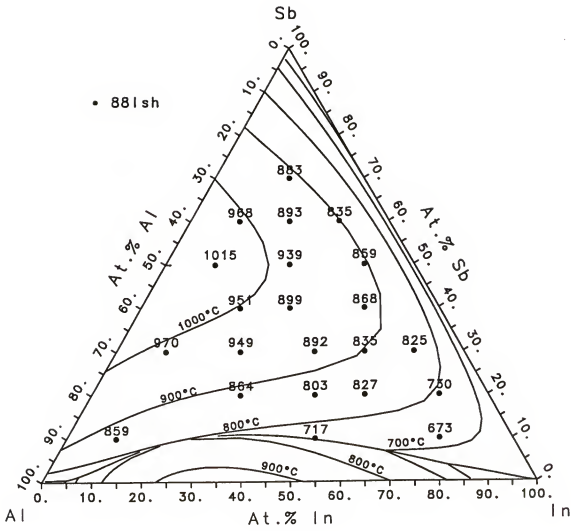

Figure 6-5

Calculated liquidus isotherms for the Al-In-Sb system, with experimental liquidus data. Calculated description obtained from extrapolation of the binary subsystems.

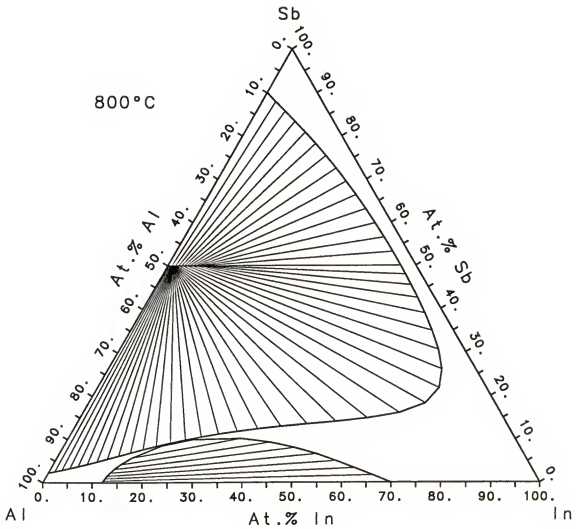

Figure 6-6

Isothermal section for the Al-In-Sb system at 800 °C. Calculated description obtained from extrapolation of the binary subsystems.

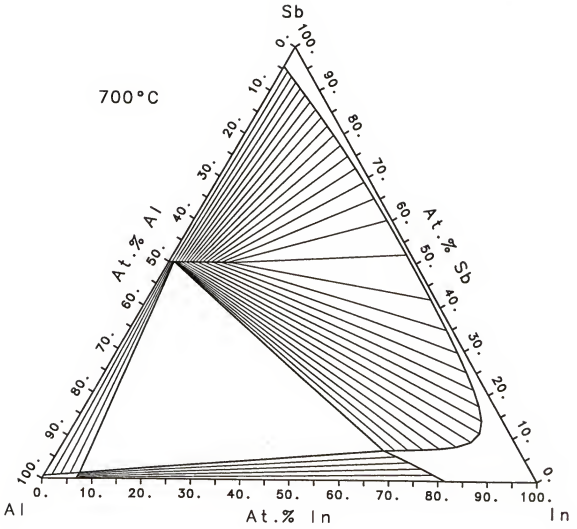

Figure 6-7

Isothermal section for the Al-In-Sb system at 700 °C. Calculated description obtained from extrapolation of the binary subsystems.

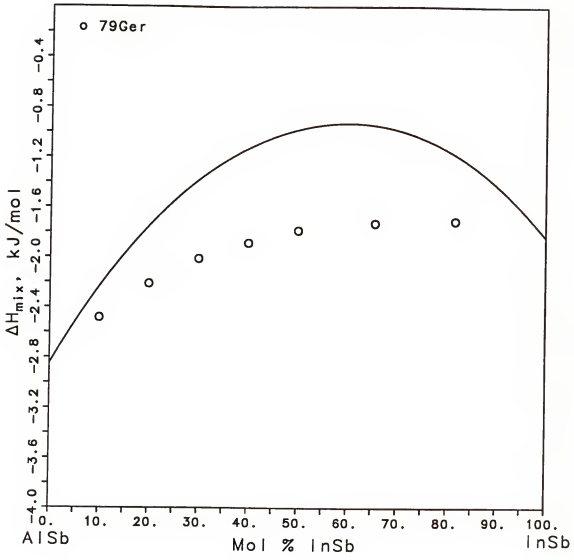

Figure 6-8

Calculated enthalpy of mixing vs. composition for the quasibinary liquid, with experimental data. Calculated description obtained from extrapolation of the binary subsystems.

This involved adding the terms, $x_{Al}x_{In}x_{Sb}H_l^E$ and $x_{Al}x_{In}H_S^E$, to Equations (6-1) and (6-2), respectively. It was found that these two ternary parameters, one for the liquid phase and one for the solid phase, were sufficient for completing the parameter set to describe the Al-In-Sb ternary. The following values for the ternary parameters were obtained from the optimization:

Al-In-Sb liquid: $H_l^E = -25536.6\ J/mol$

(Al,In)Sb solid: $H_S^E = 3800.98\ J/g-at$

Addition of these two parameters to the parameter set for the Al-In-Sb ternary improved the fit of the calculated description to all of the experimental data. The calculated quasibinary phase diagram, shown in Figure 6-9, matches the experimental data very well. Since the data show a certain amount of scatter among themselves, the passage of the calculated lines through the intermediate values is the best fit under the circumstances.

The fit of the calculated liquidus lines to the data of Ishida *et al.* [88Ish], shown in Figure 6-10, is an improvement over the fit from the binary extrapolation (Figure 6-5). Again, the experimental data exhibit some inherent scatter (see, for example, the points at 803 °C and 827 °C, which seem in reverse order), and the calculated fit would therefore be hard to improve upon. The 800 °C and 700 °C isotherms from the optimized calculation are given in Figures 6-11 and 6-12. It can be seen that the three-phase region predicted from the optimized calculation is smaller than that predicted from the binary extrapolation (compare Figures 6-12 and 6-7).

Use of the ternary parameters in the description of the Al-In-Sb system gave an excellent fit to the liquid enthalpy of mixing data of Gerdes and Predel [79Ger]. This is illustrated in Figure 6-13.

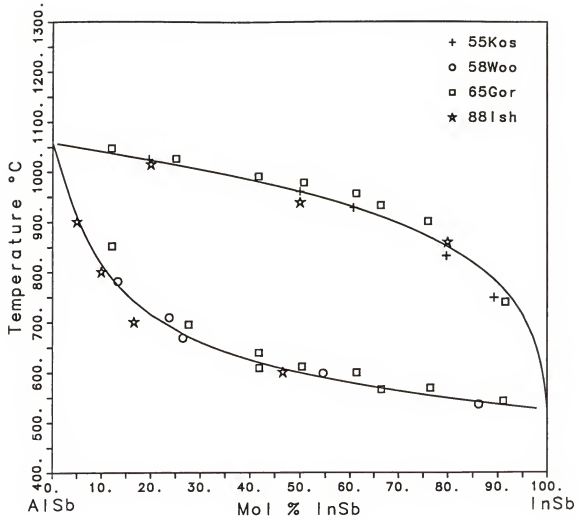

Figure 6-9

Calculated liquidus and solidus curves for the AlSb-InSb quasibinary system, with experimental quasibinary data. Calculated description obtained from optimization of the ternary data.

Comparison with Previous Calculations

Most of the calculated descriptions for the Al-In-Sb system have focussed on the quasibinary phase diagram. Many authors have used ideal, simple, regular or quasiregular solution models to describe the liquid and solid phases, with moderate success. Use of the ideal solution model for the solid phase [70Ste], for the liquid phase [74Bre], or for both phases [85Cha] gave solidus and liquidus curves that were fairly near the experimental data. Use of the simple solution model [85Cha], the regular solution model [72Str, 85Cha, 88Ish] or the quasiregular solution model [74Bre] generally improved the fit to the experimental data.

Chang, in testing several combinations of models for the solid and liquid phases of the Al-In-Sb system, found the best fit using the NRTL model for the liquid phase and the simple solution model for the solid phase [85Cha]. He obtained a good fit to the available quasibinary phase diagram data [55Kos, 58Woo, 65Gor] and also to the quasibinary liquid enthalpy of mixing data of Gerdes and Predel [79Ger]. However, his description of the Al-In-Sb ternary is bound to be hampered by his overly symmetrical description of the Al-In binary (see Chapter V).

Ishida *et al.* [88Ish] modeled the Al-In-Sb system using the regular solution model for the liquid phase and the two-sublattice model for the solid phase. Their fit of the quasibinary phase diagram is good, especially for the solidus data. They have also calculated liquidus isotherms, which compare reasonably well with their liquidus data across the ternary composition field. Their fit is comparable to the one obtained in the present study using ternary parameters. However, their isothermal section calculated for 800 °C shows a much smaller liquid-liquid, two-phase region than the one predicted in the present study (Figure 6-11). This is undoubtedly due to their adoption of the description of Ansara *et al.* [78Ans] for the Al-In binary system, wherein a critical temperature of 854 °C for the Al-In

miscibility gap was obtained. Since the description for the Al-In binary obtained in the present study gives a critical temperature of 934 °C, it is to be expected that this binary description will produce a larger miscibility gap in the ternary system, as well.

To determine the actual extent of the liquid-liquid miscibility gap in the Al-In-Sb system, liquid-phase ternary data in this region are needed. However, even binary data for the Al-In critical region would be very useful. Further data for the quasibinary liquidus and solidus are also needed, since the data currently available present a fair amount of scatter. Even the recent data of Ishida *et al.* [88Ish] do not seem to be significantly smoother than those of the earlier authors (see Figure 6-9), nor are they plentiful enough to constitute a definitive data set.

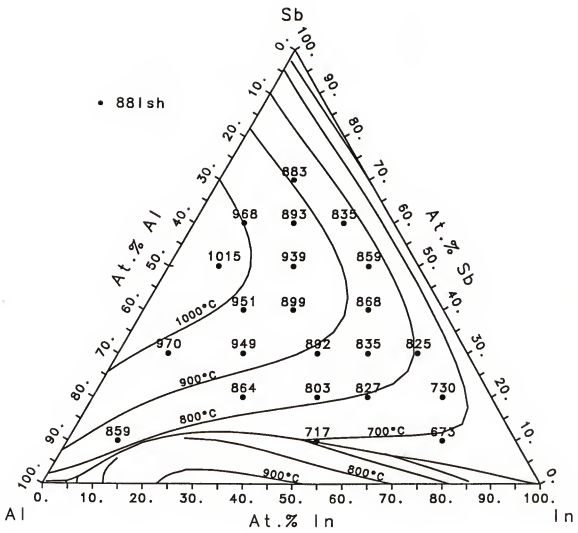

Figure 6-10

Calculated liquidus isotherms for the Al-In-Sb system, with experimental liquidus data. Calculated description obtained from optimization of the ternary data.

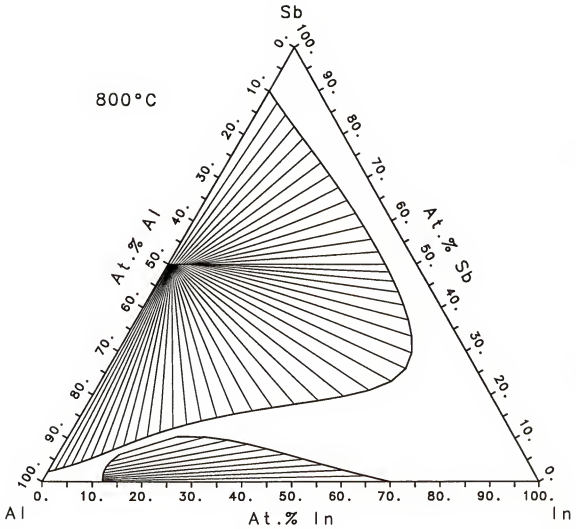

Figure 6-11

Isothermal section for the Al-In-Sb system at 800 °C. Calculated description obtained from optimization of the ternary data.

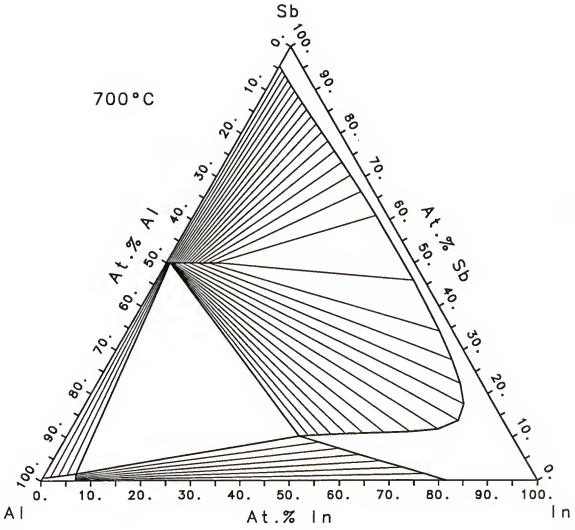

Figure 6-12

Isothermal section for the Al-In-Sb system at 700 °C. Calculated description obtained from optimization of the ternary data.

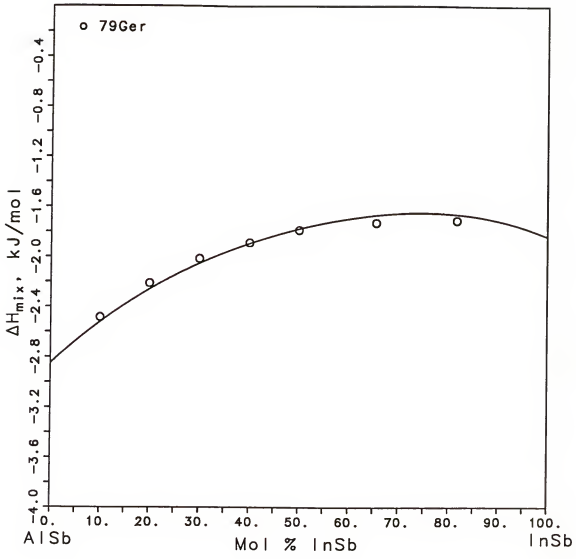

Figure 6-13

Calculated enthalpy of mixing vs. composition for the quasibinary liquid, with experimental data. Calculated description obtained from optimization of the ternary data.

CHAPTER VII

SUMMARY AND CONCLUSIONS

1. Thermodynamic data for the Al-In and Al-Sb systems were obtained using the coulometric titration technique on solid electrolyte galvanic cells. The emf data obtained for both systems match closely previous work in the literature.
2. From the emf study of the Al-Sb system, liquidus points were determined for three temperatures, 806 °C, 846 °C and 875 °C. They are in excellent agreement with phase diagram data reported by other authors.
3. The Gibbs energy of formation of the AlSb compound, calculated from the emf data, matches the value reported by Samokhval and Vecher [68Sam] within 3%.
4. The width of the homogeneity region in AlSb has been measured for the first time, by means of coulometric titration. At 846 °C, the compound width is about 0.002 mole fraction. The deviation from stoichiometry in the compound was determined to occur primarily on the Al-rich side.
5. Careful evaluation of the Al-In literature data yielded a very consistent data set. Use of this selected data set in the model description of the Al-In system gave an excellent fit to the phase diagram data and to the thermodynamic data. A critical temperature of 936 °C was calculated for the miscibility gap.

6. Optimization of the Al-Sb system was carried out using both the Redlich-kister polynomial model and the associated solution model to describe the liquid phase. While the Al-Sb data were successfully fitted with each model, the polynomial model gave somewhat better results.

7. Optimization of the Al-Sb system using the Wagner-Schottky model to describe the AlSb homogeneity region indicated that the assumption of Al_{Sb} and V_{Al} as the primary defects was consistent with the emf results obtained for the compound in this study.

8. Calculation of the Al-In-Sb ternary from the binary descriptions gave very good results. The match to the quasibinary data from the literature was especially close.

9. The optimization of the available Al-In-Sb ternary data yielded two ternary parameters, which gave an excellent fit to all of the ternary data.

10. The emf data obtained in this study and the assessment and calculation of the Al-In and Al-Sb binaries have all contributed to an improved characterization of the Al-In-Sb ternary system.

11. Recommendations for future experimental work on III-V systems using solid-electrolyte galvanic cells are contingent upon overcoming a number of experimental difficulties.

    (a) Achievement of greater precision (*e.g.* to 0.01 mV) in the emf measurements would allow data at higher x_{Al} values to be measured. For the Al-In system, this could provide further information on the miscibility gap.

    (b) Extension of the experimentally accessible temperature range to temperatures higher than 900 °C would allow the AlSb solidus to be outlined over a greater temperature range.

(c) Once thin films of AlSb are obtained for the working electrode in the solid-electrolyte galvanic cells, transient emf techniques can be used to determine the diffusion coefficient of Al in AlSb.

(d) If GaF_3 can be combined with CaF_2 to form a mixed salt analogous to the AlF_3-CaF_2 salt used in the present study, the Ga-Sb system could also be studied using solid-electrolyte galvanic cells.

12. Future assessment work upon the Al-In-Sb system is contingent on more data being obtained for the Al-In-Sb ternary or its binary subsystems. Reliable data for the miscibility gap in the Al-In system and for the liquid-phase enthalpy of mixing in the Al-Sb system are particularly needed.

APPENDIX A

EXPERIMENTAL DATA FOR THE Al-In SYSTEM

Emf versus x_{Al} Data

Coulometric titrations on the liquid Al-In system were performed at three temperatures. The emf data obtained from Cell 57 are shown in Tables A-1 to A-3, for $T = 850$, 875 and 900 °C, respectively. They span the x_{Al} range 0 to 0.05. The unadjusted emf data for Cell 59 are tabulated in the next three tables, A-4 to A-6, for the same temperatures. The x_{Al} range for Cell 59 was 0 to 0.20 mole fraction.

The titration curves at 850 °C for Cell 57 and for Cell 59, unadjusted, are shown in Figure A-1. The Cell 59 data exhibit a hump between $x_{Al} = 0.01$ and $x_{Al} = 0.04$, which was caused by emf drift in this region. By removing the five Cell 59 data points denoted by the solid black squares in Figure A-1 and shifting the Cell 59 data at larger x_{Al} values to the left until they coincided with the Cell 57 data, a set of data for Cell 59 which is adjusted to match the Cell 57 data was obtained. The match is excellent, as shown in Figure A-2. Table A-7 shows the x_{Al} shift, Δx_{Al}, required to adjust the Cell 59 data at each temperature investigated. It can be seen that the adjustment becomes smaller with increasing temperature.

Table A-1
Emf vs. x_{Al} data for the Al-In system at 850 °C. E is the net cell emf, E_I - E_{II}.

$E_{II} = 0.4257$ V

Q(C)	x_{Al}	E_I (V)	E (V)
0.000000	0.00000	0.665	0.239
0.001999	0.00006	0.646	0.220
0.005023	0.00014	0.631	0.205
0.01066	0.00030	0.6150	0.1893
0.01785	0.00050	0.6016	0.1759
0.02504	0.00071	0.5933	0.1676
0.03584	0.00101	0.5825	0.1568
0.05404	0.00152	0.5705	0.1448
0.07236	0.00204	0.5623	0.1366
0.1067	0.00300	0.5522	0.1265
0.1782	0.00500	0.5371	0.1114
0.2500	0.00700	0.5282	0.1025
0.3583	0.01000	0.5189	0.0932
0.5404	0.01501	0.5063	0.0806
0.7239	0.02000	0.4974	0.0717
1.097	0.03000	0.4831	0.0574
1.478	0.04000	0.4729	0.0472
1.867	0.05000	0.4657	0.0400

Emf versus T Data

The emf vs. T data obtained for the liquid Al-In system, shown graphically in Figure 3-4, is tabulated Tables A-8 to A-11. Data at $x_{Al} = 0.03$ and 0.05 were obtained in Cell 57, and data at $x_{Al} = 0.093$ and 0.180 (adjusted values) were obtained in Cell 59.

Table A-2
Emf vs. x_{Al} data for the Al-In system at 875 °C. E is the net cell emf, E_I - E_{II}.

$E_{II} = 0.4176$ V

Q(C)	x_{Al}	E_I (V)	E (V)
0.000000	0.00000	0.685	0.267
0.002031	0.00006	0.655	0.237
0.005031	0.00014	0.6334	0.2158
0.01003	0.00028	0.6149	0.1973
0.01781	0.00050	0.5989	0.1813
0.02502	0.00070	0.5889	0.1713
0.03583	0.00101	0.5783	0.1607
0.05403	0.00152	0.5660	0.1484
0.07235	0.00204	0.5572	0.1396
0.1067	0.00300	0.5453	0.1277
0.1782	0.00500	0.5297	0.1121
0.2500	0.00700	0.5195	0.1019
0.3583	0.01000	0.5103	0.0927
0.5404	0.01501	0.5007	0.0831
0.7239	0.02000	0.4916	0.0740
1.097	0.03000	0.4767	0.0591
1.478	0.04000	0.4667	0.0491
1.867	0.05000	0.4595	0.0419

Table A-3
Emf vs. x_{Al} data for the Al-In system at 900 °C. E is the net cell emf, E_I - E_{II}.

$E_{II} = 0.4096$ V

Q(C)	x_{Al}	E_I (V)	E (V)
0.000000	0.00000	0.680	0.270
0.002042	0.00006	0.648	0.238
0.005000	0.00014	0.6266	0.2170
0.01002	0.00028	0.6082	0.1986
0.01784	0.00050	0.5919	0.1823
0.02504	0.00071	0.5819	0.1723
0.03584	0.00101	0.5713	0.1617
0.05404	0.00152	0.5593	0.1497
0.07236	0.00204	0.5505	0.1409
0.1067	0.00300	0.5392	0.1296
0.1782	0.00500	0.5236	0.1140
0.25002	0.00700	0.5138	0.1042
0.3583	0.01000	0.5040	0.0944
0.5404	0.01501	0.4931	0.0835
0.7239	0.02000	0.4843	0.0747
1.097	0.03000	0.4693	0.0597

Table A-4
Emf vs. x_{Al} data for the Al-In system at 850 °C. E is the net cell emf, E_I - E_{II}.

$E_{II} = 0.4257$ V

Q(C)	x_{Al}	E_I (V)	E (V)
0.000000	0.00000	0.675	0.249
0.005018	0.00057	0.6095	0.1838
0.008856	0.00101	0.5922	0.1665
0.02583	0.00295	0.5579	0.1322
0.06152	0.00700	0.5302	0.1045
0.08812	0.01000	0.5214	0.0957
0.1328	0.01500	0.5159	0.0902
0.1780	0.02000	0.5140	0.0883
0.2237	0.02500	0.5090	0.0833
0.2698	0.03000	0.5053	0.0796
0.3164	0.03500	0.5013	0.0756
0.3634	0.04000	0.4940	0.0683
0.4110	0.04500	0.4878	0.0621
0.4591	0.05000	0.4821	0.0564
0.5568	0.06000	0.4730	0.0473
0.7585	0.08000	0.4601	0.0344
0.9692	0.1000	0.4524	0.0267
1.189	0.1200	0.4465	0.0208
1.539	0.1500	0.4407	0.0150
1.850	0.1750	0.4375	0.0118
2.181	0.2000	0.4355	0.0098

Table A-5
Emf vs. x_{Al} data for the Al-In system at 875 °C. E is the net cell emf, E_I - E_{II}.

$E_{II} = 0.4176$ V

Q(C)	x_{Al}	E_I (V)	E (V)
0.000000	0.00000	0.665	0.247
0.005043	0.00058	0.5989	0.1813
0.008918	0.00102	0.5812	0.1636
0.02624	0.00300	0.5476	0.1300
0.06148	0.00700	0.5205	0.1029
0.08813	0.01000	0.5108	0.0932
0.1328	0.01500	0.5043	0.0867
0.1780	0.02000	0.5011	0.0835
0.2237	0.02500	0.4949	0.0773
0.2698	0.03000	0.4875	0.0699
0.3164	0.03500	0.4803	0.0627
0.3634	0.04000	0.4744	0.0568
0.4110	0.04500	0.4690	0.0514
0.4591	0.05000	0.4648	0.0472
0.5568	0.06000	0.4578	0.0402
0.7585	0.08000	0.4484	0.0308
0.9692	0.1000	0.4420	0.0244
1.189	0.1200	0.4375	0.0199
1.539	0.1500	0.4324	0.0148
1.850	0.1750	0.4299	0.0123
2.181	0.2000	0.4284	0.0108

Table A-6
Emf vs. x_{Al} data for the Al-In system at 900 °C. E is the net cell emf, E_I - E_{II}.

$E_{II} = 0.4096$ V

Q(C)	x_{Al}	E_I (V)	E (V)
0.000000	0.00000	0.685	0.275
0.002961	0.00034	0.617	0.207
0.005072	0.00058	0.5988	0.1892
0.008851	0.00101	0.5799	0.1703
0.02626	0.00300	0.5441	0.1345
0.06147	0.00700	0.5166	0.1070
0.08814	0.01000	0.5052	0.0956
0.1328	0.01500	0.4983	0.0887
0.1780	0.02000	0.4950	0.0854
0.2237	0.02500	0.4870	0.0774
0.2698	0.03000	0.4780	0.0684
0.3164	0.03500	0.4706	0.0610
0.3634	0.04000	0.4646	0.0550
0.4110	0.04500	0.4596	0.0500
0.4591	0.05000	0.4557	0.0461
0.5568	0.06000	0.4491	0.0395
0.7585	0.08000	0.4397	0.0301
0.9692	0.1000	0.4332	0.0236
1.189	0.1200	0.4289	0.0193
1.539	0.1500	0.4240	0.0144
1.850	0.1750	0.4213	0.0117
2.180	0.2000	0.4191	0.0095

Table A-7
x_{Al} shift, Δx_{Al}, required to adjust Cell 59 data at each temperature investigated.

T (°C)	Δx_{Al}
850	-0.0200
875	-0.0073
900	-0.0070

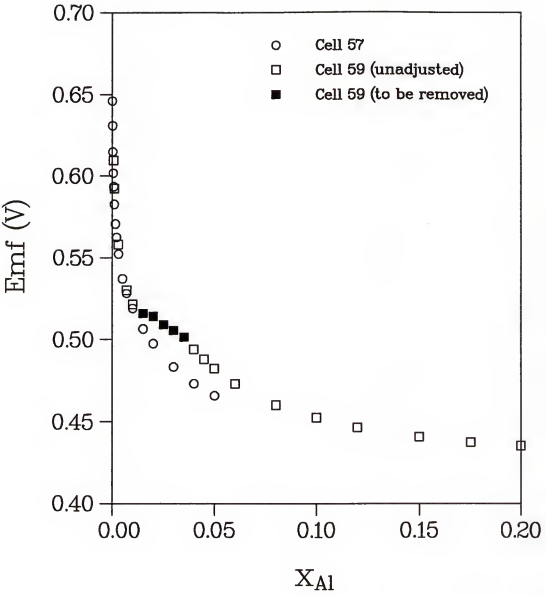

Figure A-1

Titration curves for liquid Al-In at 850 °C:
Cell 57 data and Cell 59 unadjusted data.

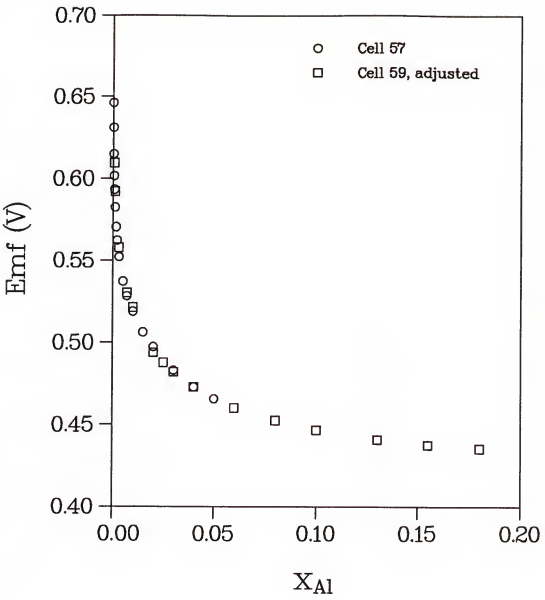

Figure A-2

Titration curves for liquid Al-In at 850 °C:
Cell 57 data and Cell 59 adjusted data.

Table A-8

Emf vs. T data for the Al-In system at $x_{Al} = 0.03$
(Cell 57). E is the net cell emf, E_I - E_{II}.

$$E_{II}\ (V) = (-0.0003215)\ T\ (°C) + (0.6989)$$

T (°C)	E_I (V)	E_{II} (V)	E (V)
850	0.4795	0.4257	0.0538
851	0.4793	0.4254	0.0539
852	0.4792	0.4250	0.0542
853	0.4790	0.4247	0.0543
854	0.4788	0.4244	0.0544
855	0.4786	0.4241	0.0545
856	0.4784	0.4238	0.0546
857	0.4782	0.4234	0.0548
858	0.4780	0.4231	0.0549
859	0.4778	0.4228	0.0550
860	0.4776	0.4225	0.0551
861	0.4774	0.4221	0.0553
862	0.4772	0.4218	0.0554
863	0.4770	0.4215	0.0555
864	0.4768	0.4212	0.0556
865	0.4766	0.4209	0.0557
866	0.4764	0.4205	0.0559
867	0.4762	0.4202	0.0560
868	0.4761	0.4199	0.0562
869	0.4759	0.4196	0.0563
870	0.4757	0.4192	0.0565
871	0.4754	0.4189	0.0565
872	0.4752	0.4186	0.0566
873	0.4750	0.4183	0.0567
874	0.4748	0.4180	0.0568

Table A-8, continued

Emf vs. T data for the Al-In system at $x_{Al} = 0.03$ (Cell 57). E is the net cell emf, E_I - E_{II}.

$$E_{II}\ (V) = (-0.0003215)\ T\ (°C) + (0.6989)$$

T (°C)	E_I (V)	E_{II} (V)	E (V)
875	0.4746	0.4176	0.0570
876	0.4744	0.4173	0.0571
877	0.4743	0.4170	0.0573
878	0.4740	0.4167	0.0573
879	0.4738	0.4164	0.0574
880	0.4736	0.4160	0.0576
881	0.4734	0.4157	0.0577
882	0.4732	0.4154	0.0578
883	0.4730	0.4151	0.0579
884	0.4728	0.4147	0.0581
885	0.4727	0.4144	0.0583
886	0.4724	0.4141	0.0583
887	0.4721	0.4138	0.0583
888	0.4719	0.4135	0.0584
889	0.4717	0.4131	0.0586
890	0.4715	0.4128	0.0587
891	0.4713	0.4125	0.0588
892	0.4711	0.4122	0.0589
893	0.4709	0.4119	0.0590
894	0.4707	0.4115	0.0592
895	0.4705	0.4112	0.0593
896	0.4703	0.4109	0.0594
897	0.4702	0.4106	0.0596
898	0.4700	0.4102	0.0598
899	0.4698	0.4099	0.0599
900	0.4696	0.4096	0.0600
901	0.4695	0.4093	0.0602

Table A-9

Emf vs. T data for the Al-In system at $x_{Al} = 0.05$
(Cell 57). E is the net cell emf, E_I - E_{II}.

$$E_{II}\ (V) = (-0.0003215)\ T\ (°C) + (0.6989)$$

T (°C)	E_I (V)	E_{II} (V)	E (V)
850	0.4659	0.4257	0.0402
851	0.4659	0.4254	0.0405
852	0.4657	0.4250	0.0407
853	0.4655	0.4247	0.0408
854	0.4653	0.4244	0.0409
855	0.4651	0.4241	0.0410
856	0.4649	0.4238	0.0411
857	0.4647	0.4234	0.0413
858	0.4644	0.4231	0.0413
859	0.4642	0.4228	0.0414
860	0.4640	0.4225	0.0415
861	0.4637	0.4221	0.0416
862	0.4635	0.4218	0.0417
863	0.4633	0.4215	0.0418
864	0.4631	0.4212	0.0419
865	0.4629	0.4209	0.0420
866	0.4627	0.4205	0.0422
867	0.4625	0.4202	0.0423
868	0.4623	0.4199	0.0424
869	0.4621	0.4196	0.0425
870	0.4619	0.4192	0.0427
871	0.4616	0.4189	0.0427
872	0.4614	0.4186	0.0428
873	0.4612	0.4183	0.0429
874	0.4610	0.4180	0.0430
875	0.4607	0.4176	0.0431

Table A-9, continued

Emf vs. T data for the Al-In system at $x_{Al} = 0.05$ (Cell 57). E is the net cell emf, E_I - E_{II}.

$$E_{II}\ (V) = (-0.0003215)\ T\ (°C) + (0.6989)$$

T (°C)	E_I (V)	E_{II} (V)	E (V)
875	0.4597	0.4176	0.0421
876	0.4594	0.4173	0.0421
877	0.4591	0.4170	0.0421
878	0.4589	0.4167	0.0422
879	0.4587	0.4164	0.0423
880	0.4585	0.4160	0.0425
881	0.4582	0.4157	0.0425
882	0.4580	0.4154	0.0426
883	0.4577	0.4151	0.0426
884	0.4575	0.4147	0.0428
885	0.4572	0.4144	0.0428
886	0.4570	0.4141	0.0429
887	0.4568	0.4138	0.0430
888	0.4566	0.4135	0.0431
889	0.4564	0.4131	0.0433
890	0.4562	0.4128	0.0434
891	0.4559	0.4125	0.0434
892	0.4557	0.4122	0.0435
893	0.4555	0.4119	0.0436
894	0.4552	0.4115	0.0437
895	0.4550	0.4112	0.0438
896	0.4547	0.4109	0.0438
897	0.4545	0.4106	0.0439
898	0.4542	0.4102	0.0440
899	0.4540	0.4099	0.0441
900	0.4537	0.4096	0.0441
901	0.4535	0.4093	0.0442

Table A-10

Emf vs. T data for the Al-In system at $x_{Al} = 0.093$ (Cell 59, adjusted). E is the net cell emf, E_I - E_{II}.

$$E_{II}\ (V) = (-0.0003215)\ T\ (°C) + (0.6989)$$

T (°C)	E_I (V)	E_{II} (V)	E (V)
850	0.4448	0.4257	0.0191
851	0.4446	0.4254	0.0192
852	0.4443	0.4250	0.0193
853	0.4441	0.4247	0.0194
854	0.4439	0.4244	0.0195
855	0.4436	0.4241	0.0195
856	0.4434	0.4238	0.0196
857	0.4432	0.4234	0.0198
858	0.4429	0.4231	0.0198
859	0.4427	0.4228	0.0199
860	0.4425	0.4225	0.0200
861	0.4422	0.4221	0.0201
862	0.4420	0.4218	0.0202
863	0.4417	0.4215	0.0202
864	0.4415	0.4212	0.0203
865	0.4412	0.4209	0.0203
866	0.4410	0.4205	0.0205
867	0.4407	0.4202	0.0205
868	0.4405	0.4199	0.0206
869	0.4403	0.4196	0.0207
870	0.4400	0.4192	0.0208
871	0.4397	0.4189	0.0208
872	0.4395	0.4186	0.0209
873	0.4393	0.4183	0.0210
874	0.4390	0.4180	0.0210
875	0.4388	0.4176	0.0212

Table A-10, continued

Emf vs. T data for the Al-In system at $x_{Al} = 0.093$ (Cell 59, adjusted). E is the net cell emf, E_I - E_{II}.

$$E_{II}\ (V) = (-0.0003215)\ T\ (°C) + (0.6989)$$

T (°C)	E_I (V)	E_{II} (V)	E (V)
876	0.4386	0.4173	0.0213
877	0.4383	0.4170	0.0213
878	0.4381	0.4167	0.0214
879	0.4378	0.4164	0.0214
880	0.4376	0.4160	0.0216
881	0.4373	0.4157	0.0216
882	0.4371	0.4154	0.0217
883	0.4368	0.4151	0.0217
884	0.4366	0.4147	0.0219
885	0.4363	0.4144	0.0219
886	0.4361	0.4141	0.0220
887	0.4359	0.4138	0.0221
888	0.4356	0.4135	0.0221
889	0.4354	0.4131	0.0223
890	0.4352	0.4128	0.0224
891	0.4350	0.4125	0.0225
892	0.4347	0.4122	0.0225
893	0.4344	0.4119	0.0225
894	0.4341	0.4115	0.0226
895	0.4338	0.4112	0.0226
896	0.4336	0.4109	0.0227
897	0.4334	0.4106	0.0228
898	0.4333	0.4102	0.0231
899	0.4331	0.4099	0.0232
900	0.4330	0.4096	0.0234

Table A-11

Emf vs. T data for the Al-In system at $x_{Al} = 0.18$ (Cell 59, adjusted). E is the net cell emf, E_I - E_{II}.

$$E_{II}\ (V) = (-0.0003215)\ T\ (°C) + (0.6989)$$

T (°C)	E_I (V)	E_{II} (V)	E (V)
850	0.4356	0.4257	0.0099
851	0.4355	0.4254	0.0101
852	0.4352	0.4250	0.0102
853	0.4350	0.4247	0.0103
854	0.4347	0.4244	0.0103
855	0.4345	0.4241	0.0104
856	0.4342	0.4238	0.0104
857	0.4339	0.4234	0.0105
858	0.4336	0.4231	0.0105
859	0.4334	0.4228	0.0106
860	0.4331	0.4225	0.0106
861	0.4329	0.4221	0.0108
862	0.4327	0.4218	0.0109
863	0.4324	0.4215	0.0109
864	0.4322	0.4212	0.0110
865	0.4319	0.4209	0.0110
866	0.4317	0.4205	0.0112
867	0.4314	0.4202	0.0112
868	0.4311	0.4199	0.0112
869	0.4309	0.4196	0.0113
870	0.4306	0.4192	0.0114
871	0.4304	0.4189	0.0115
872	0.4301	0.4186	0.0115
873	0.4298	0.4183	0.0115
874	0.4296	0.4180	0.0116
875	0.4293	0.4176	0.0117

APPENDIX B

EXPERIMENTAL ERRORS

Experimental errors for the variables measured in this study are shown in Table B-1 for the Al-In system. The errors on the thermodynamic quantities derived from the measured variables have been estimated as follows.

For variables calculated with equations involving addition or subtraction of input variables:

$$\sigma_{x+y} = \sqrt{\sigma_x^2 + \sigma_y^2}$$

where σ_i is the absolute error of variable i.

For variables calculated with equations involving multiplication or division of input variables:

$$\left(\frac{\sigma_{xy}}{xy}\right) = \sqrt{\left(\frac{\sigma_x}{x}\right)^2 + \left(\frac{\sigma_y}{y}\right)^2}$$

For variables calculated with equations involving more complex operations, such as exponentials or integrations, the errors were estimated by using the high and low values of the input variables and calculating the high and low values of the final variable.

The errors on the measured variables for the Al-Sb system are essentially the same as for the Al-In system, as are the estimated errors on the calculated variables.

Table B-1
Experimental errors for the Al-In system.

Variable	Symbol	Range of Values	Absolute Error	Relative Error
Mass of In in cell	m_{In}	0.0035 – 0.02 g	0.03 mg	0.2 – 0.9%
Temperature of the cell	T	1123 – 1173 K	1 K	0.1%
Charge passed	Q	0.005 – 2.0 C	10^{-7} – 10^{-3} C	0.01 – 0.1%
Emf of the alloy cell	E_I	0.4 – 0.7 V	0.1 mV	0.02%
Emf of the pure Al cell	E_{II}	0.40 – 0.43 V	0.2 mV	0.05%

Table B-2
Errors resulting from combined variables.

Variable	Equation	Relative Error
x_{Al}	$x_{Al} = \left(\frac{QM_{In}}{nF^2m_{In}}\right) / \left(1 + \frac{QM_{In}}{nF^2m_{In}}\right)$	0.9%
E	$E = E_I - E_{II}$	0.1 − 2%
g^M_{Al}	$g^M_{Al} = -nFE$	0.1 − 2%
a_{Al}	$a_{Al} = \exp\left[g^M_{Al}/RT\right]$	1%
γ_{Al}	$\gamma_{Al} = a_{Al}/x_{Al}$	1%
g^E_{Al}	$g^E_{Al} = RT\ln\gamma_{Al}$	1%
G^E	$G^E = (1-x_{Al})\int_0^{x_{Al}} \frac{g^E_{Al}}{(1-x_{Al})^2}dx_{Al}$	1.4 − 2.2%
G^M	$G^M = G^E + RT\left[x_{Al}\ln x_{Al} + x_{In}\ln x_{In}\right]$	1.4 − 2.5%
g^E_{In}	$g^E_{In} = \int_0^{x_{Al}} \frac{g^E_{Al}}{(1-x_{Al})^2}dx_{Al} - \frac{x_{Al}g^E_{Al}}{(1-x_{Al})}$	7%
g^M_{In}	$g^M_{In} = g^E_{In} + RT\ln(1-x_{Al})$	0.9 − 3.5%
a_{In}	$a_{In} = \exp\left[g^M_{In}/RT\right]$	0.0005 − 0.55%
x_{In}	$x_{In} = 1 - x_{Al}$	0.9%
γ_{In}	$\gamma_{In} = a_{In}/x_{In}$	1%
s^M_{Al}	$s^M_{Al} = 3Fm$	2 − 5%
s^E_{Al}	$s^E_{Al} = s^M_{Al} + R\ln x_{Al}$	11 − 38%
h^M_{Al}	$h^M_{Al} = g^M_{Al} + Ts^M_{Al}$	3 − 8%
S^M	$S^M = 3F(1-x_{Al})\int_0^{x_{Al}} \frac{m(x_{Al})}{(1-x_{Al})^2}dx_{Al}$	3%
S^E	$S^E = S^M + R\left[x_{Al}\ln x_{Al} + x_{In}\ln x_{In}\right]$	40 − 50%
H^M	$H^M = G^M + TS^M$	65 − 100%

LIST OF REFERENCES

[96Gau] H. Gautier, C. R. Hebd. Seances Acad. Sci. 123, 109 (1896).

[02Cam] W. Campbell and J. A. Mathews, J. Am. Chem. Soc. 24, 259 (1902).

[06Tam] G. Tammann, Z. Anorg. Chem. 48, 53 (1906).

[19Ura] G. G. Urazova, Zh. Russ. Fiz.-Khim. O-va Chast Khim. 51, 461 (1919).

[30Wag] C. Wagner and W. Schottky, Z. physik. Chem. B 11, 163 (1930).

[31Dix] E. H. Dix, F. Keller and L. A. Willey, Trans. Met. Soc. AIME 93, 396 (1931).

[31Loo] E. Loofs-Rassow, Hauszeitschrift VAW Erftwerk AG Aluminium 3, 20 (1931).

[31Ves] J. Veszelka, Banya- Kohomernoki Oszt. Kozl., Magy. Joszef Nador Musz. Gazdasagtud. Egy. Banya-, Koho-Erdomernoki Kar, Sopron 3, 193 (1931).

[33Gue] W. Guertler and A. Bergmann, Z. Metallk. 25, 81 (1933).

[46Rau] E. Raub and M. Engel, Z. Metallk. 37, 148 (1946).

[47Val] S. Valentiner and I. Puzicha, Z. Metallk. 38, 127 (1947).

[48Kle] W. Klemm, L. Klein, E. Hohmann, H. Volk, E. Orlamunder and H. A. Klein, Z. Anorg. Chem. 256, 240 (1948).

[52Cam] A. N. Campbell, L. B. Buchanan, J. M. Kuzmak and R. H. Tuxworth, J. Amer. Chem. Soc. 74, 1962 (1952).

[52Wag] C. Wagner, "Thermodynamics of Alloys," Addison-Wesley Press, Cambridge, Mass. (1952).

[53Wag] C. Wagner, J. Chem. Phys. 21(10), 1819 (1953).

[53Wel] H. Welker, Z. Naturforsch. 8a, 248 (1953).

[55Kos] W. Koster and B. Thoma, Z. Metallk. 46, 293 (1955).

[55Sam] L. E. Samuels, J. Inst. Met. 84, 333 (1955).

[57Kiu1] K. Kiukkola and C. Wagner, J. Electrochem Soc. 104, 308 (1957).

[57Kiu2] K. Kiukkola and C. Wagner, J. Electrochem. Soc. 104, 379 (1957).

[57Ure] R. W. Ure, J. Chem. Phys. 26(6), 1363 (1957).

[58Gla] V. M. Glazov and D. A. Petrov, Izvest. Akad. Nauk SSSR, Otdel. Tekh. Nauk 1958(4), 125 (1958).

[58Han] M. Hansen and K. Anderko, "Constitution of Binary Alloys," McGraw-Hill, New York (1958).

[58Woo] J. C. Woolley and B. A. Smith, Proc. Phys. Soc., London 72, 214 (1958).

[59Pin] B. Y. Pines and E. F. Chaikovskii, Soviet Phys.-Solid State 1, 864 (1959).

[62Gla] V. M. Glazov and S. N. Chizhevskaya, Soviet Phys.-Solid State 3(9), 1964 (1962).

[63Pie] U. Piesbergen, Z. Naturforsch. 18a, 141 (1963).

[63Wit] F. E. Wittig and G. Keil, Z. Metallk. 54(10), 576 (1963).

[65Gor] N.A. Goryunova, "The Chemistry of Diamond-like Semiconductors," The M.I.T. Press, Cambridge, Mass. (1965).

[65Pre] B. Predel, Z. Metallk., 56, 791 (1965).

[65Vec] A. A. Vecher, V. A. Geiderikh and Y. I. Gerasimov, Russ. J. Phys. Chem. 39(9), 1144 (1965).

[66Cam] A. N. Campbell and R. Wagemann, Can. J. Chem. 44, 657 (1966).

[66Mas] G. Massart, F. Durand and E. Bonnier, C. R. Acad. Sci. Paris C 262, 185 (1966).

[67Cox] R. H. Cox and M. J. Pool, J. Chem. Eng. Data 12, 247 (1967).

[68Ren] H. Renon and J. M. Prausnitz, A.I.Ch.E. Journal 14(1), 135 (1968).

[68Sam] V. V. Samokhval and A. A. Vecher, Russ. J. Phys. Chem. 42(3), 340 (1968).

[68Wag] C. Wagner, J. Electrochem. Soc. 115(9), 933 (1968).

[69Lic] B. D. Lichter and P. Sommelet, Trans. Met. Soc. AIME 245, 99 (1969).

[69Pre1] B. Predel and H. Sandig, Mater. Sci. Eng. 4(1), 49 (1969).

[69Pre2] B. Predel and U. Schallner, Mater. Sci. Eng. 5, 210 (1969/70).

[69Yaz] A. Yazawa and Y. K. Lee, J. Japan Inst. Met. 33, 318 (1969).

[70Jor] A. S. Jordan, Met. Trans. 1, 239 (1970).

[70Rap] R. A. Rapp and D. A. Shores, Tech. Metals Res. 4(Pt. 2), 123 (1970).

[70Ste] J. Steininger, J. Applied Phys. 41(6), 2713 (1970).

[71Bat] G. I. Batalin, V. E. Sokol'skii and T. B. Shimanskaya, Ukr. Khim. Zh. 37(4), 397 (1971).

[71Mas] G. Massart, Ph.D. Dissertation, Université Scientifique et Médicale, Grenoble, France (1971).

[71Pre] B. Predel and D. W. Stein, J. Less-Common Metals 24, 391 (1971).

[71Sch] H. Schmalzried, Metall. Chem., Proc. Symp. 1971, HMSO, London, 39 (1971).

[71Wag] C. Wagner, "Progress in Solid State Chemistry," vol. 6, eds. H. Reiss and J.O. McCaldin, Pergamon, New York, 1 (1971).

[72Gok] N. A. Gokcen and E. T. Chang, Scr. Metall. 6, 249 (1972).

[72Pan] M. B. Panish and M. Ilegems, Prog. Solid State Chem. 7, 39 (1972).

[72Sch] H. Schmalzried and A. D. Pelton, Ann. Rev. Mat. Sci. 2, 143 (1972).

[72Str] G. B. Stringfellow, J. Phys. Chem. Solids 33, 665 (1972).

[72Tre] Y. D. Tretyakov and A. R. Kaul, "Physics of Electrolytes, Vol. 2," ed. J. Hladik, Academic Press, New York, 623 (1972).

[73Hin] J. W. Hinze and J. W. Patterson, J. Electrochem. Soc. 120, 96 (1973).

[73Hul] R. Hultgren, P. D. Desai, D. T. Hawkins, M. Gleiser, K. Kelley and D. D. Wagman, "Selected Values of the Thermodynamic Properties of Binary Alloys," Am. Soc. Metals, Metals Park, Ohio (1973).

[74Bre] R. F. Brebick and R. J. Panlener, J. Electrochem. Soc. 121(7), 932 (1974).

[74Jor] A. S. Jordan, A. R. Von Neida, R. Caruso and C. K. Kim, J. Electrochem. Soc. 121(1), 153 (1974).

[74Mar] S. Martosudirdjo and J. N. Pratt, Thermochim. Acta 10, 23 (1974).

[74Per] A. E. C. Peres and V. F. Campos, Metal. ABM 194(3), 13 (1974).

[74Ram] T. A. Ramanarayanan and W. L. Worrell, Can. Metall. Q 13(2), 325 (1974).

[75Bau] W. Baukal, Ber. Buns. Phys. Chem. 79(11), 1148 (1975).

[75Gam] M. Gambino and J. Bros, J. Chem. Thermo. 7, 443 (1975).

[77Cra] D. F. Craig and J. J. Brown, J. Am. Cer. Soc. 60, 396 (1977).

[77Gir] C. Girard, R. Baret, J. P. Bros and P. Leydet, J. Chim. Phys. 74(10), 1061 (1977).

[77Luk] H. L. Lukas, E. T. Henig and B. Zimmerman, CALPHAD 1, 225 (1977).

[78Ans] I. Ansara, J. P. Bros and C. Girard, CALPHAD 2(3), 187 (1978).

[78Del] J. Delcet, R. J. Heus and J. J. Egan, J. Electrochem. Soc. 125(5), 755 (1978).

[79Del] J. Delcet, A. Delgado-Brune and J. J. Egan, "Calculation of Phase Diagrams and Thermochemistry of Alloy Phases," Conf. Proc. Metall. Soc. AIME, Milwaukee, 275 (1979).

[79Ger] F. Gerdes and B. Predel, J. Less-Common Metals 64, 285 (1979).

[79Jou] A. Joullie, P. Gautier and E. Monteil, J. Cryst. Growth 47, 100 (1979).

[80Ede] G. Edelin and D. Mathiot, Philosoph. Mag. B 42(1), 95 (1980).

[80Ros] C. J. Rosa, N. Rupf-Bolz, F. Sommer and B. Predel, Z. Metallk. 71(5), 320 (1980).

[80Sza] S. Szapiro, J. Phys. Chem. Solids 41, 279 (1980).

[81Ger] F. Gerdes and B. Predel, J. Less-Common Metals 79, 281 (1981).

[81Kau] L. Kaufman, J. Nell, K. Taylor and F. Hayes, CALPHAD 5(3), 185 (1981).

[81Lel] S. Lele and P. Ramachandrarao, Metall. Trans. B 12B, 659 (1981).

[81Lin] R. Linnebach and K. W. Benz, J. Crystal Growth 55, 531 (1981).

[83Alq] R. Alqasmi and J. J. Egan, Ber. Buns. Phys. Chem. 87, 815 (1983).

[83Kle] H. Kleykamp, Ber. Buns. Phys. Chem. 87, 777 (1983).

[83Kom] K. L. Komarek, Ber. Buns. Phys. Chem. 87, 709 (1983).

[83Mur] J. L. Murray, Bull. Alloy Phase Diag. 4(3), 271 (1983).

[84McA] A. J. McAlister, Bull. Alloy Phase Diagrams 5(5), 462 (1984).

[85Cha] K. M. Chang, Ph.D. Dissertation, University of Florida (1985).

[85Ega] J. J. Egan, High Temp. Sci. 19, 111 (1985).

[85Lee] J. J. Lee and F. Sommer, Z. Metallk. 76(11), 750 (1985).

[86Kat] U. Kattner, H. L. Lukas and G. Petzow, CALPHAD 10(2), 103 (1986).

[86Sau] N. Saunders and A. P. Miodownik, "Metastable Lattice Stabilities for the Elements," Report to the Scientific Group Thermodata Europe (March, 1986).

[87Gir] C. Girard, J. M. Miane, J. Riou, R. Baret and J. P. Bros, J. Less-Common Metals 128, 101 (1987).

[87Sha] R. C. Sharma, T. L. Ngai and Y. A. Chang, J. Electron. Mater. 16(5), 307 (1987).

[88Ish] K. Ishida, T. Shumiya, H. Ohtani, M. Hasebe and T. Nishizawa, J. Less-Common Metals 143, 279 (1988).

[88Sau] N. Saunders, A. P. Miodownik and A. T. Dinsdale, CALPHAD 12(4), 351 (1988).

[89Rug] B. C. Rugg and T. G. Chart, "A Critical Assessment of Thermodynamic and Phase Diagram Data for the Al-In System," presented at the CALPHAD XVIII Conference, Stockholm, Sweden (May, 1989).

BIOGRAPHICAL SKETCH

Corinne Ann Coughanowr was born in Lafayette, Indiana, the eldest child of two Ph.D.s. She called Indiana "home" for about ten years and then moved to the East Coast in 1967 and into the fast lane. Her high school years were grueling but excellent, spent at the Baldwin School, whose Latin motto translates to "learn true work." Carrying on this legacy, she went to Bryn Mawr College, where she majored in chemistry, minored in French, and took every subject and extracurricular activity she could cram in. Her next move took her across the country to the West Coast, and more academics. She finally bit the bullet and signed up for a degree in her father's field, chemical engineering, at the University of California, Berkeley. After earning the master's degree and working for a short period at DuPont, fate and determination took her on a four-month, solo trip around the world. This was definitely the major learning experience of her life. Another move across the country brought her to the University of Florida, where, in a moment of mental aberration, she signed up for the Ph.D. program in chemical engineering. Arduousness of the task notwithstanding, she has maintained the nomadic lifestyle, doing part of the work for the degree in Long Island, N.Y., and part in the Washington, D.C., area. She is meanwhile happily married and often gets to live with her husband. They are planning the next move across the Atlantic, to Grenoble, France, for as long as postdoctoral funds can be arranged.

I certify that I have read this study and that in my opinion it conforms to acceptable standards of scholarly presentation and is fully adequate, in scope and quality, as a dissertation for the degree of Doctor of Philosophy.

Timothy J. Anderson, Chair
Professor of Chemical Engineering

I certify that I have read this study and that in my opinion it conforms to acceptable standards of scholarly presentation and is fully adequate, in scope and quality, as a dissertation for the degree of Doctor of Philosophy.

Samuel O. Colgate
Associate Professor of Chemistry

I certify that I have read this study and that in my opinion it conforms to acceptable standards of scholarly presentation and is fully adequate, in scope and quality, as a dissertation for the degree of Doctor of Philosophy.

Mark E. Ozazem
Associate Professor of Chemical Engineering

I certify that I have read this study and that in my opinion it conforms to acceptable standards of scholarly presentation and is fully adequate, in scope and quality, as a dissertation for the degree of Doctor of Philosophy.

Gerald B. Westermann-Clark
Associate Professor of Chemical Engineering

This dissertation was submitted to the Graduate Faculty of the College of Engineering and the Graduate School and was accepted as partial fulfillment of the requirements for the degree of Doctor of Philosophy.

December, 1989

for Winfred M. Phillips
Dean, College of Engineering

Madelyn M. Lockhart
Dean, Graduate School